UNIVERSITY OF CALIFORNIA

Los Angeles

Cooperative Communications among Wireless Sensor Networks

A dissertation submitted in partial satisfaction of the

requirements for the degree Doctor of Philosophy

in Electrical Engineering

by

Yung-Szu Tu

2003

The dissertation of Yung-Szu Tu is approved.

Kirby A. Baker

Michael P. Fitz

Kung Yao

Gregory J. Pottie, Committee Chair

University of California, Los Angeles

2003

To my father, Tsung-Ming, my mother, Ching-Jung,

and my younger brother Yung-Cheng

Contents

List of Figures

List of Tables

ACKNOWLEDGEMENTS

I would first like to express my genuine gratitude to my advisor, Dr. Gregory J. Pottie, for his guidance and assistance. He is the most knowledgeable and caring person I have ever seen. When I am desperate in research, he encourages me like a close friend and investigates the problem with me like a cooperative colleague. Whenever I need his help, he never hesitates to assist me. His support is not limited to research. He is an indispensable part of the daily life of all his students. From time to time, he invites us to celebration activities, such as his wedding and Thanksgiving party. He cares about our needs and also creates comfortable and convenient working environments for us. I cannot imagine how I could undergo my challenging research without him.

I am indebted to Professors Kirby A. Baker, Michael P. Fitz, and Kung Yao for taking the time to serve on my Ph. D. committee. In particular, Professor Baker gives me numerous valuable and detailed suggestions on the format and wording of my dissertation.

I would also like to thank my current and previous fellow group members. They are Vishal Ailawadhi, Mohin Ahmed, Jay Gao, Kathy Sohrabi, Tommy Yu, Hong Chen, Sungsoo Kim, Huiyu Luo, Ameesh Pandya, Robert Thrasher, Yu-Ching Tong; and Sridhar Vemuri. They help me frequently in my research and make my graduate study more delightful.

I would also want to thank my friends in UCLA. They include Tai-Cheng Lee, Tzu-Chieh Kuo, Xueting Liu, Tai-Lai Tung, Li-Min Lee, Jri Lee, Jiun-Shiu Ma, Chi-Chung Chen, Jibing Wang, Joe Chen, and Da-Ching Chen. I came to UCLA without

any friend. Every seemingly trivial action, such as food shopping, was a tough task for me. It was these friends who helped and talked with me when I was hopeless. I will cherish our friendship forever.

Special thanks to Ching-Wen Fang, my cousin Charlie, and his wife Katie. Although they are not with UCLA, they are imperative part of my Ph.D. life. I share my happiness and sadness with them.

Finally, but definitely not the least, I would like to thank my family. It includes my father, Tsung-Ming, my mother, Ching-Jung, and my younger brother, Yung-Cheng. I spent the most precious part of my life with them. My Ph.D. study could not ever start without them. They are my final and most dependable shelter. They support whatever I do without any complaint. Although they are physically in the most distant place, the closet to my mind they lie.

VITA

1994	B. S., Electrical Engineering
	National Taiwan University
	Taipei, Taiwan, R. O. C.
1996	M. S., Electrical Engineering
	National Taiwan University
	Taipei, Taiwan, R. O. C.
1999-2003	Research Assistant
	University of California, Los Angeles
	Los Angeles, California
2003	Ph. D., Communications and Telecommunications
	Electrical Engineering
	University of California, Los Angeles
	Los Angeles, California

PUBLICATIONS

Yung-Szu Tu and Gregory J. Pottie, "Coherent Cooperative Transmission From Multiple Adjacent Antennas to a Distant Stationary Antenna Through AWGN Channels," *Proc. of the IEEE 54th Vehicular Technology Conference*, Spring, 2002.

Mohin Ahmed, Yung-Szu Tu, and Gregory Pottie, "Cooperative Detection and Communication in Wireless Sensor Networks," *Proc. of 38th Allerton Conference on Communication, Control, and Computing*, September 2000.

ABSTRACT OF THE DISSERTATION

Cooperative Communications among Wireless Sensor Networks

by

Yung-Szu Tu

Doctor of Philosophy in Electrical Engineering

University of California, Los Angeles, 2003

Professor Gregory J. Pottie, Chair

This dissertation addresses communications in the physical layer among wireless sensor networks, where a clock and an antenna are associated with one sensor. In this configuration, to achieve better performance, we can organize multiple sensors to communicate cooperatively. Research issues include synchronization, sensor motion, and local communication. In the scenario with multiple transmit antennas and one receive antenna in the AWGN channel, the coherent transmission approach adjusts the phase of transmit clocks so that signals combine coherently in the medium at the receive side. This requires phase-level synchronization, pre-compensation and its estimation. We propose a system to achieve this. The distribution of the phase offset for perfect combining is determined. We show the benefit of coherent combining, and the optimal power distribution between synchronization overhead and data transmission. We also devise a scheme to deal with motion of the receive antenna. In the analysis, we include the effects of the Doppler, forward and backward medium disturbances. The time correlation of the phase process associated with combined signals is explored. It is shown that coherent transmission is still beneficial.

When there are many stationary unsynchronized transmit antennas, the perceived channel depends on the phase relationships. We relate the channels having different phase relationships, and show the channel capacities are identical. The channel decomposition and the water-filling algorithm to achieve this capacity can be fixed as long as the phases of signals are compensated at baseband. The relationship between two channel decompositions with different phase statuses is also derived.

For the 3-node wireless network, we consider all communication power consumption. Initially, each information stream is divided into the relay-path and direct-path substreams. Two concepts are used in the derivation of achievable rate regions. Scenarios considered include: two sources and one common destination, one source and two destinations, and two sources and two destinations with four streams, for various normalized noise power conditions. Generally speaking, for a specific stream, if the third node is closer to the source, it should help transmission of the direct-path substream using coherent combining.

Chapter 1

Introduction

As sensor technology advances, the widespread deployment of sensor networks is envisioned to occur in the near future. They will carry out diverse tasks in a distributed fashion. Examples include security and health monitoring, over large numbers of sensors and large geographic areas for which centralized approaches are ill-suited. On the contrary, this can be easily achieved if numerous sensors are spread out in the area of interest, so that there will always be a sensor in close proximity to a source.

Sensor networks thus alleviate the data collection problem, but pose new challenges and opportunities for communications. Compared with the centralized network, the notion of the distributed network is that several low-complexity and low-cost nodes are employed to perform data collection tasks which a complicated and expensive central node cannot accomplish. The collected information has to be brought together for further processing or storage. The low complexity of sensors implies the scarcity of energy. Because communication performance degrades as transmission power is reduced, a single node in a distributed network cannot achieve the communication performance which the center node in a centralized network can achieve. On the other hand, we observe that there are several sensors in this scenario, and we may take advantage of this fact. They may cooperate to enhance the communication performance. We use the term cooperative communications to emphasize the cooperation among sensors. Although this type of

communications is motivated by the low-power sensor networks, it can also be used for other distributed networks which are not power-constrained because the communication quality scales well with power consumption. In other words, even if the power constraint on each sensor is on the order of that on the center node in a centralized network, cooperative communications may further improve the communication performance.

Cooperative communications is different from ordinary multiple input multiple output (MIMO) communications. In MIMO, because transmit antennas are co-located (as are receive antennas), some requirements for multi-antenna systems are satisfied automatically. Among them, we address the issues of synchronization and information sharing. The phases, timings, etc. of signals are dictated by the oscillator. They are assumed to be synchronized among antennas when antennas are co-located, because they are derived from the same oscillator. In sensor networks, synchronization cannot be taken for granted since each node has its own oscillator. Similarly, information sharing in ordinary MIMO communications is not a concern because it can be achieved through short-range wired communications. However, in sensor networks, information sharing among sensors is actually wireless communications. Thus, the power consumption is not trivial. In this respect, most sensors act as both the transmitter of some communication links and the receiver of others. In this dissertation, we will investigate the influences on communications when these expediencies are removed.

In Chapter 2, we consider the sensor network with multiple adjacent sensors and a remote stationary receive antenna. We determine that the coherent combining approach can boost the channel capacity. We devise a scheme to achieve coherent combining be-

yond synchronization. We neglect the communications among sensors in this scenario because they are so close that communication effort is negligible compared with the effort to communicate with the remote receive antenna. After analyzing the delay process of this scheme, we derive the influence of white Gaussian noise on it, and explore how much power should be sacrificed from information transmission and spent on synchronization for the purpose of cooperation.

In Chapter 3, we extend our work from Chapter 2 and assume the receive antenna is moving in a known orbit. We modify our communication scheme and the block diagram of the transmit antenna for this situation. Several additional imperfections, including the Doppler, medium disturbance, etc., are taken into consideration, and an analysis procedure is proposed. The optimal power distribution between information signals and synchronization signals is then numerically derived for a specific design example.

In Chapter 4, we consider stationary single-hop MIMO communications without synchronization. In other words, we suppose the synchronization in the ordinary MIMO communications with Gaussian channels does not hold. It is revealed that the channel capacity under the assumption of synchronization can still be achieved in this situation through signal processing. The only requirement is the knowledge of the synchronization offset. Although this knowledge is also required in the process of synchronization, by using this signal processing, we can remove the procedures of synchronization beyond that of acquiring of synchronization offset. Alternatively, if a new channel decomposition is made based on the new synchronization status, we also derive the relationship between the old and the new channel decomposition.

In Chapter 2 and 3, we neglect the power consumption of all local communications among transmit antennas by assuming they are very close to each other. In Chapter 5, we remove this assumption and consider a wireless network of three nodes. The famous and most simple example in this category is the relay channel[1]. This channel includes an information source, a destination, and a relay node that helps the transmission from the source to the destination. The capacity for this channel has, however, not yet been determined. Although an achievable rate region has been proposed, the converse of the capacity statement has not yet been proved. This channel includes only one information stream. We explore scenarios with multiple information streams. After revising the scheme[16] proposed by Sendonaris et al., we extend the study of the achievable rate regions to scenarios with more information streams and various relationships among noise power.

In Chapter 6, we present our conclusions and suggestions for further research.

Chapter 2

Stationary Multiple-to-One Coherent Cooperative Communications

2.1 Introduction

In the context of fading channels, the use of multiple antennas has been demonstrated to provide antenna diversity (also referred to as space diversity), which dramatically enhances system performance and channel capacity[4][7][17]. Compared with additive white Gaussian noise (AWGN) channels, the problem with fading channels, in terms of error probability, comes from the extra random attenuation of the path gain. When the channel is in deep fading, the path gain declines and consequently the error probability deteriorates given the same noise level. When the error probability is averaged over the whole possible range of path gains, the poor performance in deep fading dominates. With multiple antennas, we can take advantage of the randomness of the fading. The likelihood that all channels are in deep fades is less than the likelihood that a single channel is in a deep fade. In other words, if one channel is in a deep fade, the information may still be conveyed through other channels.

In future planetary exploration or terrestrial monitoring, it is desired to deploy large

numbers of ground sensors, and consequently an opportunity will exist to employ multiple transmitters cooperatively. The information collected from all sensors often has to be brought together at a hub. Two sensors that are far from each other may also need to exchange information. Due to the distance-squared wave propagation loss, communication through multiple short-distance hops is preferable to a single long-distance hop. However, the situation may be that these relays are not present and there are several sensors in the vicinity of the information source. The in-situ communications on Mars is an example. A Mars orbiter may be chosen as the hub. The altitude of the orbiter is on the order of a hundred kilometers, and the distance between sensors may be on the order of kilometers, but there is no relay between the orbiter and the Mars surface. Here, communication cost between sensors is insignificant, compared with communication cost between sensors and the orbiter. With cooperative communications, information is first shared among a cluster of neighboring sensors and then sensors in this cluster cooperatively convey the information to the destination, in this example the orbiter, using all resources for these sensors to achieve lower error probabilities or higher data rates. Among all resources, the energy is of the most concern. The reason is that there is no infrastructure to provide energy to sensors, while energy contained in sensors is limited because the size of sensors is small. On the other hand, transmission from the satellite is less constrained as solar energy can be more cheaply generated. Therefore, the most challenging link is from the multiple sensors to the satellite.

For this situation, we assume the channel is the AWGN channel. Line of sight (LOS) paths exist between sensors and the satellite, and there are few scatterers. Under this as-

sumption, the transmit diversity techniques can still apply but the improvement is not as substantial as for fading channels because these techniques are originally designed in view of the shortcomings of fading channels.

Another difference is the volatility of channels. Among these techniques, channel state information (CSI) is estimated by receive antennas, which are the satellites in our example, and used for detection and decoding. However, CSI is not fed back to the transmit antennas, which are the sensors in our example, for the purpose of coding and modulation. If the channel is changing fast, it is indeed useless to feed back CSI, adaptively code and modulate. Since we consider AWGN channels, the only CSI variation comes from the distance between transmit and receive antennas, and we assume the channel changes so slowly that the transmit antennas can exploit the CSI feedback.

2.2 Coherent Cooperative Transmission

Here, we focus on the single receive antenna configuration. One technique to exploit energy stored in separate transmit antennas is to adjust all EM waves so that waves emitted from each transmit antenna combine coherently at the receive antenna. Figure 2.1 illustrates this wave addition for the configuration of two transmit antennas. If the waves are of the same amplitude and perfectly coherent, the amplitude of the received wave is twice the amplitude of each component wave.

This leads to increased channel capacity. For the AWGN channel, the channel capacity is

$$C = W \log\left(1 + P_{av} / (WN_0)\right), \tag{2.1}$$

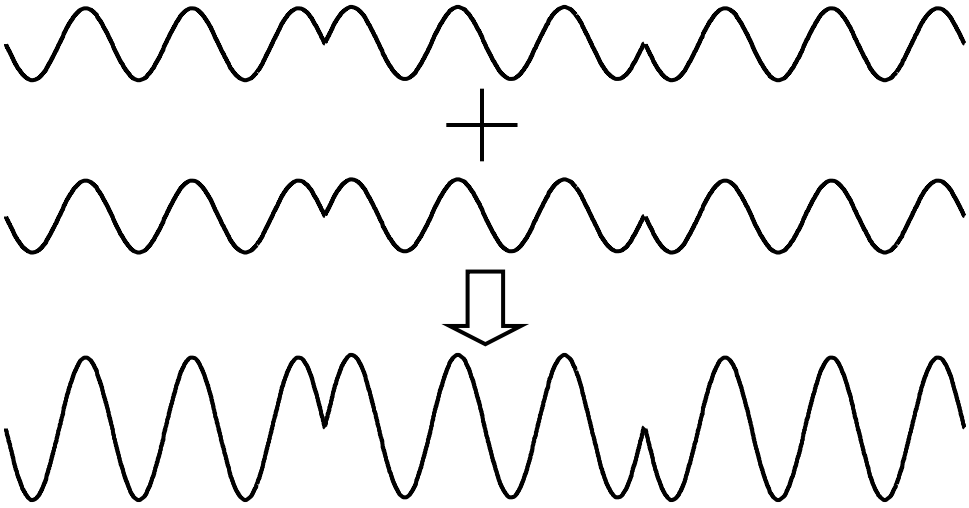

Figure 2.1: EM waves from two transmit antennas combine coherently at the receive antenna.

where W is the bandwidth in Hertz, N_0 is the one-sided power spectrum density, and P_{av} is the average received power. When each antenna transmits its own information independently, P_{av} is equal to the summation of each transmission power times individual attenuation. Assuming identical attenuation α, identical transmission power P_{tx}, and N transmit antennas, then P_{av} is equal to $\alpha N P_{tx}$. In contrast, if signals combine coherently

$$P_{av} = \left(N\sqrt{\alpha P_{tx}}\right)^2 = \alpha N^2 P_{tx}, \tag{2.2}$$

which increases with the square of the number of transmit antennas.

2.3 System Architecture

To achieve this purpose, the received carrier frequencies, the carrier phases, and the symbol timings of all EM waves have to be the same when received by the receive antenna. As clocks are triggered by oscillators, the instantaneous phase of the oscillator of

an antenna can be precisely determined by the time scale at that antenna. There are two network synchronization approaches[12] to be considered: mutual synchronization and master-slave synchronization. We will discuss which approach is better for our purposes. In addition, pre-compensation for the trip delays must be incorporated at transmit antennas.

The master-slave synchronization fits our objective better than the mutual one. With mutual synchronization, each clock collaborates with other clocks to determine the common time scale. This approach is preferred when no clock is superior to others and the robustness of the common time scale, with respect to the drift of any clock, is very crucial. However, there are two drawbacks. First, considerable overhead, which consumes energy, is required for clocks to cooperatively determine the common clock scale. Secondly, a multiple access scheme must be employed to differentiate one clock from the other in the process of coordination. Our goal is to align all EM waves coherently at the receive antenna with little extra energy consumption. Whether the common time scale is robust does not directly relate to the energy consumption of communications. Thus, we choose the master-slave synchronization approach. Once each slave clock keeps track of the variation of the master clock well, the clock drift is not an issue. The question of which antenna is the appropriate master will be discussed later.

Pre-compensation is required for each transmit antenna to compensate for unequal propagation delays. In the area of network synchronization, the propagation delays from the master clock to the slave clocks are compensated either in the master clock in advance or in the slave clocks afterward, so that at any point in time, all clocks have the

same time scale. However, our objective is more than that. We desire all waves to arrive at the receive antenna coherently. This is similar to the time requirements for the time division multiple access in satellite communications, where signals from transmit antennas must arrive at the satellite at specified time points. If the delays from all transmit antennas to the receive antenna were the same, the consequence would be just a time shift of the time scale, and all signals could arrive coherently. However, because the delays are actually different, clocks in transmit antennas have to be pre-compensated to account for different propagation delays from the transmit antennas to the receive antenna. Thus, the delays from the master to the slave clocks have to be compensated, and the delays from the transmit antennas to the receive antenna must be pre-compensated.

Two types of the combination of master-slave synchronization and pre-compensation have been investigated in [9]. The first type is the open-loop approach. For a master-slave pair, both master and slave antennas transmit their clock scales to each other. Based on the clock scales of the incoming wave and the local antenna, the clock difference and pre-compensation are constantly calculated cooperatively by the master and the slave antenna. The slave clock accordingly updates its clock and pre-compensation by changing delay, while the master updates the pre-compensation only. The slave clock makes no effort to adjust its oscillator frequency in response to the clock difference. If the master and the slave oscillator frequencies are off by a large amount, the clock difference will increase rapidly after updates, and this will result in poor synchronization. The second type is the closed-loop approach. The slave clock is a voltage-controlled oscillator (VCO). The error signal is the clock difference mentioned above,

and this signal is used to adjust the VCO frequency, rather the delay as in the open-loop approach. The problems with this approach are the stability and the tracking ability. Unlike ordinary phase-locked loops, this loop includes two significant delays, one in the master-to-slave transmission and the other in the slave-to-master transmission. Because the delay is so huge, to keep the loop stable, the loop bandwidth must be narrow, and the tracking ability will be reduced.

Our approach is illustrated in Figure 2.2. It employs a VCO at the slave antenna to track the master clock frequency which is received at the slave antenna, and the phase comparison is done locally. Thus, we avoid the problem due to long propagation delay as in the closed-loop approach, while slave clocks can track the frequency of the master clock.

Compensation for the master-slave propagation delay is implemented jointly with the pre-compensation for transmit-receive propagation delay, as illustrated in Figure 2.3. If we wanted to equalize all time scales, we would have to compensate slave clocks for the master-slave propagation delay by using delay elements, and this would require a multiple access scheme among slave antennas and a lot of signaling to determine the amount of compensation. Since what matters is whether waves arrive at the receive

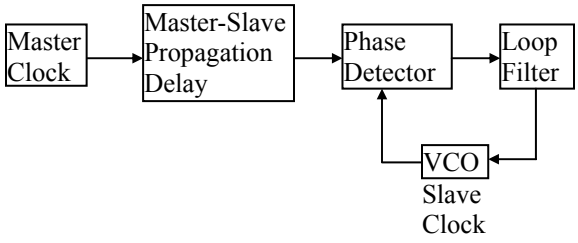

Figure 2.2: The diagram of our master-slave synchronization.

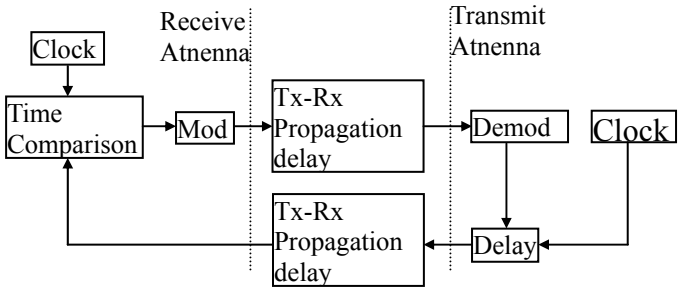

Figure 2.3: The diagram of compensation and pre-compensation.

antenna coherently, this master-slave propagation delay compensation can be combined with transmit-receive propagation delay pre-compensation. Note that the clock of the transmit antenna can be a master or a slave clock. The time difference measured at the receive antenna is the sum of both master-slave and transmit-receive propagation delays, and they are indistinguishable. This value is modulated, fed back, demodulated, and used in the single delay element. We assume that the receive antenna is moving slowly so that it can be viewed as stationary during the interval between pre-compensation estimation and coherent combining, while the value of pre-compensation has to be estimated and updated periodically. The new estimate is based upon the signal which is delayed by the previous pre-compensation estimate. Thus, this new estimate can be considered the adjustment to the previous estimate.

We choose the master clock based on the criterion of low energy consumption. The information for pre-compensation has to be modulated by the oscillator of the receive antenna, and fed back to the transmit antenna. The clock of the receive antenna can act as the master clock without consuming any extra energy since the time scale can be embedded in the carrier phase and the symbol boundary. In order to extract the time scale, the slave clocks have to remove the information sequence[14].

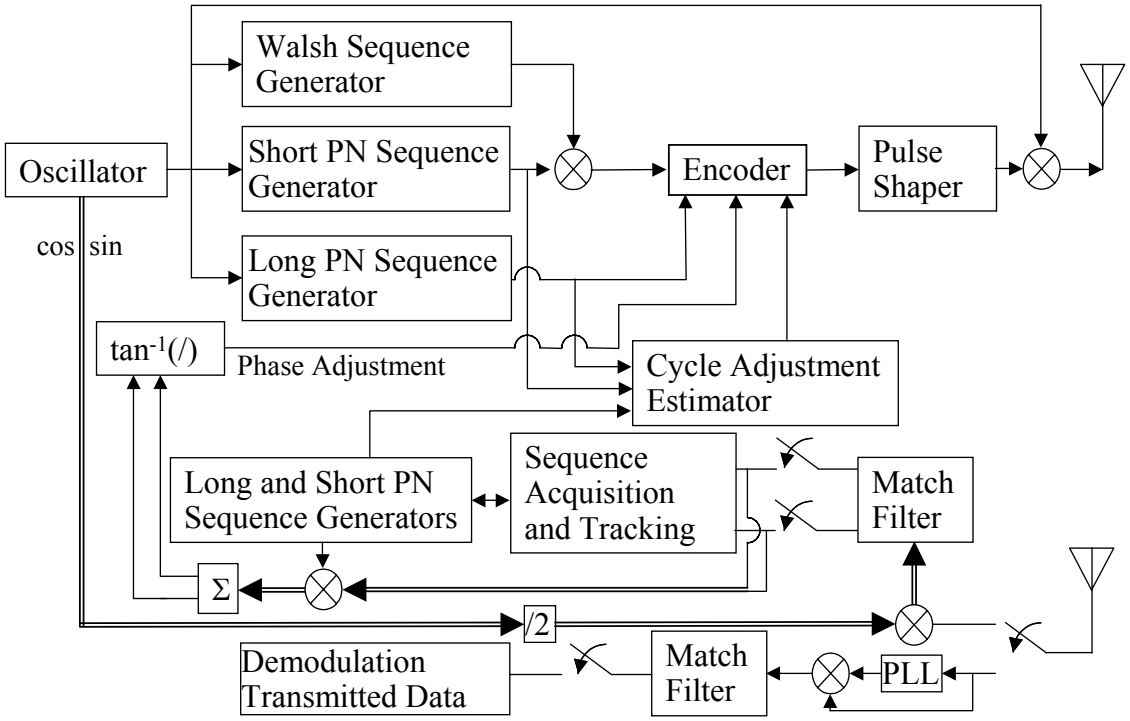

Figure 2.4: The block diagram of the receive antenna with the master clock.

Based on the preceding discussion, the block diagrams of the receive antenna with the master clock and the transmit antenna with the slave clock are illustrated in Figure 2.4 and Figure 2.5. The double line represents in-phase and quadrature components.

The time scale of the master clock is conveyed through a pseudo-noise (PN) sequence and the phase embedded in the continuous sinusoidal carrier. They work in a complementary way. The phase of the sine wave changes faster than the PN sequence. Thus, it can provide more precise timing. However, there is a severe 2π ambiguity problem. The period of the PN sequence is much longer, so it can solve this ambiguity.

On the other hand, since the chip rate is lower than the frequency of the sinusoidal carrier, the timing resolution is limited. By multiplying the PN sequence by the sine wave, precise time scale without ambiguity can be realized and transmitted to all slave clocks.

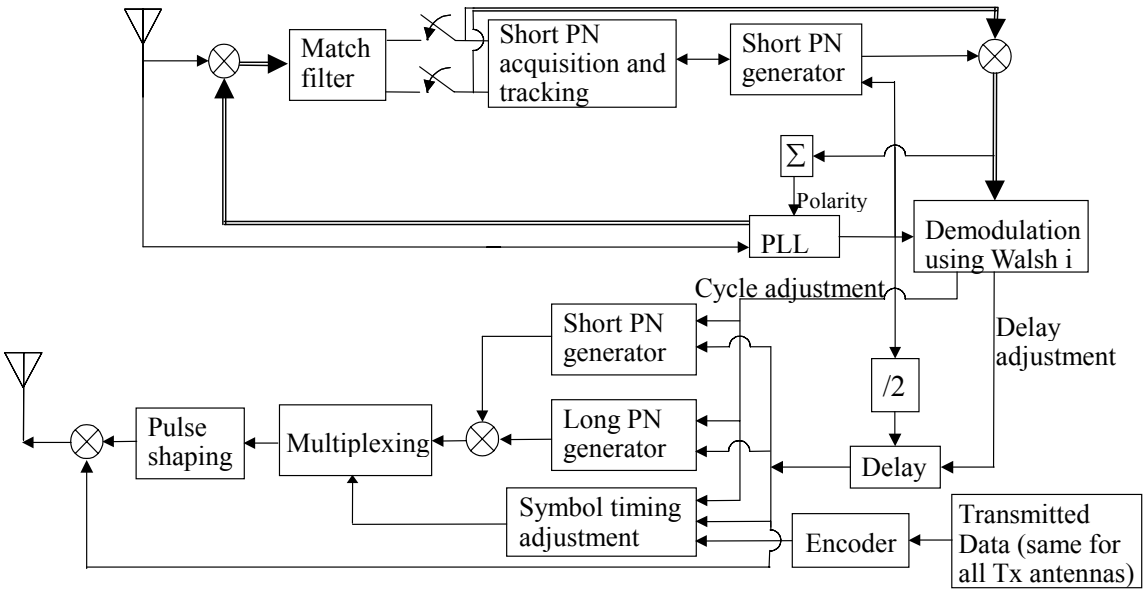

Figure 2.5: The block diagram of the transmit antenna with the slave clock.

Each slave clock uses a phase-locked loop and a delay lock loop to maintain synchronism with the carrier and the PN sequence respectively.

In order to estimate the individual pre-compensation values for each transmit antenna, every transmit antenna has to transmit its time scale back to the satellite. We also use the combination of PN sequence and sinusoidal carrier to represent the time scale. To avoid interfering with the frequency band occupied by the downlink, i.e. from the master to the slave clocks, the carrier frequency of this synchronization signal is shifted to another frequency band, while this new carrier must be derived from the retrieved carrier so that the feedback pre-compensation estimate can correspond to the retrieved time scale. To achieve this, a frequency multiplier or a divider is inserted after the output of the PLL. Additionally, the receive antenna must be able to differentiate synchronization signals from different transmit antennas. In other words, a specific multiple access scheme must be employed. DS-CDMA and TDMA are good choices for this purpose. The advantage of

these two schemes over FDMA is that all transmit antennas use the same carrier frequency, which is required in the coherent transmission. Therefore, the phase pre-compensation value can be used directly in coherent transmission without any conversion. We use DS-CDMA in Figure 2.4 and Figure 2.5 as an illustration because we would like to point out a crucial point for DS-CDMA: there must be two PN sequences multiplied together, just as in IS-95[11]. If only one sequence were used, since the different propagation delay affects the phase of the received PN sequence, there would be no way to distinguish transmit antennas. Thus, both long PN and short PN sequences are employed.

At each transmit antenna, both information and synchronization signals are transmitted. Synchronization signals are used to perform the above operations to achieve synchronization. Information signals contain the information to be conveyed from transmit antennas to the receive antenna. These two kinds of signals are multiplexed in the time or code domain, while the timing and the phase references are shared. Information signals from all transmit antennas occupy the same channel in the time or code domain. Because of the operations described above, information signals are received at the receive antenna coherently.

2.4 Mathematical Model

Assuming that the information signal and the synchronization signals are time multiplexed, at the receive antenna the received information signals from all transmit antennas are combined as

$$\sum_{n=1}^{N}\sum_{i=-\infty}^{\infty} b_i \alpha_n \sqrt{\frac{2E_b}{T_b}} \cos(\omega_n t + \theta_M + \Theta_n) \cdot h(t - iT_b + (k_n T_\omega + \Theta_n / \omega_n)), \qquad (2.3)$$

where $b_i = \pm 1$ is the information bit, α_n is the attenuation, E_b is the bit energy, ω_n is the carrier frequency, θ_M is the phase of the master oscillator, Θ_n is the phase offset and also a random process, $h(t)$ is the pulse, T_b is the symbol duration, k_n is an integer, and T_ω is the period of the carrier. $k_n T_\omega + \Theta_n / \omega_n$ represents the time offset. It is assumed that $\alpha_n = 1 \quad \forall n$, $\omega_n = \omega \quad \forall n$ due to the operation of the PLL, $k_n \approx k \quad \forall n$ which means the chip offset estimation and pre-compensation track the channel dynamics very well. Θ_n / ω_n is insignificant, compared with the support of $h(t)$. Thus, $h(t - iT_s + (k_n T_\omega + \Theta_n / \omega_n))$ is almost the same for all transmit antennas, at any point in time. Therefore, only $\cos(\omega_n t + \Theta_n)$ is of concern.

2.5 Performance Analysis

While the pre-compensation estimate is updated periodically, we assume that the propagation delays are constant during the interval from when they are estimated to when signals are coherently combined in the receive antenna. We assume all transmit antennas are independent from each other. Thus, Θ_n's are independently identically distributed. The components in Θ_n are determined by analyzing the procedures of coherent transmission, as listed in Table 2.1. At time t_1, the phase of EM wave which the slave clock n tracks is θ_M plus the phase offset φ_n due to the propagation delay. The slave clock bounces back the time scale with the PLL phase error $\theta_{e,n}(t_1)$ and the present pre-compensation

Table 2.1: Time Flow of Coherent Transmission

Time	Action	Receive Antenna	Transmit Antenna *n*
always	The master clock transmits the time scale	$\cos(\omega_M t + \theta_M)$	
t_1	The slave clock *n* receives the time scale		$\cos(\omega t + \theta_M + \varphi_n)$
t_1	The slave clock *n* bounces back the time scale		$\cos(\omega t + \theta_M + \varphi_n + \theta_{e,n}(t_1) + \theta_{est})$
t_2	The receive antenna (master clock) receives the bounce	$\cos(\omega t + \theta_M + \varphi_n + \theta_{e,n}(t_1) + \theta_{est} + \varphi_n)$	
t_2	The receive antenna estimates the new phase pre-compensation	$\theta_{est}(t_2) = 2\varphi_n + \theta_{e,n}(t_1) + \theta_{est} + \phi_{e,n}(t_2)$	
t_3	The receive antenna feeds back the estimate		
t_4	The transmit antenna *n* (slave clock) receives the new estimate, and transmit information data		$\cos(\omega t + \theta_M + \varphi_n + \theta_{e,n}(t_4) + \theta_{est} - \theta_{est}(t_2))$
t_5	Waves are coherently combined, and received by the receive antenna	$\cos(\omega t + \theta_M + 2\varphi_n + \theta_{e,n}(t_4) + \theta_{est} - \theta_{est}(t_2))$	

estimate θ_{est}. Owing to the propagation delay again, the phase received by the receive antenna is further shifted by φ_n at time t_2. The receive antenna estimates the phase pre-compensation with phase error $\phi_{e,n}(t_2)$. The new estimate $\theta_{est}(t_2)$ is sent back to the transmit antenna n, and subtracted from the old estimate θ_{est}. At time t_4, the transmit antenna transmits information data to be combined coherently with the master clock phase θ_m, the phase offset φ_n, the PLL phase error $\theta_{e,n}(t_4)$, and the updated pre-compensation $\theta_{est} - \theta_{est}(t_2)$. Therefore, the EM wave arrives at the receive antenna with phase

$$\begin{aligned} &\theta_M + 2\varphi_n + \theta_{e,n}(t_4) + \theta_{est} - \theta_{est}(t_2) \\ &= \theta_M + \theta_{e,n}(t_4) - \theta_{e,n}(t_1) + \phi_{e,n}(t_2). \end{aligned} \tag{2.4}$$

The probability density function (pdf) of $\theta_{e,n}(\cdot)$ is derived in [21] by solving the Fokker-Planck equation

$$P(\theta_{e,n}) = \frac{\exp(\eta\cos(\theta_{e,n}))}{2\pi I_0(\eta)}, \tag{2.5}$$

where η is the signal to noise ratio in the phase-locked loop. Assuming $\theta_{e,n}(t_4)$ and $\theta_{e,n}(t_1)$ are independent, after some manipulation, the pdf of $\theta_{e,n}(t_4) - \theta_{e,n}(t_1)$ is

$$P(\theta_{e,n}(t_4) - \theta_{e,n}(t_1)) = \frac{I_0[\,|\,\eta + \eta\exp(j(\theta_{e,n}(t_4) - \theta_{e,n}(t_1)))\,|\,]}{2\pi[I_0(\eta)]^2}, \tag{2.6}$$

where $I_0(\cdot)$ is the first kind Bessel function with order 0. The pdf of $\phi_{e,n}(t_2)$ is derived in [15]. Actually, independence is the worst case. If they are not independent, we can take advantage of their correlation to reduce the estimation error. The extreme is when their correlation is 1. Then, the error is equal to 0.

To investigate the effect of energy distribution between information and synchroni-

zation signals, information data is divided into groups of D symbols, and the synchronization signal, which is used for pre-compensation estimation and also called the header, is appended to form a packet of P symbols. The energy per symbol is identical in both parts. Then, the pdf of $\phi_{e,n}(t_2)$ can be written as

$$P(\phi_{e,n}) = \frac{e^{-\frac{DE_bH}{PN_0}}}{2\pi} + \sqrt{\frac{DE_bH}{\pi PN_0}}\cos(\phi_{e,n})e^{\frac{DE_bH}{PN_0}\sin^2(\phi_{e,n})} \cdot \phi\left(\sqrt{\frac{2DE_bH}{PN_0}}\cos(\phi_{e,n})\right), \quad (2.7)$$

where $H = P - D$, E_b is the total energy consumption per packet per transmit antenna divided by the number of information bits in a packet, N_0 is the one-sided noise spectrum density, and

$$\phi(x) = \frac{1}{2\pi}\int_{-\infty}^{x} e^{-\frac{w^2}{2}}dw. \quad (2.8)$$

Then, the pdf of Θ_n is determined numerically. The pdf's of random variables $\theta_{e,n}$, $\theta_{e,n}(t_4) - \theta_{e,n}(t_1)$, $\phi_{e,n}$, and Θ_n are plotted in Figure 2.6 when $\eta = 10dB$, $E_b / N_0 = 0dB$, $P = 20$, $D = 5$. It is obvious that as more and more phase errors are included, the pdf becomes wider. It goes without saying that as η and E_b / N_0 increase, their corresponding pdf's become narrower. The pdf's of different allocations between D and H are plotted in Figure 2.7. In (2.7), the appearance of D and H is symmetric, and thus the extremum occurs when D is equal to H, i.e., 10 given $P = 20$. Figure 2.7 also demonstrates this extremum in the sense that the pdf is the sharpest. If the energy per symbol is fixed for different header sizes, the larger header size will have the sharper pdf. However, what is fixed are the packet size and the energy per information symbol after averaging over the whole packet. When more symbols are allocated for the

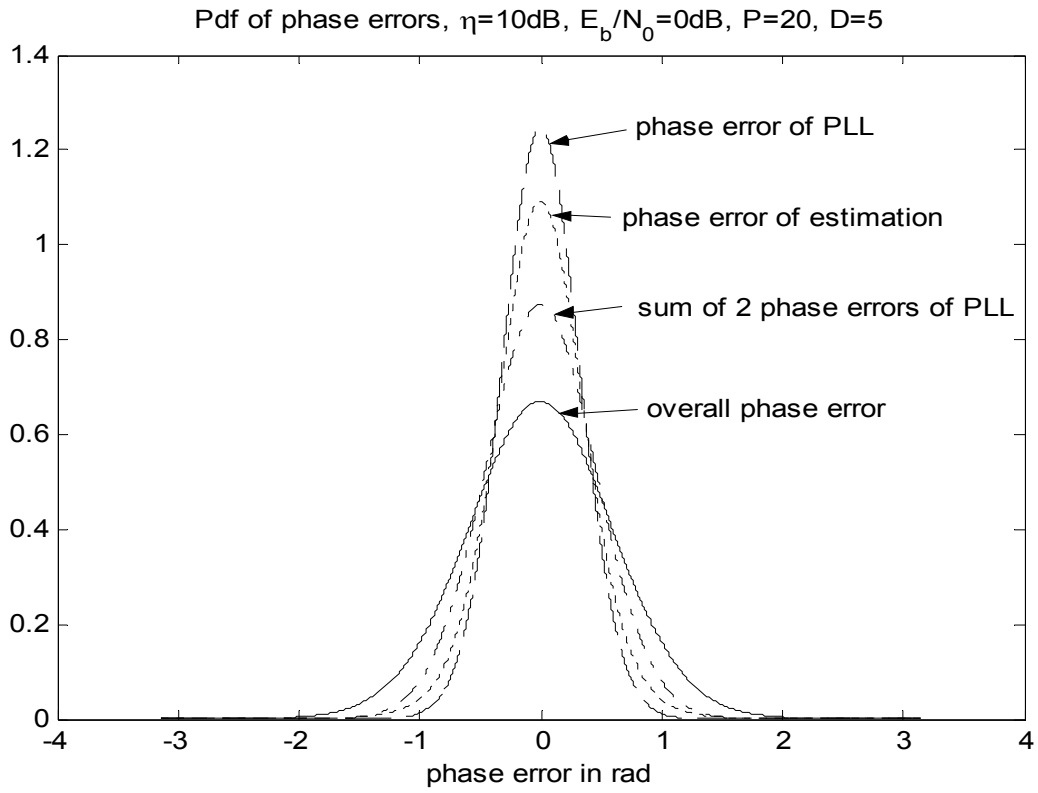

Figure 2.6: The pdf's of several random variables.

header, fewer symbols remain for the information, and thus there is less energy per packet, given the fixed energy per information symbol. This reduced total energy is shared by information and header symbols, and thus energy per symbol is also decreased. Consequently, a larger header size does not guarantee higher energy for estimation. The highest energy occurs when D is equal to H. The effect of changing P can also be predicted. Whenever $D \cdot H$ appears in the numerator, P appears in the denominator. The extremum occurs when $D \cdot H$ is minimum. Hence, as P increases, the pdf becomes sharper, as demonstrated in Figure 2.8.

The received information signals are downconverted to baseband using the local oscillator associated with the master clock. Thus, the sampled signal amplitude after the

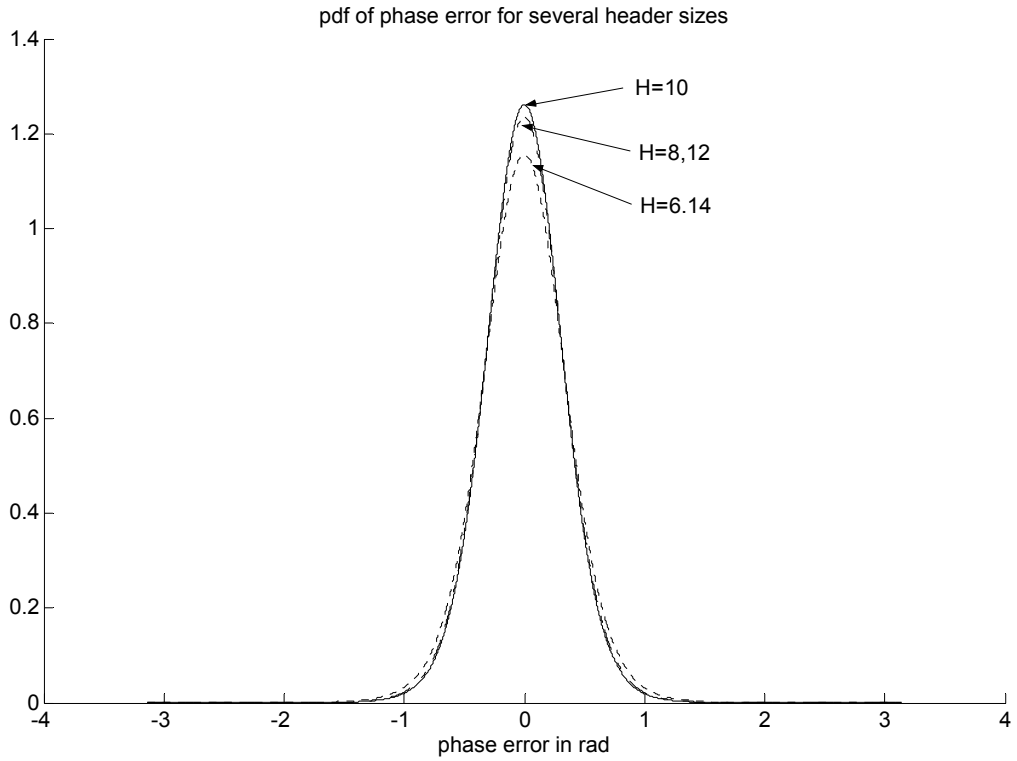

Figure 2.7: The pdf's of different header sizes.

matched filter is the summation of the cosine of Θ_n. The distribution is obtained numerically and plotted in Figure 2.9 for $\eta = 10dB$, $E_b / N_0 = 0dB$, $P = 20$, and $D = 10$. When one transmit antenna is considered, the pdf is very sharp. As more and more antennas are involved, the pdf becomes smoother and more like a Gaussian function. Nevertheless, it is obvious that the mean value increases with the number of transmit antennas. In Figure 2.10, we plot the pdf of the amplitude for various header sizes given $P = 20$. For the optimal header size, i.e. $H = 10$, the pdf is the sharpest, and has the highest mean value.

The estimate is updated per packet. The combined signal is demodulated at the receive antenna. Assuming BPSK is employed, the bit error rates for various header sizes

H are depicted in Figure 2.11. We pointed out that the optimal energy allocation for phase estimation occurs when the sizes of the header and the information are equal. However, the error rates are not symmetric in Figure 2.11. The minimum error probability does not happen at the optimal symbol allocation point. From Figure 2.7, we observe that the difference of pdf's between different header sizes around the optimal allocation is not huge. We can trade phase estimation accuracy for higher energy per information symbol. When the header size is slightly smaller than the optimal size, the benefits from higher energy for information symbol transmission overcome the deteriorated phase estimation accuracy in terms of symbol error probability.

The performance of coherent combining is also compared with other approaches with the same power consumption for a fixed number of transmit antennas. In the first configuration, power in all transmit antennas is concentrated on one transmit antenna, and thus coherent combining cannot be realized. In the second configuration, we assume that perfectly coherent combining is achieved magically without any energy dedicated to achieve synchronization. The results are demonstrated in Figure 2.12. For the curve without coherent combining, there is only one transmit antenna, whereas the power consumption grows linearly with the number of transmit antennas. For each packet size, the curves for our scheme are obtained with the optimal energy allocation between the header and information sizes. Obviously, the curve with perfectly coherent combing outperforms other curves significantly because the phases are perfectly aligned without any energy consumption for synchronization. When few sensors are involved, the transmission without coherent combining is better than our coherent combining scheme because there is no energy dedicated to accomplish synchronization. After more sensors

is no energy dedicated to accomplish synchronization. After more sensors are considered, the benefit of coherent combing overcomes this energy penalty. With the larger packet size, the error probabilities decrease because more energy per packet is available for phase estimation if a fixed portion of E_b is allocated for the header. From another point of view, if a fixed amount of energy in each packet is allocated to achieve identical performance of phase estimation, with larger packet sizes, each information symbol is required to sacrifice less energy, and thus a lower error probability is achieved. Practically speaking, however, if the packet size is too large, the channel cannot be considered stationary within the packet, and the update of phase pre-compensation estimation is not frequent enough.

2.6 Conclusion

We have proposed a transmission scheme for the setting where transmit antennas are in the vicinity while the single receive antenna is at a distance. By adjusting the carrier phase, frequencies, and symbol timings of transmit antennas, signals arrive at the receive antenna coherently, and thus combine constructively in the transmission medium. The adjustment is achieved by tracking the clock of the receive antenna, and pre-compensating transmission delays. Based on the mathematical model, we compute the system performance for the cases of the stationary and the non-stationary receive antenna. It is verified that this scheme can lower the error rates, compared with the situation where the same amount of energy emanates from a single transmit antenna. An optimal energy distribution between information and synchronization signals is observed.

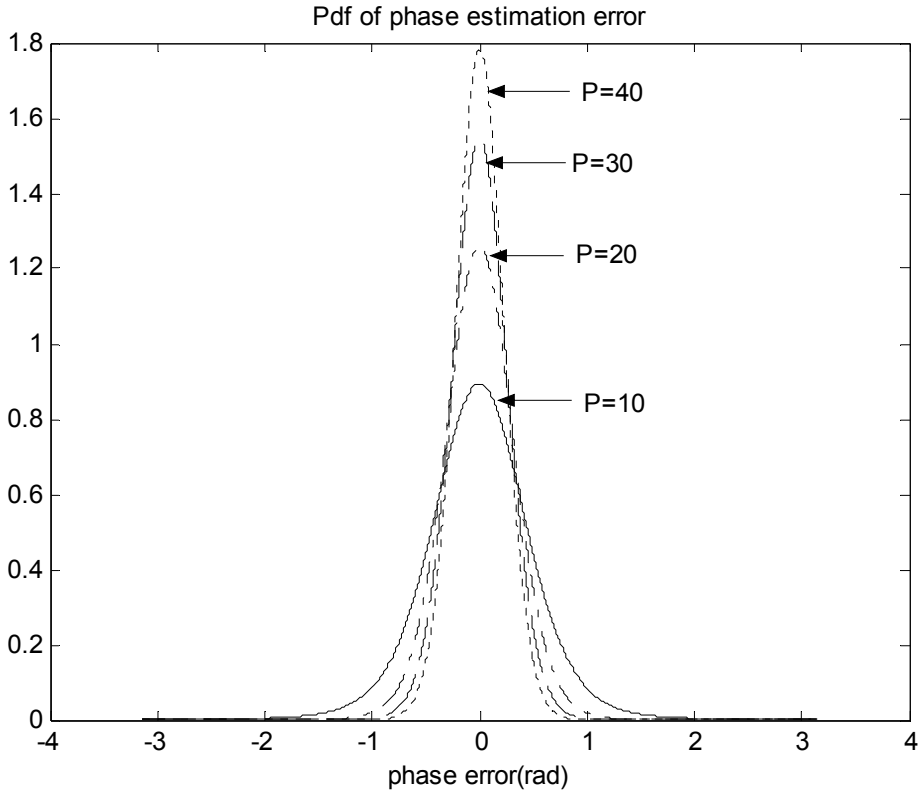

Figure 2.8: The pdf of phase estimation error for different packet sizes, with equal information and header sizes, $E_b / N_0 = 0dB$ per sensor, $\eta = 10dB$.

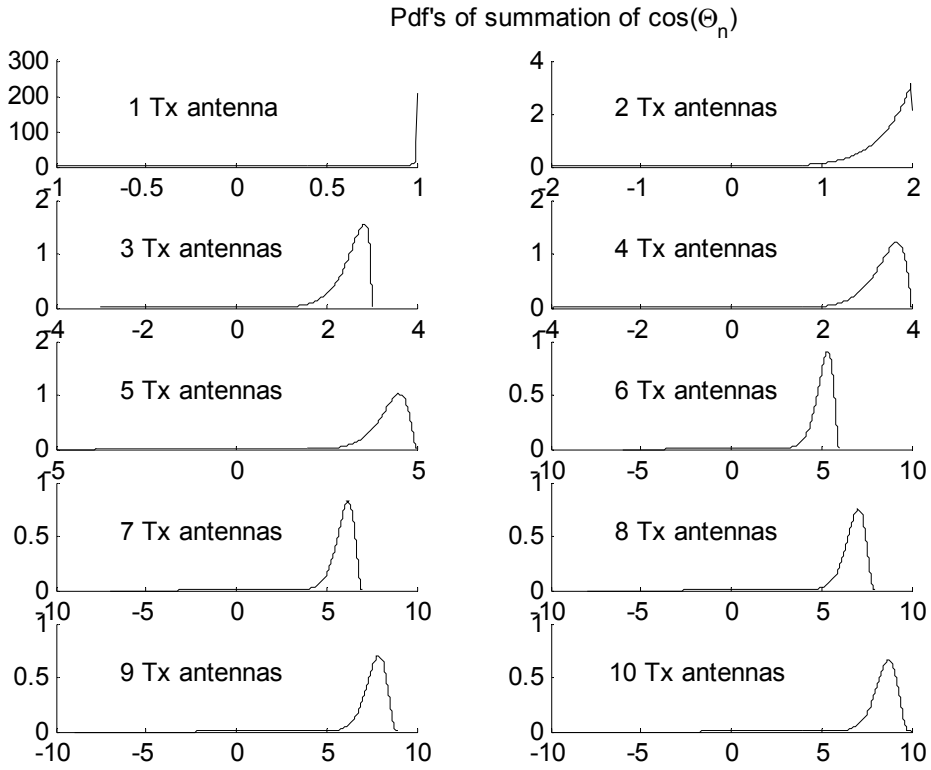

Figure 2.9: Pdf's of the summation of $\cos(\Theta_n)$

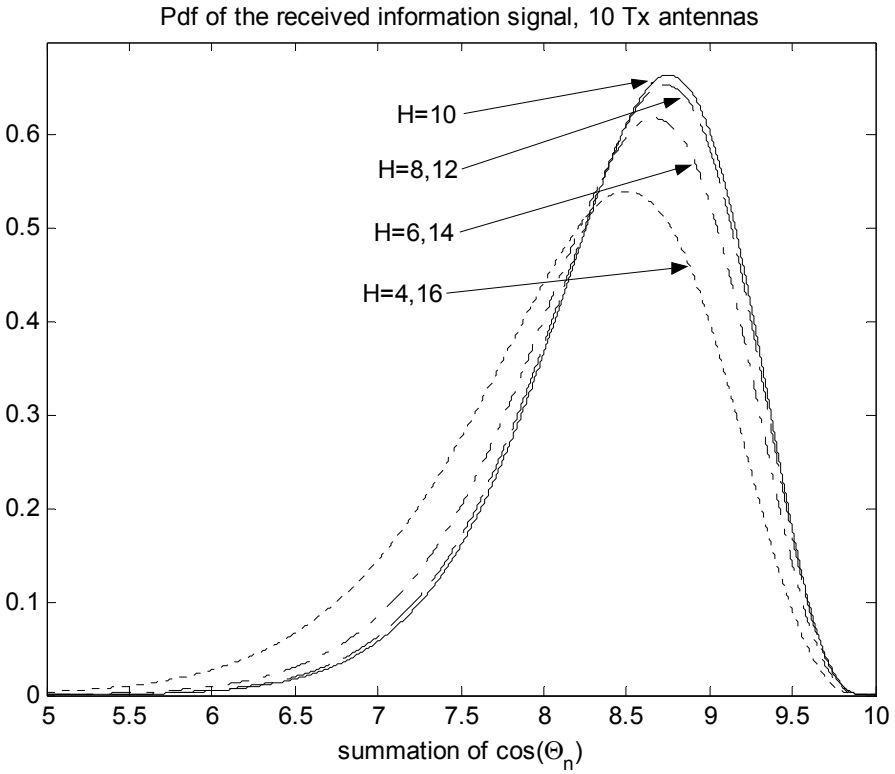

Figure 2.10: The pdf of the amplitude of the sampled received information signal, $P = 20$.

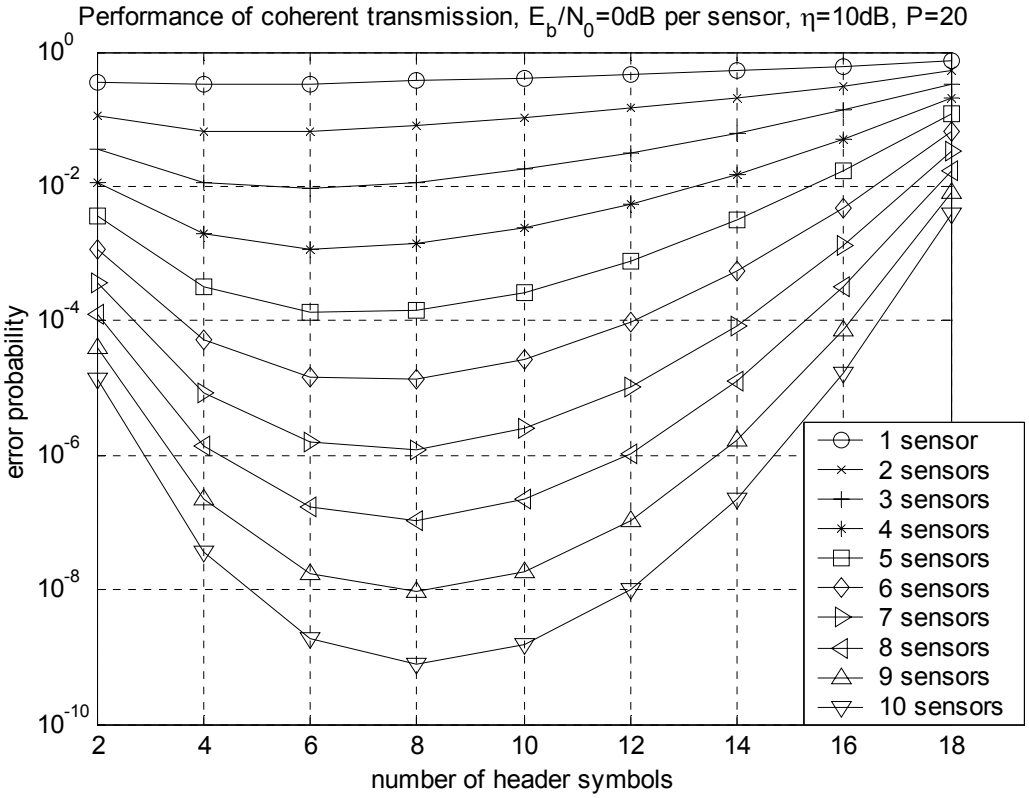

Figure 2.11: The error probabilities for various header sizes and numbers of transmit sensors

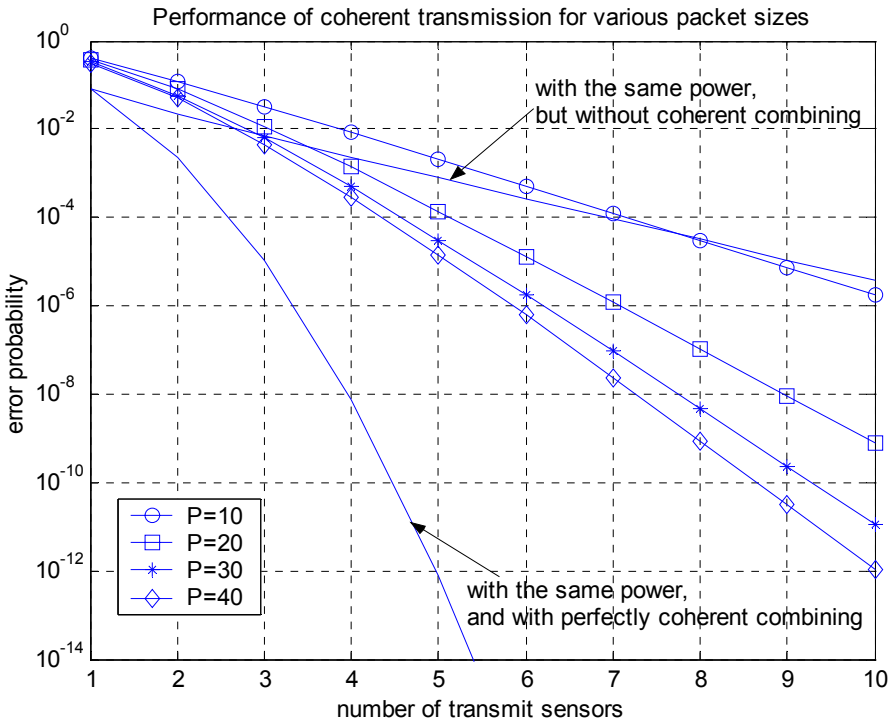

Figure 2.12: The error probabilities for various numbers of sensors and packet sizes with optimal power allocation between header and information sizes.

Chapter 3

Non-stationary Multiple-to-One Coherent Cooperative Communications

3.1 Introduction

In the last chapter, we assumed that the transmit antennas and the receive antenna were planned to be stationary. The purpose of recurrent pre-compensation estimation was just to rectify unpredictable drifts. However, there are situations where the receive antenna is moving in a known orbit. For example, the Mars orbiter may circle around Mars, rather than being geo-stationary[5] with respect to Mars. In this situation, from the point of view of the transmit antennas, the receive antenna, i.e. the orbiter, is non-stationary. Thus, the value of correct pre-compensation for coherent combining is changing. In this chapter, we revise our scheme for the stationary receive antenna in order to counteract this impediment. Finally, we analyze the system linearly and obtain the optimal power distribution numerically.

3.2 System Architecture

The consequence of the receive antenna's movement is that all propagation delays from transmit antennas to the receive antenna keep changing. In order for coherent transmission to occur, one approach is to estimate and update the pre-compensation value more frequently.

For the situation of the stationary receive antenna, the operations of pre-compensation estimation and update work alternatively. In other words, new estimation can take place only after the previous pre-compensation estimate is used by the transmit antennas and the signal compensated by this estimate is sent back to the receive antenna. The time duration of one round of operations is lower-bounded by the round-trip propagation delay. Thus, a closed loop is circumvented. If a closed loop were formed between the receive antenna and any transmit antenna, the loop would become unstable easily because the loop delay, which is the round-trip propagation delay here, is enormous. Yet avoiding a closed loop seems to place a constraint on the highest rate of pre-compensation update.

To deal with this dilemma, we use the pre-compensated clock for information signals and the un-pre-compensated clock for synchronization signals at transmit antennas. Pre-compensation estimates are computed from un-pre-compensated signals and applied to un-pre-compensated signals in return. There is no dependency on old estimates and thus it is not required for the new estimation to wait for the execution of the last estimate. Therefore, the open loop architecture is maintained, while estimation and pre-compensation can be performed without the rate constraint. The block diagram of the

transmit antenna is shown in Figure 3.1. Compared with the block diagram in the last chapter, one multiplexer is added to toggle between pre-compensated and un-pre-compensated clocks. In other words, both information and synchronization signals are transmitted and time-multiplexed. The information signal employs the pre-compensated time scale. Information signals from all transmit antennas occupy the same time slot and because of the operations described above, these signals combine coherently when received by the receive antenna. The block diagram of the non-stationary receive antenna is identical to that of the stationary receive antenna.

Another problem resulting from the non-stationary receive antenna is the Doppler shift. Because of the different Doppler shifts observed by slave clocks, i.e. transmit antennas, the frequencies that they track are not the same. Nevertheless, these frequencies

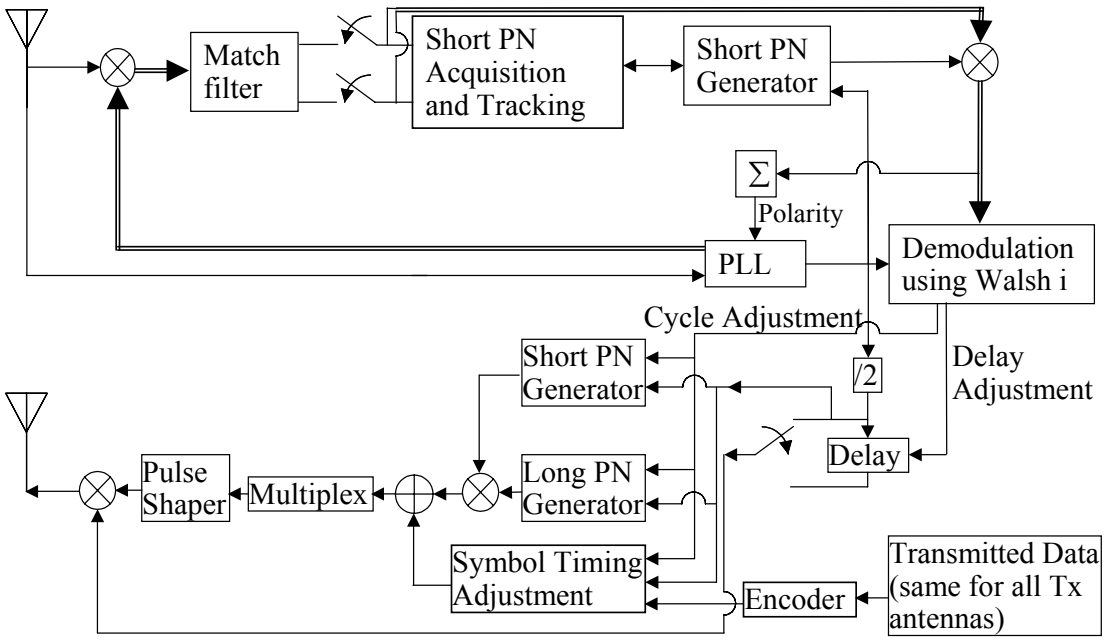

Figure 3.1: The block diagram of the receive antenna with the master clock.

are more confined, compared with situations without this synchronization.

3.3 Performance Analysis

Since the modification is on the procedure of estimation and pre-compensation, the mathematical representation of transmitted information signals is the same as in the last chapter and the phase error still comes from the difference between pre-compensation estimates and the perfect pre-compensation values when signals are coherently combined.

The whole procedure is decomposed into blocks in Figure 3.2. In addition to the white noise considered in the estimation and the phase-locked loops, we also take into consideration Doppler, time dilation[19], and medium noise[22]. When the object is moving at high speed, the effects of special relativity are not insignificant. The effect that is relevant to our analysis is time dilation. The medium noise means the effect of the disturbance of the medium on the propagation delay of EM waves. Both the transmissions from the satellite forward to the sensor and from the sensor back to the satellite experience this kind of disturbance. Their power spectrum densities are denoted by $S_{m,f}$ and $S_{m,b}$, respectively. The reason that the medium noise blocks are placed closer to the PLL

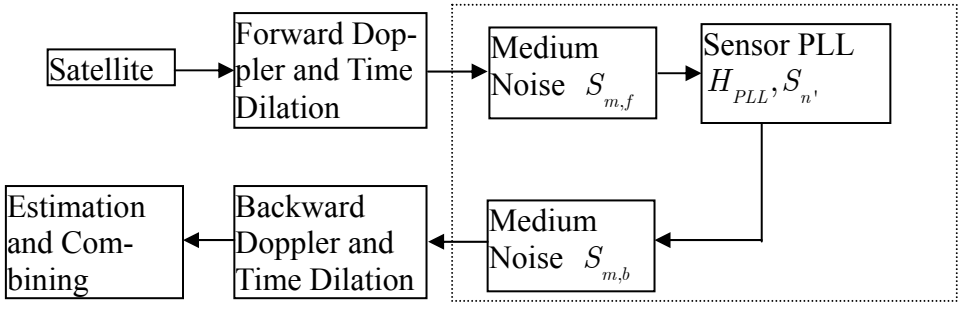

Figure 3.2: The block diagram for coherent combining analysis.

block than the Doppler and time dilation blocks is as follows. First, they come from the same medium. Thus, both noise blocks are in the same time reference and should be placed at the same side, either the right or the left side, of Doppler and time dilation blocks. Secondly, they are placed on the right side of the medium because they are relatively stationary with respect to the sensors, so it is more intuitive to place them close to the sensor PLL block.

The dash-lined box in Figure 3.2 can be further decomposed as in Figure 3.3. $n'(t)$ is the angular phase disturbance, defined in [13, (3.2-3)]. This random process is a function of the input amplitude and the power spectrum of white noise. $F(s)$ is the loop filter transfer function. K_D is the phase detector gain. L is the ratio of received carrier frequency to the transmitted carrier frequency. $m_f(t)$ is the forward medium noise and $m_b(t)$ is the backward medium noise. Given a fixed propagation delay disturbance, the effect of phase disturbance on the received signals is L times that on the transmitted signals because the received carrier frequency is L times the transmitted carrier frequency.

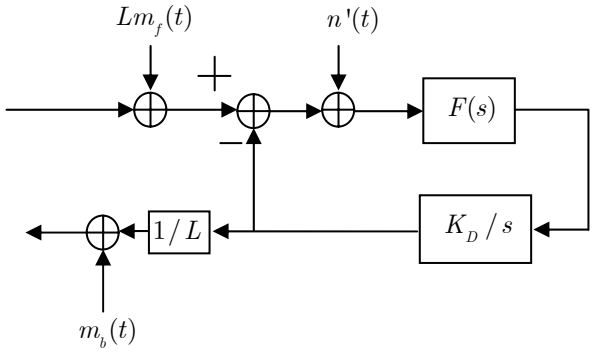

Figure 3.3: The model for the phase-locked loop in the slave clock.

In order to determine the statistics of pre-compensation estimates and the perfect pre-compensation values, we must investigate the effects of each block in Figure 3.2. The effect of Doppler and time dilation is frequency transformation. Assuming the carrier frequency of the master clock is f_0, the master clock is moving at speed V and the relative motion makes an angle $90+\varphi$ with the line connecting the source and observer, as depicted in Figure 3.4, then the observed frequency is

$$\frac{\sqrt{1-V^2/c^2}}{1+(V/c)\sin\varphi} f_0 . \tag{3.1}$$

Hence, the Doppler and time dilation block can be modeled by a power spectrum transformation, as illustrated in Figure 3.5. Notice the dilation in time converts to contraction in frequency and increase in amplitude.

The slave clocks track the observed frequency and transmit information and synchronization signals back to the receive antenna, i.e. the master clock. Therefore, after

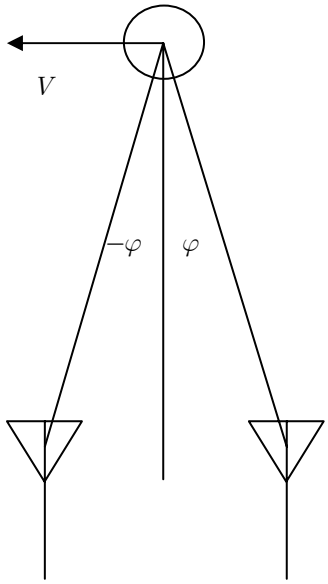

Figure 3.4: The setting of the master clock and the sensors.

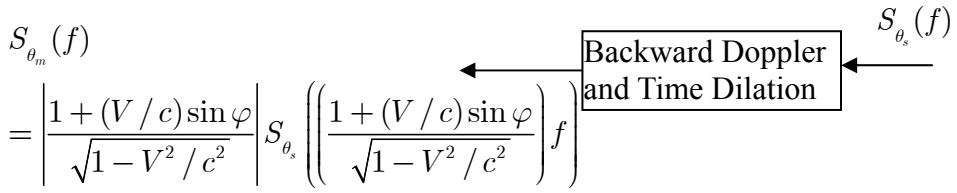

Figure 3.5: Power spectrum transformation due to Doppler ant time dilation.

forward and backward Doppler and time dilation, the frequency observed by the receive antenna is

$$f_m = \frac{1 - V^2/c^2}{\left(1 + (V/c)\sin\varphi\right)^2} f_0 . \tag{3.2}$$

There are three components associated with the pre-compensation estimate. The first one is the clean signal at frequency f_m computed using (3.2). This component is determined by the forward and backward Doppler and time dilation blocks. The second component is the phase noise process $\theta_m(t)$ at the output of backward Doppler time dilation block. The power spectrum of this process is represented by S_{θ_m}. This component is determined by the sensor PLL block and two medium noise blocks. The last noise component, which appears in the estimation and combining block, is the white Gaussian noise.

We determine the expression of pre-compensation estimates by approximation and assume the pulse shape is rectangular. It is also assumed that decision-directed loops[14] are employed so that we can neglect the phases associated with each bit and consider the synchronization signal as a pure sine wave without modulation. We first determine the phase pre-compensation estimate without considering the white Gaussian noise. The phase-offset estimate is

$$\theta_{appr} = \tan^{-1}\left(\frac{-\int_{\Delta t_i} \sin w_0 t[\cos(w_m t + \theta_m(t) + \theta_0)]dt}{\int_{\Delta t_i} \cos w_0 t[\cos(w_m t + \theta_m(t) + \theta_0)]dt}\right),$$

where Δt_i is the estimation duration, $\omega_0 = 2\pi f_0$, $\omega_m = 2\pi f_m$ and θ_0 is the initial phase offset. We make the following manipulations,

$$\frac{\sin\theta_{appr}}{\cos\theta_{appr}} = \frac{-\int_{\Delta t_i} \sin w_0 t[\cos(w_m t + \theta_m(t) + \theta_0)]dt}{\int_{\Delta t_i} \cos w_0 t[\cos(w_m t + \theta_m(t) + \theta_0)]dt},$$

$$-\int_{\Delta t_i} \sin w_0 t \cos\theta_{appr}[\cos(w_m t + \theta_m(t) + \theta_0)]dt$$

$$= \int_{\Delta t_i} \cos w_0 t \sin\theta_{appr}[\cos(w_m t + \theta_m(t) + \theta_0)]dt,$$

$$\int_{\Delta t_i} \sin(w_0 t + \theta_{appr})[\cos(w_m t + \theta_m(t) + \theta_0)]dt = 0, \tag{3.3}$$

$$\int_{\Delta t_i} \sin(\Delta w t - \theta_{appr} + \theta_m(t) + \theta_0)]dt = 0, \tag{3.4}$$

$$\int_{\Delta t_i} (\Delta w t - \theta_{appr} + \theta_m(t) + \theta_0)dt \approx 0, \tag{3.5}$$

where $\Delta w = w_m - w_0$. (3.4) is obtained from (3.3) because the $\sin((w_m + w_0)t + \theta_m(t) + \theta_0)$ term is neglected in the integration. The reason that (3.5) holds is as follows. The values of Δw and $\theta_m(t)$ are small and thus the value of $\Delta w t - \theta_{appr} + \theta_m(t) + \theta_0$ in the interval of integration does not vary significantly. In this case, the only way (3.4) can be satisfied is the value of $\Delta w t - \theta_{appr} + \theta_m(t) + \theta_0$ is around 0. Thus, (3.4) can be approximated by (3.5) and the phase pre-compensation estimate can be expressed as

$$\theta_{appr} \approx \frac{1}{\Delta t_i}\left(\frac{\Delta w \Delta t_i^2}{2} + \int_{\Delta t_i} \theta_m(t)dt\right) + \theta_0. \tag{3.6}$$

Then, we examine the effect of white Gaussian noise on this phase pre-compensation estimate. First, we have to compute the amplitude of the phasor without white Gaussian noise. The square of it is

$$\begin{aligned} A^2 &= \left[\int A_m \sin w_0 t \cos(w_m t + \theta_m(t))dt\right]^2 + \left[\int A_m \cos w_0 t \cos(w_m t + \theta_m(t))dt\right]^2 \\ &= \left[0.5\int A_m \sin((w_0 - w_m)t - \theta_m(t))dt\right]^2 \\ &\quad + \left[0.5\int A_m \cos((w_0 - w_m)t - \theta_m(t))dt\right]^2 \qquad (3.7) \\ &= \left[0.5A_m\int \sin\Delta wt\cos\theta_m(t) + \cos\Delta wt\sin\theta_m(t))dt\right]^2 \\ &\quad + \left[0.5A_m\int \cos\Delta wt\cos\theta_m(t) - \sin\Delta wt\sin\theta_m(t))dt\right]^2 \\ &\approx \left[0.5A_m\int \sin\Delta wt\cos\theta_m(t)\right]^2 + \left[0.5A_m\int \cos\Delta wt\cos\theta_m(t)dt\right]^2, \qquad (3.8) \end{aligned}$$

where A_m is the amplitude of the input signal. (3.7) holds because the high-frequency terms are ignored and (3.8) holds because $\sin\theta_m(t)$ is close to 0 regardless of the beginning of integration. In order to deal with the random process $\theta_m(t)$, we use the technique in [15, p. 52]. Then,

$$\begin{aligned} A^2 &\approx \left[0.5A_m E[\cos\theta_m(t)]\int_{t_2}^{t_1} \sin\Delta wtdt\right]^2 + \left[0.5A_m E[\cos\theta_m(t)]\int_{t_2}^{t_1} \cos\Delta wtdt\right]^2 \\ &= 0.25E[\cos\theta_m(t)]^2\left(\frac{A_m}{\Delta w}\right)^2\left[\left(-\cos\Delta wt_1 + \cos\Delta wt_2\right)^2 + \left(\sin\Delta wt_1 - \sin\Delta wt_2\right)^2\right] \\ &= 0.25\left(\frac{A_m E[\cos\theta_m(t)]}{\Delta w}\right)^2(2 - 2\cos\Delta w\Delta t_i) \\ &= 0.25\left(\frac{A_m E[\cos\theta_m(t)]}{\Delta w}\right)^2 4\sin^2\frac{\Delta w\Delta t_i}{2} \end{aligned},$$

where $t_1 - t_2 = \Delta t_i$. Thus,

$$A = \frac{A_m E[\cos\theta_m(t)]}{\Delta w} \sin\frac{\Delta w \Delta t_i}{2}. \tag{3.9}$$

The noise is decomposed into in-phase and quadrature components and these two components are integrated. The results are denoted by n_c and n_s. Then the phase offset with white Gaussian noise is

$$\theta_{noisy} = \tan^{-1}\left(\frac{\sin\theta_{appr} + n_s / A}{\cos\theta_{appr} + n_c / A}\right). \tag{3.10}$$

After the following manipulations,

$$\frac{\sin\theta_{noisy}}{\cos\theta_{noisy}} = \frac{\sin\theta_{appr} + n_s / A}{\cos\theta_{appr} + n_c / A}$$
$$(n_c \sin\theta_{noisy} - n_s \cos\theta_{noisy}) / A = \sin(\theta_{appr} - \theta_{noisy}) \approx \theta_{appr} - \theta_{noisy},$$

we obtain

$$\theta_{noisy} \approx \theta_{appr} + (n_c \sin\theta_{noisy} - n_s \cos\theta_{noisy}) / A.$$

The term $n_c \sin\theta_{noisy} - n_s \cos\theta_{noisy}$ is also Gaussian distributed, and has the same statistics as n_c and n_s. Its distribution is independent of θ_{noisy} and this term is denoted by n_{master}. Consequently, the expression of the pre-compensation estimate is

$$\theta_{noisy} \approx \frac{1}{\Delta t_i}\left(\frac{\Delta w \Delta t_i^2}{2} + \int_{\Delta t_i} \theta_m(t)dt\right) + \theta_0 + n_{master} / A. \tag{3.11}$$

In (3.11), the only random variable whose statistics are unknown is $\theta_m(t)$. In order to investigate the statistics of the integration of $\theta_m(t)$, we have to obtain the power spectrum, denoted by $S_{\theta_m}(f)$, which in turn can be derived from the power spectrum of $\theta_s(t)$, denoted by $S_{\theta_s}(f)$ through the frequency transformation in Figure 3.5. Conse-

quently, we have to determine the characteristics of $\theta_s(t)$. It includes the noise inside the phase-locked loop, the forward and backward medium phase noises. The effect of the former can be analyzed by the techniques in [13]. It is assumed that the medium phase noises are independent across transmit antennas, but forward and backward medium phase noises of each transmit antenna are correlated. Thus, we have to investigate the effect of their correlation on $\theta_s(t)$. To focus on this effect, we define

$$\tilde{\theta}_s(t) = m_b(t) + \int h_{PLL}(\tau) m_f(t-\tau) d\tau ,$$

where $h_{PLL}(\bullet)$ is the impulse response of the phase-locked loop. Since it is assumed that both $m_b(t)$ and $m_f(t)$ are Gaussian distributed, $\tilde{\theta}_s(t)$ is also Gaussian distributed. The autocorrelation is

$$\begin{aligned}\phi_{\tilde{\theta}_s}(\tau) &= E[\tilde{\theta}_s(\tau)\tilde{\theta}_s(0)] \\ &= E[m_b(\tau)m_b(0) + \iint h_{PLL}(\alpha)h_{PLL}(\beta)m_f(\tau-\alpha)m_f(0-\beta)d\alpha d\beta \\ &\quad + \int m_b(\tau)h_{PLL}(\beta)m_f(0-\beta)d\beta + \int m_b(0)h_{PLL}(\alpha)m_f(\tau-\alpha)d\alpha].\end{aligned}$$

Thus, the power spectrum of $\theta_s(t)$ is

$$\begin{aligned}S_{\tilde{\theta}_s}(f) &= S_{mb}(f) + \left|H_{PLL}(f)\right|^2 S_{mb}(f) + \Phi_{mb,mf}(f)H^*_{PLL}(f) \\ &+ \Phi^*_{mb,mf}(f)H_{PLL}(f)\end{aligned} . \qquad (3.12)$$

From (3.12), we can compute the power spectrum of the integration of $\theta_m(t)$ in (3.6) and the statistics of pre-compensation estimate θ_{noisy}.

This spectrum of $\theta_s(t)$ can be used to compute the correlation between the medium phase noise components of the pre-compensation estimate and of the perfect

pre-compensation value when signals are coherently combined. The time relationship between these two values is illustrated in Figure 3.6. The propagation delay increases with time because the satellite is assumed to move away from the surface. The correlation r is determined from the autocorrelation $R_{\theta_m}(t)$

$$r = \frac{E[\theta_1, \theta_2]}{\sigma_1 \sigma_2} \triangleq \frac{E[\theta_m(\tau + t_2), \frac{1}{\Delta t_i}\int_0^{\Delta t_i} \theta_m(\tau + \alpha) d\alpha]}{\sigma_1 \sigma_2}$$
$$= \frac{\frac{1}{\Delta t_i}\int_0^{\Delta t_i} E[\theta_m(\tau + t_2), \theta_m(\tau + \alpha)] d\alpha}{\sigma_1 \sigma_2} = \frac{\int_0^{\Delta t_i} R_{\theta_m}(t_2 - \alpha) d\alpha}{\Delta t_i \sigma_1 \sigma_2}, \tag{3.13}$$

where σ_1 is the standard deviation of θ_m and σ_2 is the standard deviation of $\frac{1}{\Delta t_i}\int_0^{\Delta t_i} \theta_m(\tau + \alpha) d\alpha$. The difference between the pre-compensation estimate and the perfect pre-compensation value is

$$\theta_2 - \theta_1 + \underbrace{(\frac{\Delta w \Delta t_i}{2} - \Delta w \times t_2)}_{\text{Doppler effect}} + \underbrace{n_{master} / A}_{\text{white Gaussian noise in estimation}}. \tag{3.14}$$

In (3.14), $\theta_2 - \theta_1$ is independent of the Doppler and the white Gaussian noise in estima-

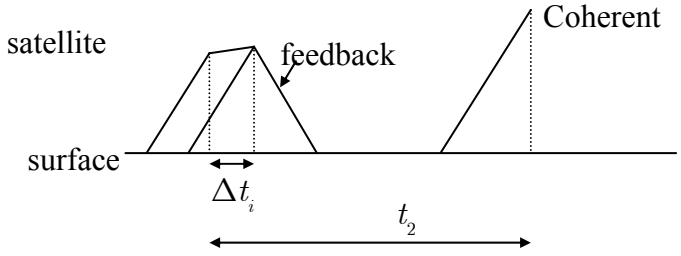

Figure 3.6: Time relationship between pre-compensation estimates and perfect values.

tion. Given the correlation r, the joint pdf of θ_1 and θ_2 is

$$f(\theta_1,\theta_2)=\frac{1}{2\pi\sigma_1\sigma_2\sqrt{1-r^2}}\exp\left(-\frac{1}{2(1-r^2)}\left(\frac{\theta_1^2}{\sigma_1^2}-\frac{2r\theta_1\theta_2}{\sigma_1\sigma_2}+\frac{\theta_2^2}{\sigma_2^2}\right)\right).$$

Thus, the pdf of $\theta_2-\theta_1$ is

$$\begin{aligned}
&f(\Delta\theta)=\int f(\Delta\theta=\theta_2-\theta_1,\theta_2)d\theta_2\\
&=\frac{1}{2\pi\sigma_1\sigma_2\sqrt{1-r^2}}\int\exp\left(-\frac{1}{2(1-r^2)}\left(\frac{(\theta_2+\Delta\theta)^2}{\sigma_1^2}-\frac{2r(\theta_2+\Delta\theta)\theta_2}{\sigma_1\sigma_2}+\frac{\theta_2^2}{\sigma_2^2}\right)\right)d\theta_2\\
&=\frac{1}{\sqrt{2\pi}\sqrt{\sigma_1^2+\sigma_2^2-2r\sigma_1\sigma_2}}\exp(-\frac{\Delta\theta^2}{2(\sigma_1^2+\sigma_2^2-2r\sigma_1\sigma_2)}).
\end{aligned}$$

3.4 Numerical Results

Given the framework of analysis in the last section, we will demonstrate the performance of coherent transmission when the receive antenna is moving, with models of the medium noise and the phase-lock loop, in this section.

The power spectrum densities of forward and backward medium noise are modeled as in [22]

$$S_{mf}(f)=S_{mb}(f)=\left|\frac{\omega_s b}{j2\pi f+\omega_s}\right|^2, \tag{3.15}$$

where ω_s and b are coefficients. The variance of noise is $\sigma_s^2=\omega_s b^2/2$. Furthermore, the relationship between $m_f(t)$ and $m_b(t)$ is modeled by a time lag. Specifically, $m_b(t)$ is assumed to be the advanced version of $m_f(t)$ with time lag τ_0. The reason is as follows. For the signal received by the receive antenna, the effect of the forward medium phase noise takes place when the clock from the satellite is received by the sensor.

This occurs before the signal which contains this effect arrives at the receive antenna from the transmit antenna. The time lag τ_0 is equal to the propagation delay from the transmit antenna to the receive antenna. This relationship is characterized by

$$m_f(t) = m_b(t - \tau_0). \tag{3.16}$$

Thus, the power spectrum density of correlation between $m_b(t)$ and $m_f(t)$ is

$$\Phi_{mb,mf}(f) = e^{j2\pi f\tau_0}\Phi_{mb,mb}(f).$$

Regarding the phase-lock loop, we employ a second-order loop with transfer function[13]

$$H(s) = \frac{2\zeta\omega_n s + \omega_n^2}{s^2 + 2\zeta\omega_n s + \omega_n^2}, \tag{3.17}$$

where ω_n is the natural frequency and ζ is the loop damping ratio. The single-sided loop noise bandwidth[13] of (3.14) is

$$B_L = \frac{\zeta\omega_n}{2}\left(1 + \frac{1}{4\zeta^2}\right).$$

The signal-to-noise ration in the loop and given the symbol ρ

$$\rho = \frac{A_s^2}{N_0 B_L},$$

where A_s is the amplitude of received signals from the satellite, divided by $\sqrt{2}$,.The power spectrum of θ_m is

$$S_{\theta_m}(\omega) = d_0\left(\frac{(\omega_s b)^2}{(d_0\omega)^2+\omega_s^2}+\frac{N_0/2}{A_s^2}\right)\frac{1+4\zeta^2(d_0\omega)^2/\omega_n^2}{(1-(d_0\omega)^2/\omega_n^2)^2+4(d_0\omega)^2\zeta^2/\omega_n^2}$$
$$+\frac{(\omega_s b)^2}{(d_0\omega)^2+\omega_s^2}\left[\begin{matrix}1+e^{-jd_0\omega\tau_0}\dfrac{(\omega_n^2+2\zeta j(d_0\omega)\omega_n)}{-(d_0\omega)^2+2\zeta\omega_n j(d_0\omega)+\omega_n^2}\\ +e^{jd_0\omega\tau_0}\dfrac{(\omega_n^2-2\zeta j(d_0\omega)\omega_n)}{-(d_0\omega)^2-2\zeta\omega_n j(d_0\omega)+\omega_n^2}\end{matrix}\right], \tag{3.18}$$

where d_0 represents the frequency translation due to Doppler and time dilation. The value of d_0 is

$$d_0 = \frac{1+(V/c)\sin\varphi}{\sqrt{1-V^2/c^2}}.$$

As we pointed out, (3.18) includes the effects of white Gaussian noise and the medium disturbance. (3.18) is multiplied by $\Delta t_i \cdot \left[\sin c(\omega\Delta t_i/(2\pi))\right]^2$ to obtain the power spectrum of the pre-compensation estimate. Then, σ_2 in (3.13) can be calculated numerically. Besides, the autocorrelation function $R_{\theta_m}(t)$ in (3.13) is equal to $R_{\theta_s}(t/d_0)$ and $R_{\theta_s}(t)$ can be decomposed into R_{noise}, R_{mf}, R_{mb}, and $Cov_{mf,mb}$, corresponding to the inverse Laplace transforms of $H(s)H(-s)N_0/(2A_s^2)$, $H(s)H(-s)S_{mf}(s)$, $S_{mb}(s)$, and $\Phi_{mb,mf}(s)H_{PLL}(-s)+\Phi_{mb,mf}(-s)H_{PLL}(s)$, respectively. Notice our $Cov_{mf,mb}$ is not the conventional definition of cross-correlation between $m_f(t)$ and $m_b(t)$. Actually, it captures the relationship between $m_b(t)$ and the influence of $m_f(t)$ on the output of the phase-locked loop. $R_{mb}(t)$ is

$$R_{mb}(t) = \frac{\omega_s b^2}{2}e^{-\omega_s|t|}.$$

After making the following definitions,

$$b_0 \triangleq \frac{-4\zeta^2 - 1}{4\zeta\omega_n}$$

$$a_1 \triangleq \frac{-b_0 - 0.5/\omega_s}{\omega_s - 2\zeta\omega_n + \omega_n^2/\omega_s}$$

$$a_2 \triangleq \frac{0.5 + a_1\omega_n^2}{\omega_s}$$

$$b_1 \triangleq \frac{-b_0 + 0.5/\omega_s}{\omega_s + 2\zeta\omega_n + \omega_n^2/\omega_s}$$

$$b_2 \triangleq \frac{0.5 - b_1\omega_n^2}{\omega_s}$$

$$a_{11} \triangleq \frac{2\zeta/\omega_n - 1/\omega_s}{\omega_s - 2\zeta\omega_n + \omega_n^2/\omega_s}$$

$$a_{21} \triangleq \frac{1 + a_{11}\omega_n^2}{\omega_s}$$

$$b_{11} \triangleq \frac{2\zeta/\omega_n + 1/\omega_s}{\omega_s + 2\zeta\omega_n + \omega_n^2/\omega_s}$$

$$b_{21} \triangleq \frac{1 - b_{11}\omega_n^2}{\omega_s},$$

we can express R_{noise}, R_{mf}, and $Cov_{mf,mb}$ as

$$R_{noise}(t) = \frac{1}{L^2}\frac{N_0}{2A_s^2}\Big(0.5\omega_n^2 \mid t \mid e^{-\omega_n|t|} - b_0\omega_n^2(e^{-\omega_n|t|} + \mid t \mid (-\omega_n)e^{-\omega_n|t|})\Big),$$

$$R_{mf}(t) = \frac{\omega_n^2\omega_s^2b^2}{2\omega_s}\Big((a_2 - a_1\zeta\omega_n + b_2 - b_1\zeta\omega_n)e^{-\zeta\omega_n|t|} \mid t \mid + (a_1 + b_1)e^{-\zeta\omega_n|t|} - (a_1 - b_1)e^{-\omega_s|t|}\Big),$$

$$Cov_{mf,mb}(t) = \frac{\omega_n^2 \omega_s^2 b^2}{2\omega_s} \begin{bmatrix} \begin{pmatrix} (a_{21} - a_{11}\zeta\omega_n + b_{21} - b_{11}\zeta\omega_n)e^{-\zeta\omega_n(t-\tau_0)}(t-\tau_0) \\ +(a_{11}+b_{11})e^{-\zeta\omega_n(t-\tau_0)} \end{pmatrix} u(t-\tau_0) \\ + \begin{pmatrix} (a_{21} - a_{11}\zeta\omega_n + b_{21} - b_{11}\zeta\omega_n)e^{-\zeta\omega_n(-t-\tau_0)}(-t-\tau_0) \\ +(a_{11}+b_{11})e^{-\zeta\omega_n(-t-\tau_0)} \end{pmatrix} u(-t-\tau_0) \\ -a_{11}e^{-\omega_s(t-\tau_0)}u(t-\tau_0) \\ -a_{11}e^{-\omega_s(-t-\tau_0)}u(-t-\tau_0) \\ +b_{11}e^{-\omega_s(t+\tau_0)}u(t+\tau_0) \\ +b_{11}e^{-\omega_s(-t+\tau_0)}u(-(t-\tau_0)) \end{bmatrix},$$

when $\zeta = 1$. Otherwise, when $\zeta < 1$,

$$R_{noise}(t) = \frac{N_0\omega_n^2}{2A_s^2L^2}\left(\frac{0.5 + b_0\zeta\omega_n}{\sqrt{1-\zeta^2}\omega_n}e^{-\zeta\omega_n|t|}\sin(\sqrt{1-\zeta^2}\omega_n \mid t \mid) - b_0 e^{-\zeta\omega_n|t|}\cos(\sqrt{1-\zeta^2}\omega_n \mid t \mid)\right)$$

$$R_{mf}(t) = \frac{\omega_n^2\omega_s^2 b^2}{2\omega_s}\begin{pmatrix} \frac{a_2 - a_1\zeta\omega_n + b_2 - b_1\zeta\omega_n}{\sqrt{1-\zeta^2}\omega_n}e^{-\zeta\omega_n|t|}\sin(\sqrt{1-\zeta^2}\omega_n \mid t \mid) \\ +(a_1+b_1)e^{-\zeta\omega_n|t|}\cos(\sqrt{1-\zeta^2}\omega_n \mid t \mid) - (a_1-b_1)e^{-\omega_s|t|} \end{pmatrix},$$

$$Cov_{mf,mb}(t)=\frac{\omega_n^2\omega_s^2b^2}{2\omega_s}\left[\begin{array}{l}\left(\begin{array}{l}\frac{a_{21}-a_{11}\zeta\omega_n+b_{21}-b_{11}\zeta\omega_n}{\sqrt{1-\zeta^2}\omega_n}e^{-\zeta\omega_n(t-\tau_0)}\\ \sin(\sqrt{1-\zeta^2}\omega_n(t-\tau_0))\\ +(a_{11}+b_{11})e^{-\zeta\omega_n(t-\tau_0)}\cos(\sqrt{1-\zeta^2}\omega_n(t-\tau_0)\end{array}\right)u(t-\tau_0)\\ +\left(\begin{array}{l}\frac{a_{21}-a_{11}\zeta\omega_n+b_{21}-b_{11}\zeta\omega_n}{\sqrt{1-\zeta^2}\omega_n}e^{-\zeta\omega_n(-t-\tau_0)}\\ \sin(\sqrt{1-\zeta^2}\omega_n(-t-\tau_0))\\ +(a_{11}+b_{11})e^{-\zeta\omega_n(-t-\tau_0)}\cos(\sqrt{1-\zeta^2}\omega_n(-t-\tau_0)\end{array}\right)u(-t-\tau_0)\\ -a_{11}e^{-\omega_s(t-\tau_0)u(t-\tau_0)}u(t-\tau_0)\\ -a_{11}e^{-\omega_s(t-\tau_0)u(-t-\tau_0)}u(-t-\tau_0)\\ +b_{11}e^{-\omega_s(t+\tau_0)}u(t+\tau_0)\\ +b_{11}e^{-\omega_s(-t+\tau_0)}u(-(t-\tau_0))\end{array}\right].$$

Then σ_1 and the integration of $R_{\theta_m}(t)$ in (3.13) can be evaluated through

$$R_{\theta_m}(t)=R_{noise}(t/d_0)+R_{mf}(t/d_0)+R_{mb}(t/d_0)+Cov_{mf,mb}(t/d_0).$$

We now consider the scenario of low-Mars orbit. We will examine the influences of changing parameters around their nominal values. The satellite, i.e. the receive antenna, is moving at the speed of $3361m/s$, and at the height of $400km$. Correspondingly, the one-way propagation delay is $1.33ms$. The carrier frequency is $400MHz$. The received signal to noise ratio is $E_b/N_0=0dB$ per transmitter. L is set to 2. ω_n is $2\pi*50$ rad/s, ζ is 0.7, ρ is 10dB, and the fading bandwidth $Ws=\omega_s/2$ [22] is twice B_L. b is chosen so that σ_s^2 is 0.1. When one sensor is considered, ϕ is 0°. In the simulation results, the parameters are at their nominal values if not specified. The auto-

correlation function $R_{noise}(t/d_0)$ is plotted in Figure 3.7 for various natural frequencies. With lower natural frequencies, the autocorrelation function changes more slowly. Notice A_s is also scaled down as the natural frequency increases so that ρ keeps constant, and the variance $R_{noise}(0)$ is identical across natural frequencies. Otherwise, with higher natural frequencies, the autocorrelation would scale up accordingly. In Figure 3.8, the autocorrelation function is plotted for various damping factors. These curves conform to the general concept about the damping factor.

The autocorrelation $R_{mf}(t/d_0)$ is illustrated in Figure 3.9, where ω_s also changes

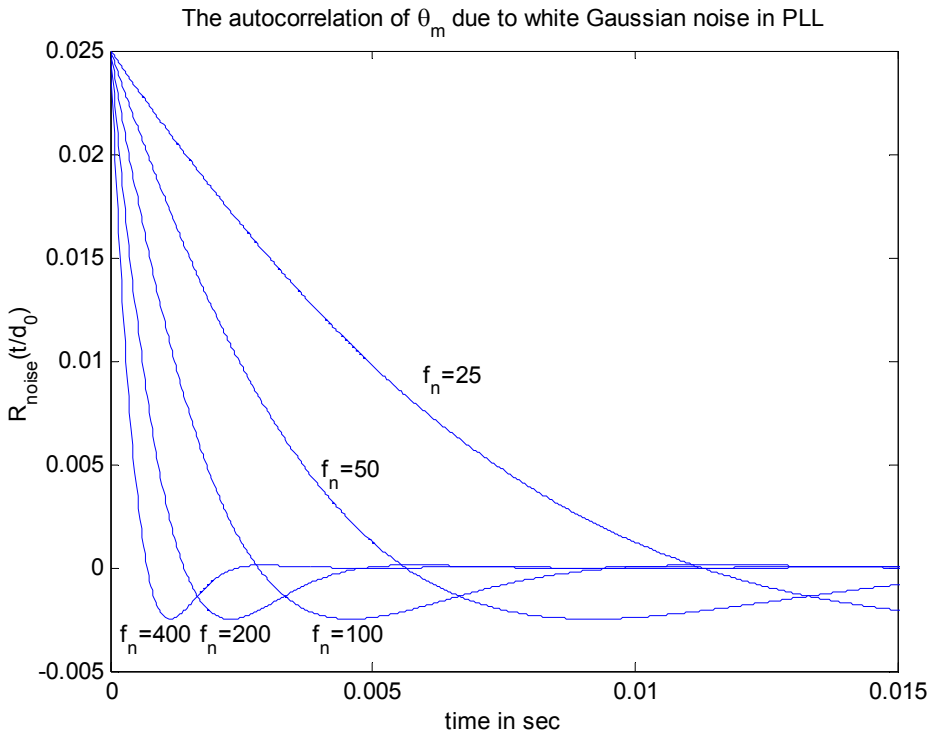

Figure 3.7: $R_{noise}(t/d_0)$, the autocorrelation of theta due to the white Gaussian noise in PLL, with $\rho = 10dB$, $\phi = 0^\circ$.

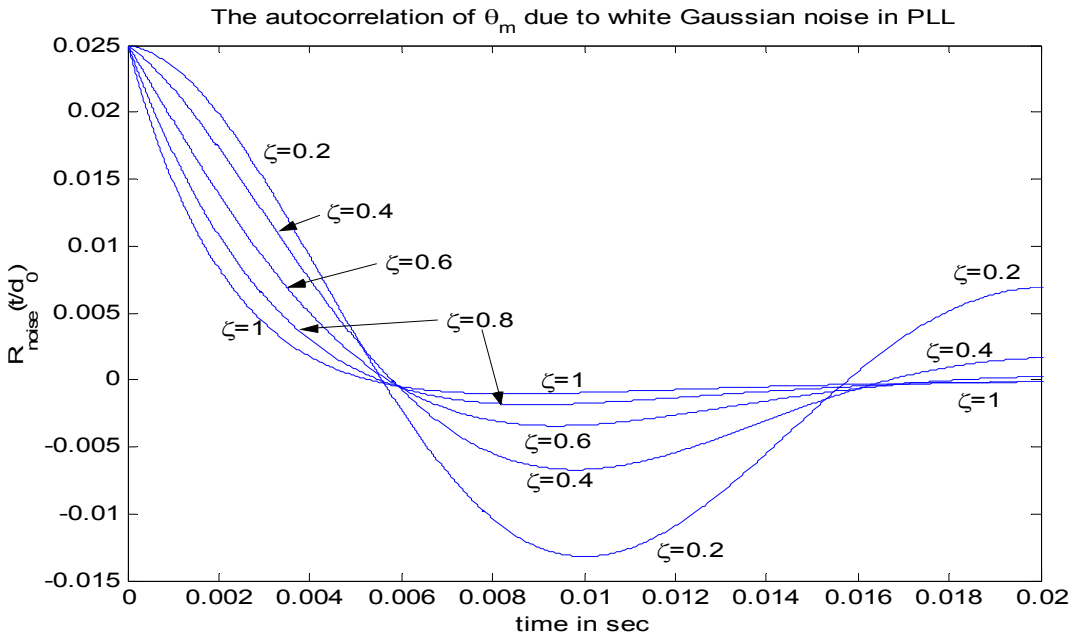

Figure 3.8: $R_{noise}(t/d_0)$, the autocorrelation of theta due to the white Gaussian noise in PLL with several ζ, $\rho = 10dB$, and $\phi = 0^\circ$.

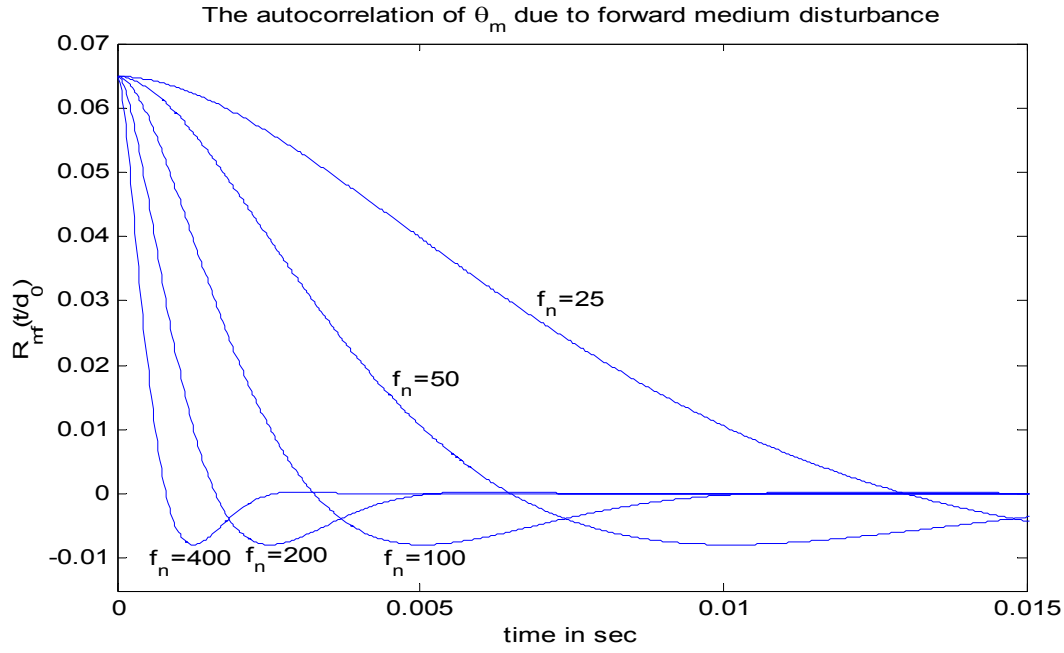

Figure 3.9: $R_{mf}(t/d_0)$, the autocorrelation of theta due to the forward medium disturbance with $\omega_s = 4B_L$, $\phi = 0^\circ$.

with the natural frequency so that the value is equal to $4B_L$, and thus the variance $R_{mf}(0)$ is fixed. Again, the lower natural frequencies result in slower autocorrelation decay. Figure 3.10 demonstrates the autocorrelation $R_{mf}(t/d_0)$ for various ω_s. Since we keep σ_s^2 constant, with higher ω_s, the noise power is spread over a wider bandwidth, and the noise power at each frequency is lower. Because f_n is fixed at 50Hz, lower ω_s leads to lower noise power due to forward medium disturbance at the output of the phase-locked loop.

$Cov_{mf,mb}(t/d_0)$ is shown in Figure 3.11 while ρ is fixed. Because of (3.16), the

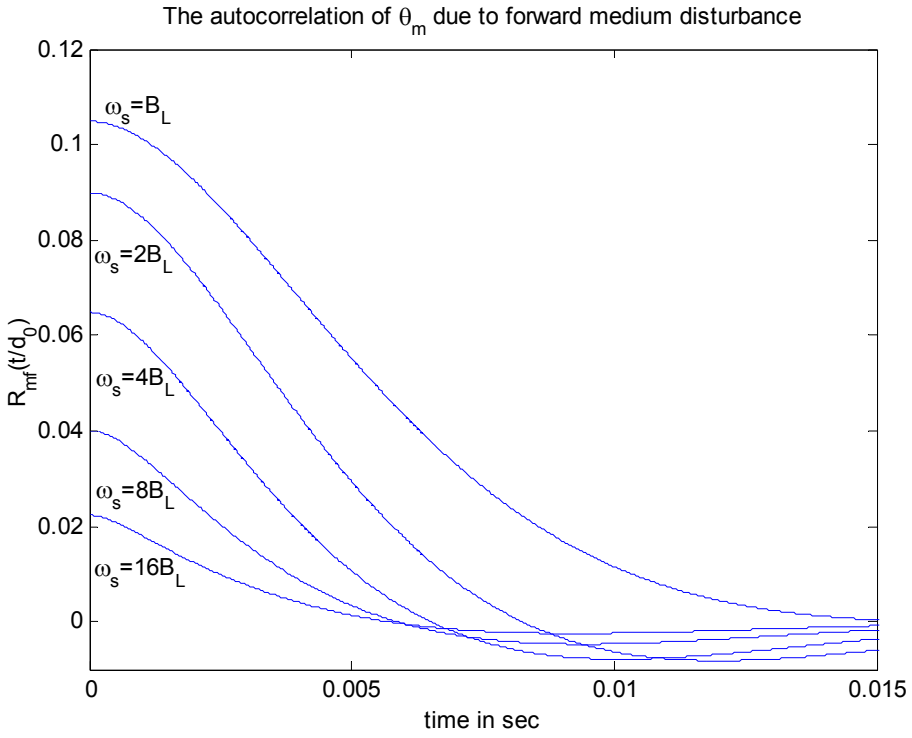

Figure 3.10: $R_{mf}(t/d_0)$, the autocorrelation of theta due to the forward medium disturbance with $f_n = 50Hz$, $\phi = 0^\circ$.

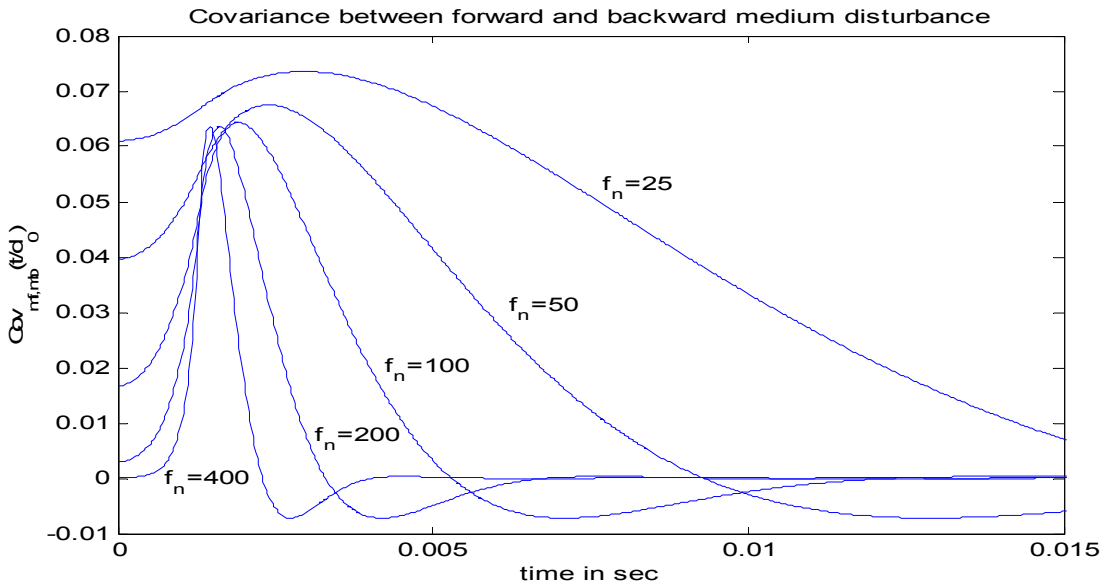

Figure 3.11: $Cov_{mf,mb}(t/d_0)$, the covariance between forward and backward medium disturbance with $\phi = 0^\circ$.

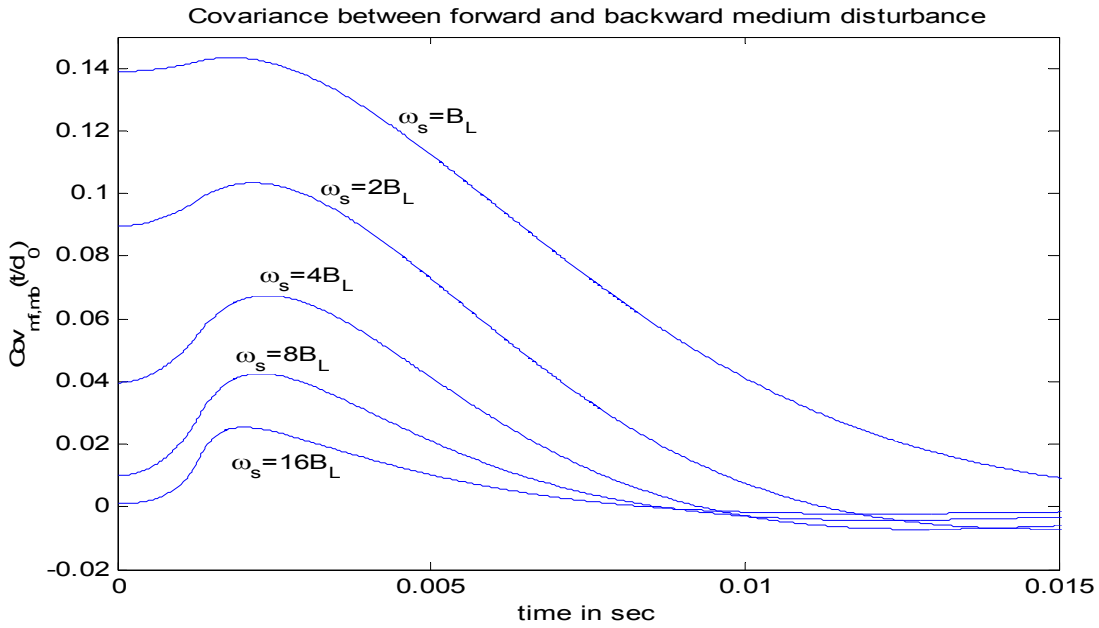

Figure 3.12: $Cov_{mf,mb}(t/d_0)$, the covariance between forward and backward medium disturbance with various ω_s and $\phi = 0^\circ$.

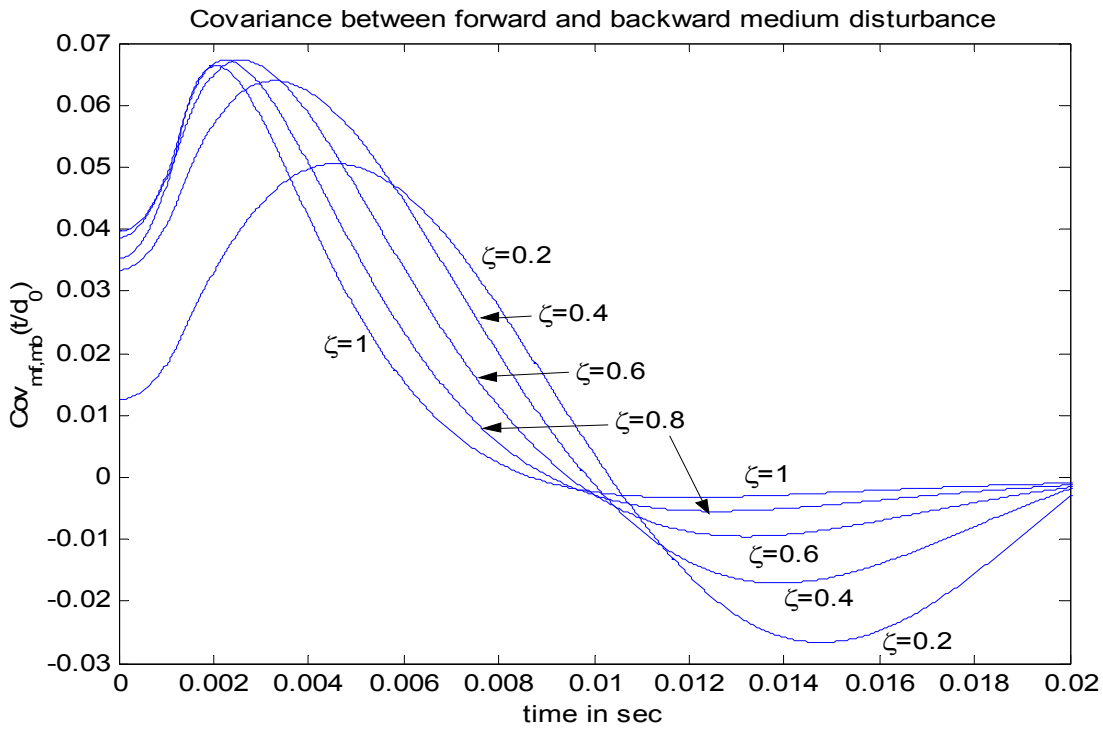

Figure 3.13: $Cov_{mf,mb}(t/d_0)$, the covariance between forward and backward medium disturbance with various ζ and $\phi = 0^\circ$.

peak occurs slightly after τ_0. As the natural frequency decreases, the response of the phase-locked loop is slower and the peak is further delayed. Figure 2.12 shows the effect of ω_s on $Cov_{mf,mb}(t/d_0)$. As in Figure 3.10, the wider ω_s of medium disturbance, the less noise power at the output of phase-locked loop. The impact of the damping factor ζ is depicted in Figure 3.13

For coherent combining, the locations of sensors and the satellite play an important role in the analysis. This influence is captured in terms of the angle spread in Figure 3.4. When the angle spread is wide, the Doppler effects for sensors expressed in (3.1) vary across a wide range, and the coherent combining cannot be achieved for a long period of

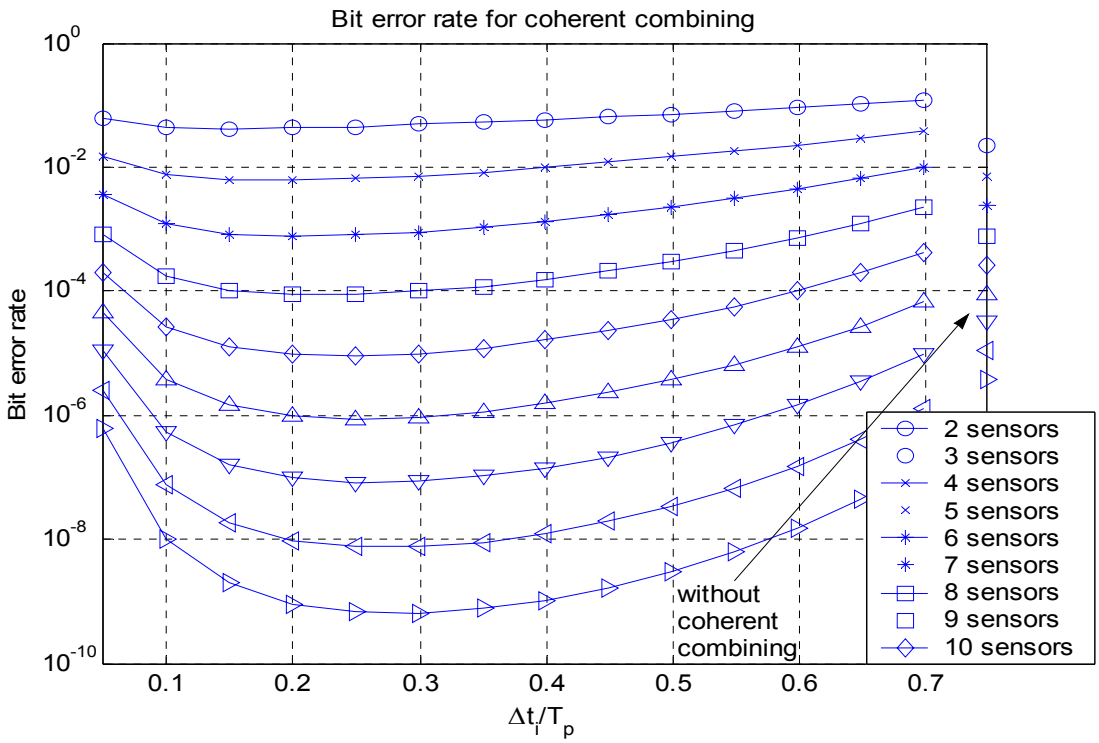

Figure 3.14: Simulation results of coherent transmission with a non-stationary receive antenna.

time. Given the locations of sensors, the worst coherent combining performance occurs when the satellite is on top of them, as shown in Figure 3.4. For one sensor, the perfect pre-compensation value decreases, and for the other, it increases. Thus, they cannot combine well. If they are at the same side of the satellite, although the perfect pre-compensation values change more rapidly, the difference of these values between two sensors is less. In this situation, to demodulate the coherently combined signal, a training sequence must be inserted, or a phase-locked loop in the satellite, as illustrated in, is required so that the satellite can determine the phase of the combined signal. To precede our analysis, we project the phasors of constituent signals onto the phasor with angle equal to the average of all constituent phasors without the consideration of phase distur-

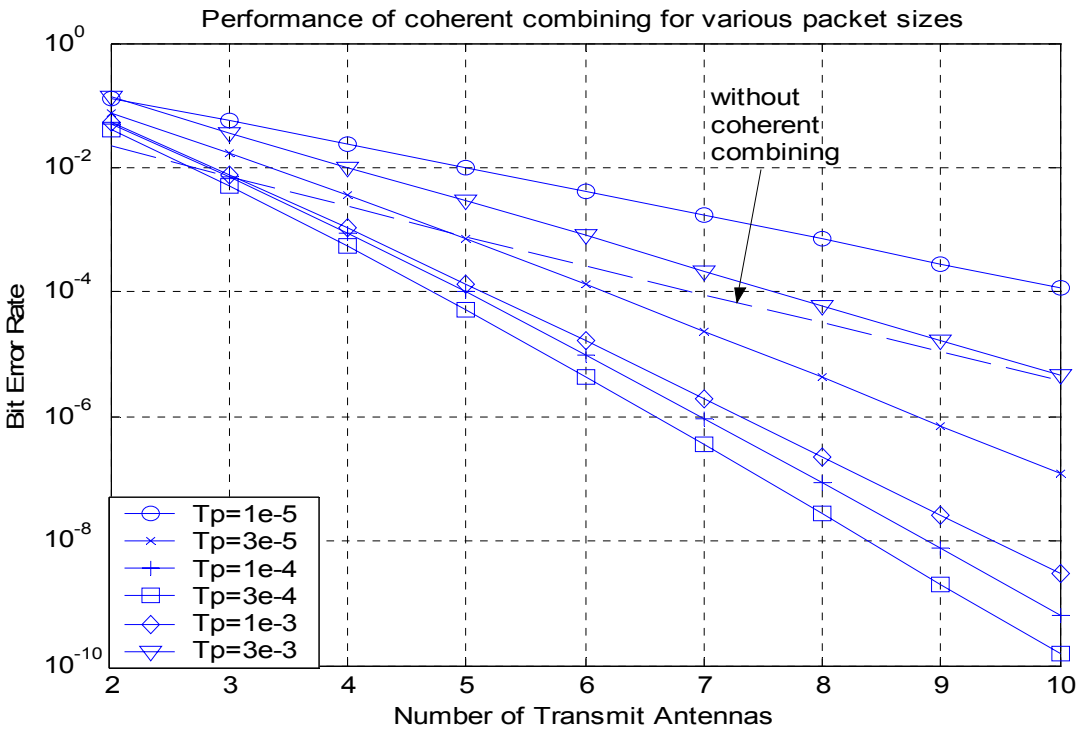

Figure 3.15: Performance of coherent combining for various packet sizes at their optimal power allocation between the header and the information segments

bance due to noise. In the real situation the performance is better because the phase-locked loop is able to track the phase dynamics. In our simulation, we nominally assume the angle spread of 0.15° no matter how many sensors are employed.

As in the last chapter, we divide information data into packets. Each packet is $0.1ms$ long, and contains 100 symbols used either by the information segment or by the header. The number of symbols in the header multiplied by the symbol duration is equal to Δt_i. BPSK modulation is also employed.

The simulation results are shown in Figure 3.14. It is the performance of coherent transmission at the moment immediately before a new pre-compensation estimate is employed. In this respect, this is the worst-case performance. Like the result for the station-

ary receive antenna, it is observed coherent transmission can achieve lower bit error rates than the transmission with all power in one transmit antenna. Furthermore, the optimal power distributions between synchronization and information signals are observed. In Figure 3.15, we investigate the effect of various header sizes T_p on the bit error rates. The optimal power allocation between the header and information segments are numerically obtained for each packet size and employed. It is obvious that the packet size can not be either too large or too small. If it is too small, the power available for pre-compensation estimation is not enough to make an accurate estimation. Thus, the performance is poor. As the packet size grows, the available power increases. Consequently, the optimal $\Delta t_i / T_p$ required to make a moderate estimation is decreased. Meanwhile, more power remains for information transmission. The performance should improve. However, as the packet size increases, the pre-compensation estimate becomes more obsolete and more distinct from the ideal value at the end of packet. Therefore, the bit error rates deteriorate. The performance without coherent combining is also plotted to reveal that coherent combining is beneficial only for a specific range of packet sizes. Also, as in the last chapter, if the number of transmit antennas is less than three, it is not helpful to employ coherent combining because the overhead to conduct synchronization cannot be paid off by coherent combining.

3.5 Conclusion

Based on the framework of coherent transmission for the stationary receive antenna, we devised a scheme for the situation where the receive antenna is moving. These modifica-

tions result from the concept to estimate the pre-compensation upon the un-pre-compensated signal so as to reduce the estimation and pre-compensation cycle to less than one round-trip propagation delay. We also examined this system linearly. In our analysis, we considered several disturbances, including the white Gaussian noise at both the transmit and the receive antennas, the medium propagation delay disturbance, and the Doppler effect. In the last section, using the proposed analysis approach, we derived the statistics of all random variables related to the coherent combining. Based on these statistics, the performance in terms of bit error rates was obtained. In addition to the dominance of coherent combining, we also observed the optimal power distributions between the synchronization and information segments. Finally, we examined the influence of the packet size on the performance and obtained the optimal range of the packet size.

Chapter 4

Stationary MIMO Coherent Cooperative Communications

4.1 Introduction

The channel capacity of some multiple input multiple output (MIMO) channels has been investigated by Foschini[4] and Telatar[18]. In particular, when the channel is stationary and the noise is white and Gaussian, the channel capacity is determined. Assume there are n_t transmit antennas and n_r receive antennas, and denote the transmitted signal vector as s, the white Gaussian noise as n, the channel matrix as H with dimension $n_r \times n_t$, then the received signal vector is $r = Hs + n$. The mutual information is

$$\begin{aligned} I(r;s) &= \log_2 \det(I_{n_r} + HQH^\dagger) \\ &= \log_2 \det(I_{n_t} + QH^\dagger H), \end{aligned} \tag{4.1}$$

where Q is the covariance matrix of the transmitted signal s. The channel capacity C_s is the maximum mutual information over Q, subject to the power constraint.

In order to achieve the channel capacity, it is suggested to decompose the MIMO channel into several independent single input single output (SISO) channel by linear transformation at both the transmit and the receive antenna array. First, H is expressed

into its singular value decomposition as $H = UDV^{\dagger}$. Thus, $r = UDV^{\dagger}s + n$. Let $\tilde{r} = U^{\dagger}r$, $\tilde{s} = V^{\dagger}s$, then the original channel is equivalent to the channel

$$\tilde{r} = D\tilde{s} + \tilde{n}. \tag{4.2}$$

This means the transmitted signal vector s is V times the signal vector $\tilde{s}$, where each element is independent and parallel. At the receiver side, the received signal vector is left multiplied by $U^{\dagger}$ to obtain the signal vector $\tilde{r}$, where each element is independent.

In the process of derivation, it is assumed implicitly that all the antennas, including transmit and receive antennas, are synchronized in all respects, such as phases and frequencies. In this chapter, we will investigate the effect of phase offset on the channel capacity and the suggested linear transformation. Throughout this chapter, it is still assumed that frequencies are synchronized.

4.2 Phase offset at the receive antennas

Denote H as the channel matrix measured when all antennas are synchronized to a common time scale. Now, assume the transmit antennas are not synchronized. The clock in the first antenna lags the common time scale by θ_1, and so on. The new channel matrix perceived by the receive antenna array can be expressed as

$$H_r = \begin{bmatrix} e^{j\theta_{r,1}} & 0 & \cdots & 0 \\ 0 & e^{j\theta_{r,2}} & \ddots & \vdots \\ \vdots & \ddots & \ddots & 0 \\ 0 & \cdots & 0 & e^{j\theta_{r,n_r}} \end{bmatrix} H \triangleq D_r H .$$

Then the channel capacity C_r is

$$
\begin{aligned}
C_r &= \max_{Q} \log_2 \det(I_{n_r} + H_r Q H_r^{\dagger}) \\
&= \max_{Q} \log_2 \det(I_{n_t} + Q H_r^{\dagger} H_r) \\
&= \max_{Q} \log_2 \det(I_{n_t} + Q H^{\dagger} D_r^{\dagger} D_r H) \,. \\
&= \max_{Q} \log_2 \det(I_{n_t} + Q H^{\dagger} H) \\
&= C_s
\end{aligned}
$$

Thus, the channel capacity is identical to the channel capacity when all antennas are synchronized.

We then derive the channel transformation in the form of (4.2). We write the received signal as

$$
\begin{aligned}
r &= H_r s + n \\
&= D_r U D V^{\dagger} s + n
\end{aligned}
\,.
$$

Denote $U_r \triangleq D_r U$, $\widehat{r} \triangleq U_r^{\dagger} r = U^{\dagger} D_r^{\dagger} r$, and $\widehat{n} = U_r^{\dagger} n = U^{\dagger} D_r^{\dagger} n$ then

$$
\widehat{r} = D\tilde{s} + \widehat{n} \,. \tag{4.3}
$$

Because $U_r^{\dagger}$ is a unitary matrix, $\widehat{n}$ has the same distribution as n and $\tilde{n}$. Since D is unchanged, the power distribution determined by the water filling approach[18] is the same as the distribution when antennas are synchronized. The difference is the received signal r must be multiplied by $D_r^{\dagger}$ additionally before being multiplied by $U^{\dagger}$. Thus, the role of U is replaced by $U_r = D_r U$. Notice $D_r^{\dagger}$ is nothing more than phase advances on individual received signals by the amount of phase lags with respect to the common scale. In other words, before the received signals are processed assuming the receive antennas were synchronized, each received signal is rotated in reverse by the amount of phase offset so that the synchronization status is transparent to the channel

transformation (4.2).

As a result, the requirement that all receive antennas are synchronized in phase is converted to the requirement that phase offsets are known. Generally speaking, the latter is less stringent than the former because phase synchronization contains many procedures, one of which is the acquisition of phase offset information.

4.3 Phase offset at the transmit antennas

In this section, we consider the situation where transmit antennas are not synchronized with respect to the common time scale. First, we will derive the channel capacity C_t. The new channel matrix perceived by the receive antenna array is

$$H_t = H \begin{bmatrix} e^{j\theta_{t,1}} & 0 & \cdots & 0 \\ 0 & e^{j\theta_{t,2}} & \ddots & \vdots \\ \vdots & \ddots & \ddots & 0 \\ 0 & \cdots & 0 & e^{j\theta_{t,n_t}} \end{bmatrix} \triangleq HD_t .$$

The positive phase means the clock advances the common time scale so that the receive antennas consider the signal goes through extra phase rotation. In [18], $H^\dagger H$ is decomposed as $U^\dagger \Lambda U$, then we obtain

$$\det(I_r + HQH^\dagger) = \det(I_r + \Lambda^{1/2} U Q U^\dagger \Lambda^{1/2}) .$$

Using the same approach, we write $H_t^\dagger H_t = D_t^\dagger H^\dagger H D_t$, then with the new power allocation $\breve{Q}$,

$$\det(I_r + H_t \breve{Q} H_t^\dagger) = \det(I_r + \Lambda^{1/2} U D_t \breve{Q} D_t^\dagger U^\dagger \Lambda^{1/2}) .$$

It is obvious any mutual information achieved for a specific Q when antennas are synchronized can be realized when receive antennas are not synchronized by choosing $\breve{Q} = D_t^{\dagger} Q D_t$. Conversely, by $Q = D_t \breve{Q} D_t^{\dagger}$, any mutual information achieved in the unsynchronized situation can be obtained in the synchronized situation. Therefore, the channel capacity C_t is equal to C_s.

As in the last section, we will derive the method to realize the equivalence to the synchronous channel. In the unsynchronized situation, the received signal is

$$r = H_t s + n = UDV^{\dagger} D_t s + n . \tag{4.4}$$

Multiplying (4.4) by $U^{\dagger}$, we get

$$U^{\dagger} r = DV^{\dagger} D_t s + U^{\dagger} n . \tag{4.5}$$

Denote $D_t s$ as $\breve{s}$, then (4.5) is in the same form as (4.2) with the replacement of s by $\breve{s}$, and the MIMO channel can be decomposed into several parallel and independent SISO channels. The value of $\tilde{s} = V^{\dagger} D_t s$ is again determined by the water-filling algorithm. If transmit antennas are synchronized, the transmitted signal is $V\tilde{s}$ as mentioned in the first section. In the unsynchronized situation, the transmitted signal is further multiplied by $D_t^{\dagger}$, which is exactly the phase delay on individual transmitted signals. Because the water-filling algorithm considers the channel matrix under synchronization, signals must undergo this further step to counteract the effect of advanced clocks before being transmitted. The signal which is finally transmitted is $s = D_t^{\dagger} V \tilde{s}$. By the definition $V_t \triangleq D_t^{\dagger} V$, the role of V is replaced by V_t. Consequently, from the point of view

of the water-filling algorithm, all antennas appear to be synchronized in phase.

As in the last section, the requirement of phase synchronization is converted to the requirement of phase offset information. This provides an alternative to phase synchronization.

4.4 Relationship between synchronization conditions

In the previous sections, we assumed the water-filling algorithms were executed when the clocks were synchronized, and investigated the techniques to counteract any phase offset afterwards. In some situations, perfect synchronization is not achievable due to reasons such as noise disturbance, etc. Thus, the execution of the water-filling algorithm and channel decomposition at two points in time are actually based on different synchronization conditions. In this section, we will explore the relationship between these two executions.

This exploration also applies if we discard the concept of phase synchronization. The channel decomposition and water-filling algorithms are performed regardless of the synchronization status. If the clocks drift, no effort is made to compensate the phase offsets, as in previous two sections. Instead, channel decomposition and water-filling algorithms are performed again for this new condition. In essence, these two scenarios are identical in that the set of channel decomposition and water-filling algorithms is executed at two points in time with different synchronization conditions but the same locations of antennas.

The observed channel is denoted as H_1 for a specific relationship among clocks at time 1. H_1 can be expressed in terms of the channel H in the conceived status of synchronization as $H_1 = D_{r,1} H D_{t,1}$, where $D_{r,1}$ and $D_{t,1}$ are examples of D_r and D_t, respectively. Accordingly, the U and V matrixes are replaced by $U_{r,1} \triangleq D_{r,1} U$ and $V_{t,1} \triangleq D_{t,1}^{\dagger} V$. With another time relationship at time 2, the observed channel is H_2, i.e. $H_2 = D_{r,2} H D_{t,2}$, and the new U and V are $U_{r,2} = D_{r,2} U$ and $V_{t,2} = D_{t,2}^{\dagger} V$. We can relate these two executions of channel decomposition and water-filling through the conceived synchronization as

$$H_2 = (D_{r,2} D_{r,1}^{\dagger}) H_1 (D_{t,1}^{\dagger} D_{t,2}) \tag{4.6}$$

$$U_{r,2} = (D_{r,2} D_{r,1}^{\dagger}) U_{r,1} \tag{4.7}$$

$$V_{t,2} = D_{t,2}^{\dagger} D_{t,1} V_{t,1} = (D_{t,1}^{\dagger} D_{t,2})^{\dagger} V_{t,1}. \tag{4.8}$$

Notice

$$D_{r,2} D_{r,1}^{\dagger} = \begin{bmatrix} e^{j(\theta_{r,1,2} - \theta_{r,1,1})} & 0 & \cdots & 0 \\ 0 & e^{j(\theta_{r,2,2} - \theta_{r,2,1})} & \ddots & \vdots \\ \vdots & \ddots & \ddots & 0 \\ 0 & \cdots & 0 & e^{j(\theta_{r,n_r,2} - \theta_{r,n_r,1})} \end{bmatrix},$$

which is also in the form of D_r. Similarly,

$$D_{t,1}^{\dagger}D_{t,2} = \begin{bmatrix} e^{j(\theta_{t,1,2}-\theta_{t,1,1})} & 0 & \cdots & 0 \\ 0 & e^{j(\theta_{t,2,2}-\theta_{t,2,1})} & \ddots & \vdots \\ \vdots & \ddots & \ddots & 0 \\ 0 & \cdots & 0 & e^{j(\theta_{t,n_t,2}-\theta_{t,n_t,1})} \end{bmatrix}$$

is also in the same form. Thus, from the point of view of the first point in time with channel matrix H_1, the channel H_2 is measured when the transmit antenna clocks are offset by $D_{t,1}^{\dagger}D_{t,2}$ and the receive antenna clocks are offset by $D_{r,2}D_{r,1}^{\dagger}$. According to our studies in the previous two sections, their channel capacities are the same. The outcome of the second channel decomposition is equivalent to the phase offset methods in the previous two sections. The channel H_2 is decomposed into parallel subchannels with the same D. $U_{r,2}$ is $U_{r,1}$ left multiplied by $D_{r,2}D_{r,1}^{\dagger}$, which is the phase difference of receive antenna clocks at time 2 with respect to time 1. $V_{t,2}$ is $V_{t,1}$ left multiplied by the Hermitian of $D_{t,1}^{\dagger}D_{t,2}$, which is the phase difference of transmit antenna clocks at time 2 with respect to time 1. If the condition at time 1 is perfect synchronization, (4.6)—(4.8) degenerate to the results in the previous two sections.

Therefore, when the relationships among transmit and receive antenna clocks change so that the channel decomposition is obsolete, there are two approaches to deal with this change. The first one is to measure the new perceived channel matrix and make a new channel decomposition, which results in the same water-filling algorithm but different U and V. The second one is to determine the amount of phase change, and remove this change by modifying U and V. Both approaches are equivalent and lead to

the same mathematical expressions.

4.5 Conclusion

In this chapter, we examine the effects of phase offset on the channel capacity. It is revealed that phase offset at either the transmit or the receive antenna does not change the channel capacity. In addition to rigorous clock synchronization in the phase level, two alternatives to counteract the phase offset are also explored. They are equivalent mathematically. The first one is to discard the previous channel matrix as well as the associated channel decomposition, and measure a new channel matrix and perform a new channel decomposition. The second approach is to work with the phase change, with respect to the nominal condition when the channel decomposition is performed. When a clock is different from the nominal value by a phase θ, the way to cancel out this effect is to rotate the signal in the opposite direction at the baseband processing units closest to the channel, as demonstrated in Figure 4.1. When lack of synchronism occurs at the clock of any transmit antenna, the processing unit is immediately before the baseband signal modulates the carrier. When this occurs at the clock of any receive antenna, the processing unit is immediately after the RF signal is down-converted to the baseband signal. Therefore, the channel decomposition does not have to be executed again, and the lack of synchronism is not apparent to the other side of communication link and the water-filling algorithm.

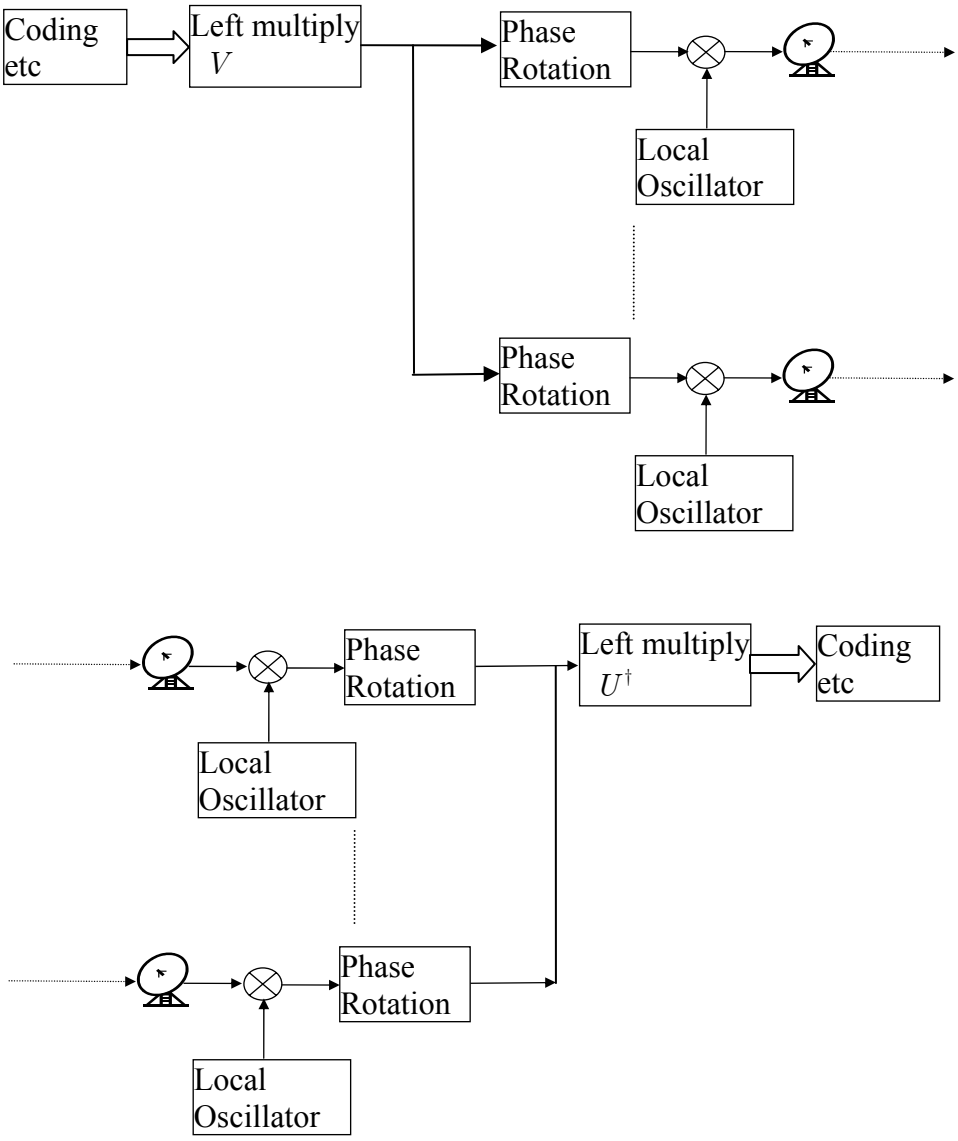

Figure 4.1: Phase adjustment at baseband when clocks are not synchronized.

Chapter 5

Achievable Rate Regions in the 3-node Wireless Network

5.1 Introduction

Network information theory has been investigated for decades. However, there are many unsolved problems. Due to the multiplicity of nodes, numerous problems arise and most of them remain to be answered. The most general problem is illustrated in Figure 5.1. This example contains several fundamental networks. In order to explore the behavior of the whole network, it is crucial to fully understand all these fundamental elements. Some elements are as follows.

In Figure 5.1, the three transmitters, nodes A, B and C, send information to the

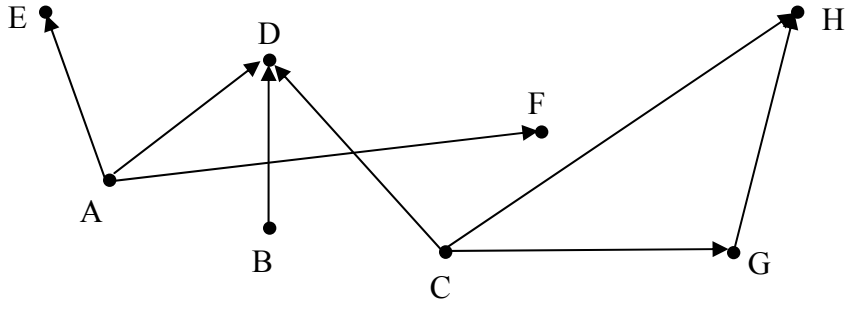

Figure 5.1: An example of network information flows

common receiver node D. This is called the multiple access channel. The capacity of this channel has been determined. When one common transmitter sends information to multiple receivers, this is called the broadcast channel. Transmission from node A to node D, E and F is an example. Although this is just a simple extension from the one-transmitter-one-receiver channel, only the degraded broadcast channel is solved, and the general problem is still open. In addition to problems coming from the number of transmitters or receivers, some nodes may act as helpers, which create another dimension for network information theory. In Figure 5.1, node G receives information from node C, and meanwhile it can send information to node H. Thus, by relaying information meant for node H, it can help information transportation from node C to H. When there is only one information stream, whose source is node C and destination is node H, it is called relay channel. The capacity is determined only for the physically degraded relay channel. Beyond these three simple networks, many network topologies can be imagined. For example, there may be multiple relay levels, where each level is composed of multiple

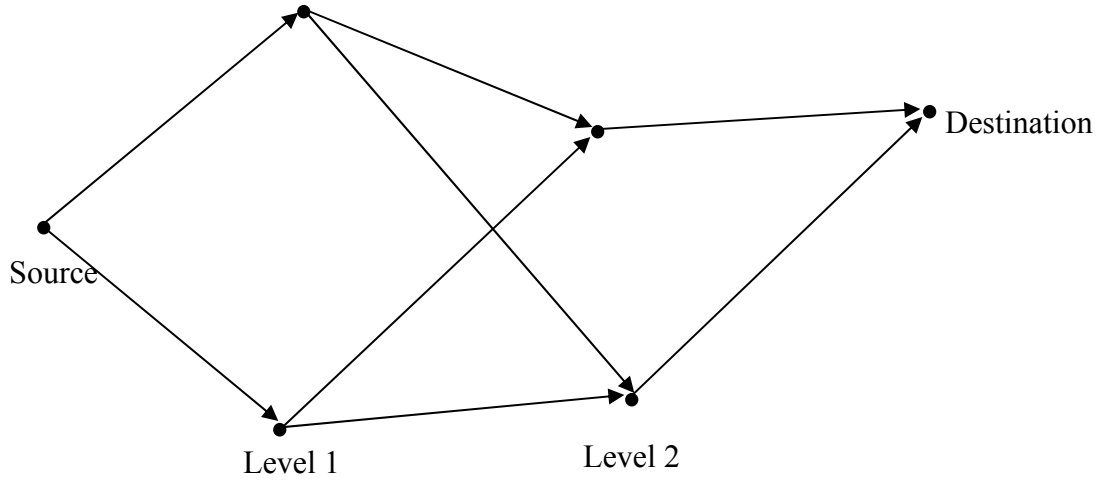

Figure 5.2: A decode-and-forward network with multiple levels, and multiple nodes in each level.

nodes. This is illustrated in Figure 5.2. In this figure, the link represents the designed communication link. Because it is a wireless network, signals transmitted from the information source can be overheard by the information destination, although they are meant to be received only by nodes at level 1. In other words, these signals are interference signals at the information destination.

There are two approaches to implement the function of a relay. The first one, which is more intuitive from the point of view of information theory, is called decode-and-forward[8][10][16] here. First, relay nodes decode the received signal into information data. Then, they encode the data into clean signals, and these signals are transmitted to the assigned receivers, which do not have to be the information destination, as shown in Figure 5.2. In the second approach, called magnify-and-forward[6][10], each node magnifies whatever signal it receives and forwards the magnified signal to the information destination. With this approach, relay nodes do not know the information data they relay since they do not decode the received signals. Noise is also magnified and forwarded along with the information-bearing signal. Due to this specific implementation

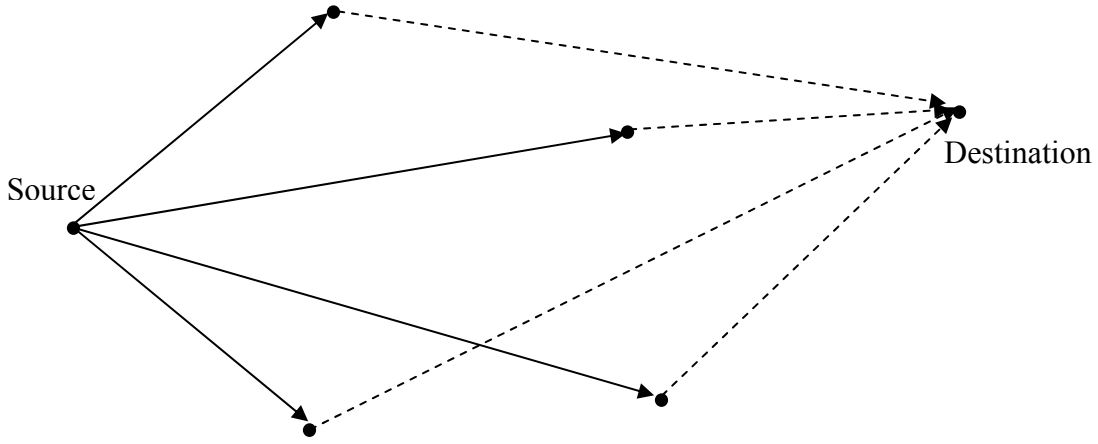

Figure 5.3: A network with magnify-and-forward relay nodes.

of a relay, there are two limitations associated with this approach. First, only one level of relay nodes is allowed, as shown in Figure 5.3. Because nodes do not decode signals, they cannot delete any interference. With a one-layer topology, we can avoid inter-level interference. Secondly, the communications from the source to the relay nodes, as in the solid lines in Figure 5.3, and from the relay nodes to the destination, as in the dashed lines in Figure 5.3, must be multiplexed. The reason is to avoid the interference between these two communication stages. Finally, it is not easy, although it may not be impossible, to support multiple information streams. Because relay nodes do not decode signals, they cannot distinguish signals of different streams.

In contrast, the decode-and-forward approach can support multiple information streams at least conceptually, which will be demonstrated in this chapter. However, there are two drawbacks with this approach. First of all, although interference can be removed from the clean signal by decoding the received signal, interference is strongly dependent on node locations. In Figure 5.2, signals from nodes in level 1 are received at the destination as interference. When there is more than one node in a level, the component interference signals from these nodes may combine coherently under some node location settings. In this case, the interference is significant. On the other hand, under some location settings, interference signals may combine destructively so that no interference is detected. Secondly, it is very challenging to derive the capacity, although some achievable rate regions are proposed.

In this chapter, we focus on the network composed of three nodes with a decode-and-forward implementation, which is the network of node C, G and H in Figure

5.1. We will consider several combinations of information flow. Achievable rate regions and the associated optimal power allocation will be determined based on some communication schemes.

5.2 Two Sources and One Destination

In this section, we consider the situation where two information sources send information to a common destination, as depicted in Figure 5.4. An achievable rate region was derived in [16] based on the proposed communication scheme. Since we will determine the optimal power allocation, which was not studied in [16], and since the analysis in the following sections uses a similar concept, the achievable rate region and the communication scheme are briefly described here.

5.2.1 The Achievable Rate Region Without Power Optimization

The received signals at node 1, 2 and 0 are given by

$$Y_0 = K_{10}X_1 + K_{20}X_2 + Z_0$$
$$Y_1 = K_{21}X_2 + Z_1$$
$$Y_2 = K_{12}X_1 + Z_2$$

where X_1 and X_2 are transmitted signals from nodes 1 and 2, respectively, K_{ij} is the path gain from node i to node j, and Z_i, which is distributed as $\mathrm{N}(0, N_i)$, is the

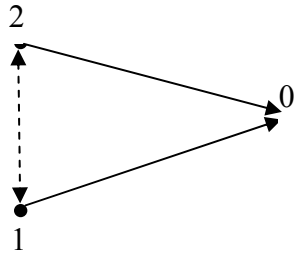

Figure 5.4: the network with 2 information sources and one common destination

noise at node i. For the sake of brevity, the following explanation is based on the operation at node 1. The same reasoning applies to node 2. Suppose the information from node 1 to node 0, denoted as W_1, is divided into two parts: W_{10}, to be sent directly to node 0, and W_{120}, to be sent to node 0 cooperatively with node 2. Accordingly, the transmitted signal X_1 is composed of 3 components, which are outputs of 3 encoders:

$$X_1 = X_{10} + X_{120} + U_{10},$$

where X_{10} is used to convey W_{10}, X_{120} is used to transmit W_{120} to node 2, and U_{10} is the signal intended to be combined coherently with signals from node 2. To expedite our discussion, we call X_{10} the direct-path signal, X_{120} the relay-path signal, and U_{10} the coherent-combining signal. Coherent combining was interpreted in the previous chapters. These are their major tasks, and the other arguments of the encoders will be described in detail later. Accordingly, the total power is divided into

$$P_1 = P_{10} + P_{120} + P_{U10}.$$

The transmission continues for B blocks of length n each. Both B and n are assumed to be large, and the transmission is performed block by block. This means the earliest time when coherent combining can take place is one block after X_{120}, which is equivalent to W_{120}, has been sent from node 1. If we look at one block, denoted as block b, we have

$$X_{10} = \sqrt{P_{10}}\tilde{X}_{10}(W_{10}(b), W_{120}(b-1), W_{210}(b-1))$$
$$X_{120} = \sqrt{P_{120}}\tilde{X}_{120}(W_{120}(b), W_{120}(b-1), W_{210}(b-1))$$
$$U_{10} = \sqrt{P_{U10}}\tilde{U}\,(W_{120}(b-1), W_{210}(b-1)),$$

where X_{10}, X_{120} and U_{10} are vectors of length n. Notice that $W_{120}(b-1)$ and $W_{210}(b-1)$ are also arguments of $\tilde{X}_{10}$ and $\tilde{X}_{120}$, and $\tilde{U}$ is a function not only of $W_{120}(b-1)$ but also of $W_{210}(b-1)$. Besides, node 2 uses the identical encoder $\tilde{U}$ for the coherent combining signal so that these two coherent combining signals can be combined coherently.

The decoding procedure is implemented in two stages. In the forward decoding stage, W_{120} is decoded immediately so that it can be used for coherent combining at the next block. We initialize the transmission by setting $(W_{120}(0), W_{210}(0)) = (0,0)$. Thus, at block 1, U_{10} is known for node 2, and X_{10} is regarded as noise when node 2 tries to decode $W_{120}(1)$ from $X_{10}(1)$. The rate constraint is

$$R_{120} < C\left(\frac{K_{12}^2 P_{120}}{K_{12}^2 P_{10} + N_2}\right). \tag{5.1}$$

At block 2, $U_{10}(2)$ is still known in advance because $W_{120}(1)$ was decoded at block 1 and $W_{210}(1)$ is produced at node 2. Therefore, as long as (5.1) holds, node 2 can decode W_{120} as the block index goes forward. At the second stage, called the backward decoding stage, node 0 decodes W_{10}, W_{120}, W_{20} and W_{210} from the last block backward to the first block. We assume there is no new information at the last block, i.e. $(W_{10}(B), W_{120}(B), W_{20}(B), W_{210}(B)) = (0,0,0,0)$. Since B is a very large number, the effect of this information rate reduction by the factor (B-1)/B is negligible. Thus, all of $X_{10}(B)$, $X_{20}(B)$, $X_{120}(B)$, $X_{210}(B)$, $U_{10}(B)$, and $U_{20}(B)$ are solely determined by

$W_{120}(B-1)$ and $W_{210}(B-1)$. In other words, the rate constraint is

$$R_{120} + R_{210} < C\left(\frac{K_{10}^2 P_1 + K_{20}^2 P_2 + 2K_{10}K_{20}\sqrt{P_{U10}P_{U20}}}{N_0}\right). \tag{5.2}$$

The factor $\sqrt{P_{U10}P_{U20}}$ results from the coherent combining of U_{10} and U_{20}. Now, we consider block B-1. Node 0 is required to decode $W_{10}(B-1)$, $W_{20}(B-1)$, $W_{120}(B-2)$, and $W_{210}(B-2)$. According to the multiple access channel capacity formulation, it is easy to obtain

$$R_{10} < C\left(\frac{K_{10}^2 P_{10}}{N_0}\right)$$

$$R_{20} < C\left(\frac{K_{20}^2 P_{20}}{N_0}\right)$$

$$R_{10} + R_{20} < C\left(\frac{K_{10}^2 P_{10} + K_{20}^2 P_{20}}{N_0}\right)$$

Since $X_{10}(B-1)$, $X_{20}(B-1)$, $X_{120}(B-1)$, $X_{210}(B-1)$, $U_{10}(B-1)$, and $U_{20}(B-1)$ are all functions of $W_{120}(B-2)$ and $W_{210}(B-2)$, (5.2) is still valid in this block. However, these signals are also functions of $W_{10}(B-1)$ and $W_{20}(B-1)$, so

$$R_{10} + R_{20} + R_{120} + R_{210} < C\left(\frac{K_{10}^2 P_1 + K_{20}^2 P_2 + 2K_{10}K_{20}\sqrt{P_{U10}P_{U20}}}{N_0}\right) \tag{5.3}$$

is also required. Since the region of (5.2) is contained in the region of (5.3), the final result of the achievable rate region is

$$R_{120} < C\left(\frac{K_{12}^2 P_{120}}{K_{12}^2 P_{10} + N_2}\right) \tag{5.4}$$

$$R_{210} < C\left(\frac{K_{21}^2 P_{210}}{K_{21}^2 P_{20} + N_1}\right) \tag{5.5}$$

$$R_{10} < C\left(\frac{K_{10}^2 P_{10}}{N_0}\right) \tag{5.6}$$

$$R_{20} < C\left(\frac{K_{20}^2 P_{20}}{N_0}\right) \tag{5.7}$$

$$R_{10} + R_{20} < C\left(\frac{K_{10}^2 P_{10} + K_{20}^2 P_{20}}{N_0}\right) \tag{5.8}$$

$$R_{10} + R_{20} + R_{120} + R_{210} < C\left(\frac{K_{10}^2 P_1 + K_{20}^2 P_2 + 2K_{10}K_{20}\sqrt{P_{U10}P_{U20}}}{N_0}\right). \tag{5.9}$$

5.2.2 Power Optimization

This achievable rate region was derived in [16], but the optimal power allocation was not determined. Our goal is to maximize the achievable rate region of $(R_1 = R_{10} + R_{120}, R_2 = R_{20} + R_{210})$, and we will investigate the associated power allocation between P_{10} and P_{120}. This issue is related to how W_1 is divided into W_{10} and W_{120}. By adding (5.4) and (5.6), we obtain

$$\begin{aligned} R_1 &= R_{10} + R_{120} \\ &< \frac{1}{2}\log\left(\frac{K_{12}^2 P_{10} + N_2 + K_{12}^2 P_{120}}{K_{12}^2 P_{10} + N_2}\right) + \frac{1}{2}\log\left(\frac{N_0 + K_{10}^2 P_{10}}{N_0}\right) \\ &= \frac{1}{2}\log\left(\frac{K_{12}^2 (P_{10} + P_{120}) + N_2}{N_0} \times \frac{K_{10}^2 P_{10} + N_0}{K_{12}^2 P_{10} + N_2}\right) \end{aligned} \tag{5.10}$$

Suppose the power allocation between P_{U10} and $P_{10} + P_{120}$ is fixed, then the only variable in (5.10) is P_{10}. We denote $P_{10} + P_{120}$ as $P_{1,non-coherent}$. The optimal P_{10} is

$$P_{10} = \begin{cases} P_{1,non-coherent} & \text{, if } \dfrac{N_0}{K_{10}^2} < \dfrac{N_2}{K_{12}^2} \\ 0 & \text{, if } \dfrac{N_0}{K_{10}^2} \geq \dfrac{N_2}{K_{12}^2} \end{cases}$$

In other words, to maximize the achievable region, the choice of P_{120} and P_{10} depends on the values of N_0 / K_{10}^2 and N_2 / K_{12}^2. If N_2 / K_{12}^2 is greater, which means node 2 is noisier than node 0, then it is intuitive that node 2 cannot help node 0 and all $P_{1,non-coherent}$ should be allocated to transmit X_{10}, which is now not a function of W_{120}. Consequently, if a similar situation occurs for W_2, i.e. $N_0 / K_{20}^2 < N_1 / K_{21}^2$, the achievable rate region for the whole network reduces to that of the multiple access channel. If N_0 / K_{10}^2 is greater, node 2 can relay signals to node 0. All $P_{1,non-coherent}$ should be allocated to convey information W_{120}, and W_{10} does not play a role. This strategy might seem unreasonable at first sight, and it might be expected that there should be a smooth transition between 0 and $P_{1,non-coherent}$ for both P_{120} and P_{10}. The secret lies in the fact that W_{120} can perform whatever functions W_{10} is designed to perform. X_{10}, which is the only signal component dependent on W_{10}, is designed to be received by node 0. X_{120}, which is a function of the current value of W_{120}, received and relayed by node 2, is also received by node 0. This reception at node 0 is similar to that of X_{10}. From this point of view, the role of W_{10} can in effect be replaced by W_{120}. The fact that node 0 takes advantage of this received power is revealed in (5.2), where the right hand side contains P_{120}, which is part of P_1. Furthermore, the optimization indicates that the role of W_{10} has to be effectively replaced by W_{120}. This is due to the constraint (5.4). If some power were allocated to P_{10}, the achievable rate constraint of R_{120} would be reduced. Because node

0 is noisier, the increase in the R_{10} constraint cannot compensate for the decrease in the R_{120} constraint. Thus, P_{10} is set to 0. In the next section, with another decoding procedure, we will show that there is some freedom of power allocation between P_{10} and P_{120}.

To conclude, when $N_0 / K_{10}^2 \geq N_2 / K_{12}^2$ and $N_0 / K_{20}^2 \geq N_1 / K_{21}^2$, the achievable rate region is given by

$$R_1 < C\left(\frac{K_{12}^2(P_1 - P_{U10})}{N_2}\right) \tag{5.11}$$

$$R_2 < C\left(\frac{K_{21}^2(P_2 - P_{U20})}{N_1}\right) \tag{5.12}$$

$$R_1 + R_2 < C\left(\frac{K_{10}^2 P_1 + K_{20}^2 P_2 + 2K_{10}K_{20}\sqrt{P_{U10}P_{U20}}}{N_0}\right). \tag{5.13}$$

Notice that (5.6), (5.7) and (5.8) disappear because $P_{10} = P_{20} = 0$. In (5.11), P_{120} has been replaced by $P_1 - P_{U10}$ since P_{10} is 0, and a similar replacement is used in (5.12). The achievable rate region cannot be further expanded by appropriate power allocation between P_{120} and P_{U10}. When P_{U10} grows, the constraint (5.13) is released, while the right hand side of (5.11) is decreased.

When $N_0 / K_{10}^2 > N_2 / K_{12}^2$ and $N_0 / K_{20}^2 < N_1 / K_{21}^2$, node 2 can help the transmission of W_1, but node 1 is too noisy to help node 2. The achievable rate region is

$$R_1 < C\left(\frac{K_{12}^2(P_1 - P_{U10})}{N_2}\right) \tag{5.14}$$

$$R_2 < C\left(\frac{K_{20}^2(P_2 - P_{U20})}{N_0}\right) \tag{5.15}$$

$$R_1 + R_2 < C\left(\frac{K_{10}^2 P_1 + K_{20}^2 P_2 + 2K_{10}K_{20}\sqrt{P_{U10}P_{U20}}}{N_0}\right). \tag{5.16}$$

Notice because $P_{10} = P_{210} = 0$, (5.5) and (5.6) disappear while (5.8) duplicates (5.7). Further, (5.14)—(5.16) are almost the same as (5.11)—(5.13) except that the denominator in (5.15) is N_0.When $N_0 / K_{10}^2 < N_2 / K_{12}^2$ and $N_0 / K_{20}^2 \geq N_1 / K_{21}^2$, the achievable rate region can be derived in a similar fashion.

5.2.3 Degeneration to the Physically Degraded Gaussian Relay Channel

The channel capacity for the physically degraded Gaussian relay channel has been derived in [2], where an achievable rate region for the Gaussian relay channel is proposed, and the degradedness is exploited to show no higher rate is achievable. In this relay channel with 3 nodes, there is only one transmitter, whereas 2 transmitters were considered in the previous subsection. Thus, the result in the previous subsection should be able to degenerate to the result in [2].

In the Gaussian relay channel, it is assumed the destination, i.e. node 0, is noisier than the relay node, which can be node 1 or 2. If we start from (5.11), (5.12) and (5.13), by settting $P_2 = P_{U20}$, which means node 2 is the relay node, we obtain

$$R_1 < C\left(\frac{K_{12}^2(P_1 - P_{U10})}{N_2}\right)$$

$$R_1 < C\left(\frac{K_{10}^2 P_1 + K_{20}^2 P_2 + 2K_{10}K_{20}\sqrt{P_{U10}P_2}}{N_0}\right),$$

which is equivalent to the capacity of the degraded Gaussian relay channel:

$$C = \max_{0\le\alpha\le 1} \min\left\{ C\left(\frac{K_{12}^2 \alpha P_1}{N_2}\right), C\left(\frac{K_{10}^2 P_1 + K_{20}^2 P_2 + 2K_{10}K_{20}\sqrt{\bar{\alpha} P_1 P_2}}{N_0}\right)\right\}, \tag{5.17}$$

where $\bar{\alpha} \triangleq 1-\alpha$. The same result can be derived from (5.14), (5.15) and (5.16).

5.3 One Source and Two Destinations

In this section, we will propose an achievable region for the scenario where two information streams come from the same source but arrive at different destinations, as depicted in Figure 5.5. In the following section, we will study some scenarios which are more complicated and contain this one as a special case. The reason for discussing this case in advance is that it is the first step in extending the achievable rate region derived by Sendonaris et al.[16], and that it reveals some insights and techniques which will facilitate the exploration of more complicated scenarios.

The destinations of information streams are node 1 and node 2, with node 0 as the source. Node 1 and node 2 can communicate with each other. This scenario is simpler in terms of the number of information sources, compared with the network in Figure 5.4. However, in terms of the number of nodes which are transmitting signals, there are three nodes here, instead of the two nodes in Figure 5.4. Based on the same technique in the

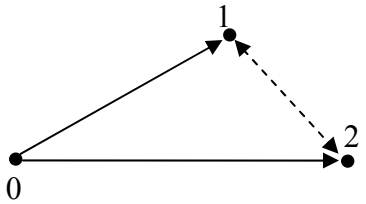

Figure 5.5: the network with 1 common information source and two destinations

previous section, W_1 is divided into W_{01} and W_{021}, and likewise for W_2. Thus, we can write X_0 as

$$X_0 = X_{01} + X_{021} + U_{021} + X_{02} + X_{012} + U_{012}.$$

where X_{01}, X_{021} and U_{021} stand respectively for the direct-path, relay-path, and co-herently combined signals for the first information stream, and X_{01}, X_{021} and U_{021} are for the second information stream. Notice we have two coherent-combining signals to combine with coherent-combining signals from nodes 1 and node 2, respectively. The power is divided likewise. Although nodes 1 and 2 are not information sources, they may relay signals in the form of

$$X_1 = U_{12}$$
$$X_2 = U_{21}$$

If we focus on block b, these signals are the outputs of encoders

$$U_{012} = \sqrt{P_{U012}}\tilde{U}_2(W_{012}(b-1))$$
$$U_{021} = \sqrt{P_{U021}}\tilde{U}_1(W_{021}(b-1))$$
$$U_{12} = \sqrt{P_{U12}}\tilde{U}_2(W_{012}(b-1))$$
$$U_{21} = \sqrt{P_{U21}}\tilde{U}_1(W_{021}(b-1))$$
$$X_{01} = \sqrt{P_{01}}\tilde{X}_{01}(W_{01}(b), W_{012}(b-1), W_{021}(b-1))$$
$$X_{021} = \sqrt{P_{021}}\tilde{X}_{021}(W_{021}(b), W_{012}(b-1), W_{021}(b-1))$$
$$X_{02} = \sqrt{P_{02}}\tilde{X}_{02}(W_{02}(b), W_{012}(b-1), W_{021}(b-1))$$
$$X_{012} = \sqrt{P_{012}}\tilde{X}_{012}(W_{012}(b), W_{012}(b-1), W_{021}(b-1)).$$

The received signal at nodes 1 and 2 are

$$Y_1 = K_{01}X_0 + K_{21}X_2 + Z_1$$
$$Y_2 = K_{02}X_0 + K_{12}X_1 + Z_2.$$

By using the 2-stage decoding approach discussed in the last section, in the forward decoding stage, nodes 1 and 2 decode W_{012} and W_{021}, respectively, so that in the following block data can be relayed to the destinations.

Assuming that the direct-path signals W_{01} and W_{02} are decoded in the backward decoding stage, the rate constraint R_{012} at node 1 is

$$\begin{aligned} R_{012} &< C\left(\frac{K_{01}^2 P_{012}}{K_{01}^2(P_{01}+P_{021}+P_{02}+P_{U021})+K_{21}^2 P_{U21}+2K_{01}K_{21}\sqrt{P_{U21}P_{U021}}+N_1}\right) \\ &= C\left(\frac{P_{012}}{P_{01}+P_{021}+P_{02}+\left(P_{U021}+\frac{K_{21}^2 P_{U21}}{K_{01}^2}+\frac{2K_{21}\sqrt{P_{U21}P_{U021}}}{K_{01}}+\frac{N_1}{K_{01}^2}\right)}\right) \end{aligned} \tag{5.18}$$

and the rate constraint R_{021} at node 2 is

$$\begin{aligned} R_{021} &< C\left(\frac{K_{02}^2 P_{021}}{K_{02}^2(P_{01}+P_{012}+P_{02}+P_{U012})+K_{12}^2 P_{U12}+2K_{12}K_{02}\sqrt{P_{U012}P_{U12}}+N_2}\right) \\ &= C\left(\frac{P_{021}}{P_{01}+P_{012}+P_{02}+\left(P_{U012}+\frac{K_{12}^2 P_{U12}}{K_{02}^2}+\frac{2K_{12}\sqrt{P_{U012}P_{U12}}}{K_{02}}+\frac{N_2}{K_{02}^2}\right)}\right) \end{aligned} \tag{5.19}$$

We denote $P_{U021}+K_{21}^2 P_{U21}/K_{01}^2+2K_{21}\sqrt{P_{U21}P_{U021}}/K_{01}+N_1/K_{01}^2$ in (5.18) by O_1, and $P_{U012}+K_{12}^2 P_{U12}/K_{02}^2+2K_{12}\sqrt{P_{U012}P_{U12}}+N_2/K_{02}^2$ in (5.19) by O_2. The relationship between O_1 and O_2 leads to some interesting consequences. Either $O_2 > O_1$ or $O_2 \le O_1$ holds, and the consequence of one is simply the opposite of the other. For the sake of brevity, we only illustrate the situation when $O_2 > O_1$. Then

$$C\left(\frac{P_{021}}{P_{01}+P_{012}+P_{02}+O_2}\right) < C\left(\frac{P_{021}}{P_{01}+P_{02}+O_1}\right). \tag{5.20}$$

Because of (5.19) and (5.20), any achievable rate R_{021} has the property:

$$R_{021} < C\left(\frac{P_{021}}{P_{01}+P_{02}+O_1}\right). \tag{5.21}$$

The inequality (5.21) is exactly the constraint for node 1 if it would decode W_{021} in the forward decoding stage after W_{012} is decoded. This decoding is not mandatory in the scheme since W_{021} is intended to be decoded after signals from node 0 and 2 are coherently combined. However, this decoding is achievable without any additional constraint because (5.21) holds without adding new constraints to the original set of constraints. In other words, the destination node, i.e. node 1, can decode the data intended to be relayed before they are relayed by the relay node, i.e. node 2. Therefore, it is suggested that W_{021} not be employed. Consequently, P_{021}, P_{U021}, and P_{U21} are set to 0, and (5.21) is discarded. This reduces O_1 to N_1 / K_{01}^2 and increases the difference between O_1 and O_2. Then (5.18) is rewritten as

$$R_{012} < C\left(\frac{P_{012}}{P_{01}+P_{02}+N_1/K_{01}^2}\right). \tag{5.22}$$

Since W_{021} is not used, node 2 is not required to send U_{21} to node 1; W_{01} can be decoded in the forward decoding stage, and the rate constraint is

$$R_{01} < C\left(\frac{P_{01}}{P_{02}+N_1/K_{01}^2}\right). \tag{5.23}$$

Even if W_{01} is decoded in the backward decoding stage, the constraint is the same.

In the backward decoding stage, no data remain to be decoded at node 1. Node 2 has

to decode W_{02} and W_{012}. The procedure is similar to the procedure in the last section. The constraints are

$$R_{02} < C\left(\frac{P_{02}}{P_{01} + N_2 / K_{02}^2}\right) \tag{5.24}$$

$$R_{02} + R_{012} < C\left(\frac{K_{02}^2(P_{02} + P_{012} + P_{U012}) + K_{12}^2 P_{U12} + 2K_{12}K_{02}\sqrt{P_{U12}P_{U012}}}{P_{01} + N_2 / K_{02}^2}\right). \tag{5.25}$$

Now the achievable rate region is determined by (5.22)—(5.25).

If W_{01} and W_{02} are decoded in the forward decoding stage, instead of in the backward decoding stage, the rate constraints at node 1 are

$$R_{012} < C\left(\frac{P_{012}}{P_{021} + P_{02} + O_1}\right) \tag{5.26}$$

$$R_{01} < C\left(\frac{P_{01}}{P_{021} + P_{02} + O_1}\right) \tag{5.27}$$

$$R_{012} + R_{01} < C\left(\frac{P_{012} + P_{01}}{P_{021} + P_{02} + O_1}\right). \tag{5.28}$$

The constraints at node 2 are

$$R_{021} < C\left(\frac{P_{021}}{P_{012} + P_{01} + O_2}\right) \tag{5.29}$$

$$R_{02} < C\left(\frac{P_{02}}{P_{012} + P_{01} + O_2}\right) \tag{5.30}$$

$$R_{021} + R_{02} < C\left(\frac{P_{021} + P_{02}}{P_{012} + P_{01} + O_2}\right). \tag{5.31}$$

With the same assumption of $O_2 > O_1$, node 1 can further decode W_{02} and W_{021} after removing P_{012} and P_{01}. The reason is as follows. The rate constraints to perform this decoding are

$$R_{021} < C\left(\frac{P_{021}}{O_1}\right) \tag{5.32}$$

$$R_{02} < C\left(\frac{P_{02}}{O_1}\right) \tag{5.33}$$

$$R_{021} + R_{02} < C\left(\frac{P_{021} + P_{02}}{O_1}\right). \tag{5.34}$$

Because $O_2 > O_1$, the region of (5.32)—(5.34) contains the region of (5.29)—(5.31). In other words, node 1 can decode W_{02} and W_{021} without imposing any new constraint. Since W_{021} can be obtained by node 1 before it is relayed by node 2, W_{021} is not helpful in the scheme. This result is the same as in the case when W_{01} and W_{02} are decoded in the backward decoding stage. The set of constraints (5.26)—(5.31) reduces to

$$R_{012} < C\left(\frac{P_{012}}{P_{02} + N_1 / K_{01}^2}\right) \tag{5.35}$$

$$R_{01} < C\left(\frac{P_{01}}{P_{02} + N_1 / K_{01}^2}\right) \tag{5.36}$$

$$R_{012} + R_{01} < C\left(\frac{P_{012} + P_{01}}{P_{02} + N_1 / K_{01}^2}\right). \tag{5.37}$$

$$R_{02} < C\left(\frac{P_{02}}{P_{012} + P_{01} + O_2}\right) \tag{5.38}$$

In the backward decoding stage, node 1 has nothing to decode, and node 2 has to decode W_{012} only because W_{02} has been obtained. The rate constraint is

$$R_{012} < C\left(\frac{K_{02}^2(P_{02} + P_{012} + P_{U012}) + K_{12}^2 P_{U12} + 2K_{12}K_{02}\sqrt{P_{U12}P_{U012}}}{P_{01} + N_2 / K_{02}^2}\right). \tag{5.39}$$

The achievable rate region is now (5.35)—(5.39).

Now, we focus on the interaction between R_{01} and R_{012} in both approaches. We compare (5.35)—(5.37) with (5.22) and (5.23). The former achievable rate region is lar-

ger than the latter. The difference is depicted in Figure 5.6. If W_{01} is decoded in the backward decoding stage, the region determined by R_{012} and R_{01} is a rectangle. If W_{01} is decoded along with W_{012} in the forward decoding stage, the constraint on R_{012} is relaxed, and the constraint on $R_{012}+R_{01}$ is introduced. In the former case, the signal containing W_{01} is regarded as noise. In the latter case, W_{01} is on the contrary decoded as well as W_{012} using the concept of decoding in the multiple access channel. Therefore, less noise is involved when W_{012} is decoded and meanwhile the rate constraint on R_{01} is not sacrificed. This concept of decoding messages as in the multiple access channel will be discussed further in the next section.

Consequently, if we decode W_{02} in the backward decoding stage, the achievable region is determined by (5.35)—(5.37), (5.24) and (5.25). For convenience, they are repeated here

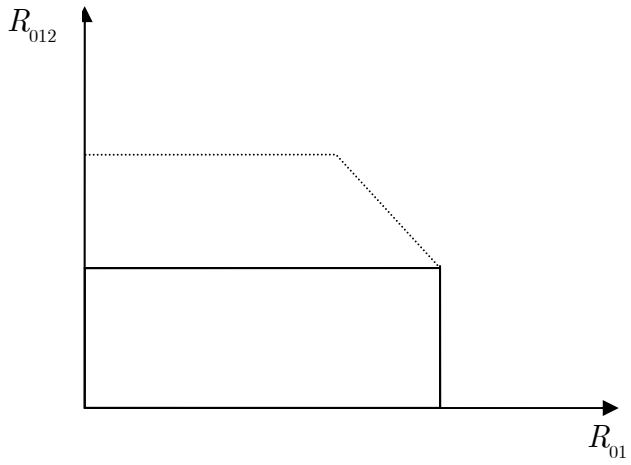

Figure 5.6: The different rate constraints for two decoding schemes.

$$R_{012} < C\left(\frac{P_{012}}{P_{02} + N_1 / K_{01}^2}\right) \tag{5.40}$$

$$R_{01} < C\left(\frac{P_{01}}{P_{02} + N_1 / K_{01}^2}\right) \tag{5.41}$$

$$R_{012} + R_{01} < C\left(\frac{P_{012} + P_{01}}{P_{02} + N_1 / K_{01}^2}\right). \tag{5.42}$$

$$R_{02} < C\left(\frac{P_{02}}{P_{01} + N_2 / K_{02}^2}\right) \tag{5.43}$$

$$R_{02} + R_{012} < C\left(\frac{K_{02}^2(P_{02} + P_{012} + P_{U012}) + K_{12}^2 P_{U12} + 2K_{12}K_{02}\sqrt{P_{U12}P_{U012}}}{P_{01} + N_2 / K_{02}^2}\right). \tag{5.44}$$

This region is illustrated in Figure 5.7. Among the set of constraints, the benefit of coherent combining is revealed in (5.44). Because of the terms $K_{02}^2 P_{U012}$, $K_{12}^2 P_{U12}$, and $2K_{12}K_{02}\sqrt{P_{U12}P_{U012}}$, the constraint (5.71) on $R_{02} + R_{012}$ is very loose. It could be even

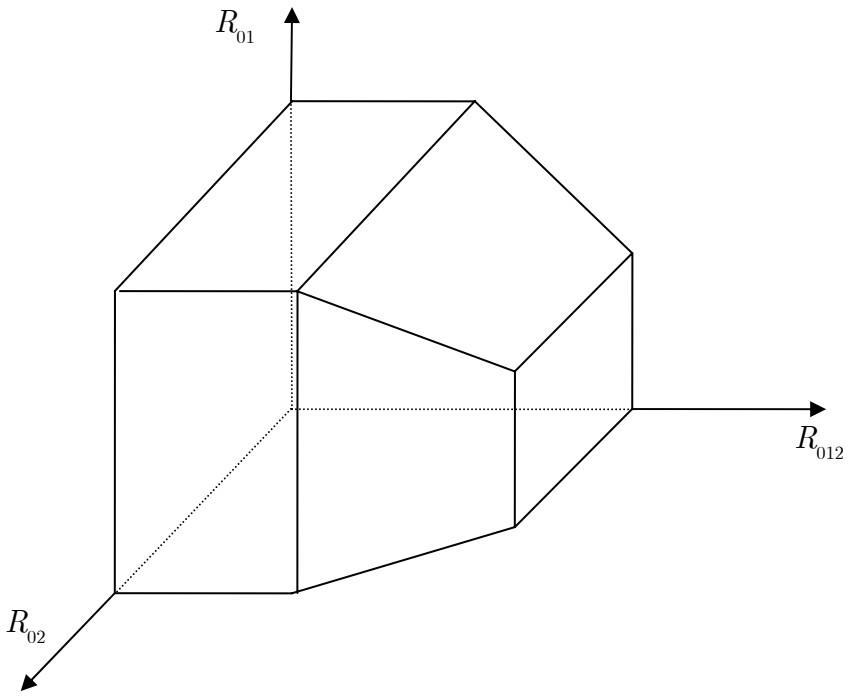

Figure 5.7: The achievable rate region for the case with one source and two destinations.

looser than the summation of (5.40) and (5.43), and thus should be invisible in Figure 5.7. As in the last section, it is worthwhile to investigate the optimal power allocation between the relay-path and direct-path signals. The only relay-path message used is W_{012}. Thus, our objective is to determine the power allocation between P_{02} and P_{012} so that $R_2 = R_{012} + R_{02}$ is maximum. The right hand side of (5.44) is invariant with respect to power allocation between P_{02} and P_{012} as long as their summation is fixed. We denote their summation as $P_{2,non-coherent}$ as in the last section. By adding (5.40) and (5.43), we obtain

$$\begin{aligned} R_{02} + R_{012} &< \frac{1}{2}\log\left(\frac{P_{02} + P_{01} + N_2 / K_{02}^2}{P_{01} + N_2 / K_{02}^2}\frac{P_{02} + P_{012} + N_1 / K_{01}^2}{P_{02} + N_1 / K_{01}^2}\right) \\ &= \frac{1}{2}\log\left(\frac{P_{2,non-coherent} + N_1 / K_{01}^2}{P_{01} + N_2 / K_{02}^2}\frac{P_{02} + (P_{01} + N_2 / K_{02}^2)}{P_{02} + (N_1 / K_{01}^2)}\right). \end{aligned} \tag{5.45}$$

Generally speaking, this constraint is tighter than (5.44) because it does not include the power related to coherent combining. Then, as in the previous section, the optimal power allocation depends on the values of $P_{01} + N_2 / K_{02}^2$ and N_1 / K_{01}^2. The optimal P_{02} is

$$P_{02} = \begin{cases} P_{2,non-coherent} & \text{, if } P_{01} + \dfrac{N_2}{K_{02}^2} < \dfrac{N_1}{K_{01}^2} \\ 0 & \text{, if } P_{01} + \dfrac{N_2}{K_{02}^2} \geq \dfrac{N_1}{K_{01}^2} \end{cases} \tag{5.46}$$

The explanation and implication are similar to those for the power allocation between P_{10} and P_{120} in the last section.

The comparison between O_1 and O_2 can be viewed differently if we look at the first decoding block, i.e. block 1. At this time, $W_{021}(0)$ and $W_{012}(0)$ are known a priori

as zero . If we decode W_{01} and W_{02} in the backward decoding stage, the rate constraints on R_{012} and R_{021}, which are determined in the forward decoding stage, are

$$R_{012} < C\left(\frac{P_{012}}{P_{01} + P_{021} + P_{02} + N_1 / K_{01}^2}\right)$$
$$R_{021} < C\left(\frac{P_{021}}{P_{01} + P_{012} + P_{02} + N_2 / K_{02}^2}\right).$$

We want to determine if node 2 can decode W_{012} or node 1 can decode W_{021} before these messages are relayed at block 2. The concern is the noise power of $P_{01} + P_{02} + N_1 / K_{01}^2$ and $P_{01} + P_{02} + N_2 / K_{02}^2$. They differ in N_2 / K_{02}^2 and N_1 / K_{01}^2. Either $N_2 / K_{02}^2 \geq N_1 / K_{01}^2$ or $N_2 / K_{02}^2 < N_1 / K_{01}^2$ holds. If $N_2 / K_{02}^2 \geq N_1 / K_{01}^2$, then

$$C\left(\frac{P_{021}}{P_{01} + P_{02} + N_1 / K_{01}^2}\right) > C\left(\frac{P_{021}}{P_{01} + P_{012} + P_{02} + N_2 / K_{02}^2}\right) > R_{021}. \qquad (5.47)$$

Inequality (5.47) means that node 1 can decode $W_{021}(1)$ as long as it can be decoded at node 2. Then, at block 2, node 1 can also decode $W_{021}(2)$, and so on. Thus, all signal power terms related to W_{021}, such as P_{U021} and P_{U21}, are not regarded as noise at node 1, and it is not helpful to have node 2 relay any message. On the other hand, node 2 cannot decode W_{012}. Thus, in the following block, the signals associated with P_{U012} and P_{U12} cannot be decoded and are regarded as noise. This causes the noise power in node 2 to increase to $P_{U012} + K_{12}^2 P_{U12} / K_{02}^2 + N_2 / K_{02}^2$, which makes the noise power at node 2 further larger than that at node 1. The same result can be obtained if W_{01} and W_{02} are decoded in the forward decoding stage.

Now we include our analysis regarding optimal power allocation. Since $N_2 / K_{02}^2 > N_1 / K_{01}^2$, $P_{01} + N_2 / K_{02}^2$ is greater than N_1 / K_{01}^2. Therefore, according to (5.46), the optimal P_{02} is zero. All information intended for node 2 should be sent through the relay path. To conclude, when N_2 / K_{02}^2 is greater than N_1 / K_{01}^2, the achievable rate region is

$$R_{01} < C\left(\frac{P_{01}}{N_1 / K_{01}^2}\right) \tag{5.48}$$

$$R_{012} < C\left(\frac{P_{012}}{N_1 / K_{01}^2}\right) \tag{5.49}$$

$$R_{01} + R_{012} < C\left(\frac{P_{01} + P_{012}}{N_1 / K_{01}^2}\right) \tag{5.50}$$

$$R_{012} < C\left(\frac{K_{02}^2(P_{012} + P_{U012}) + K_{12}^2 P_{U12} + 2K_{12}K_{02}\sqrt{P_{U12}P_{U012}}}{P_{01} + N_2 / K_{02}^2}\right). \tag{5.51}$$

Among (5.48)—(5.51), (5.49) and (5.51) are constraints on R_{012}. Their relationship cannot be determined, so both of them must be considered. It is also easy to derive the capacity of the physically degraded Gaussian relay channel (5.17) as a special case of this achievable rate region.

To conclude, we have shown how and when the relay-path signals can be removed. We have also demonstrated that the achievable rate region can be enlarged if a node simultaneously decodes messages even though some messages are not needed so urgently.

5.4 Revision to the Achievable Rate Region

In the last section, we observed the benefits of decoding direct-path messages along with the relay-path messages in the forward decoding stage rather than in the backward de-

coding stage. In other words, it is beneficial to simultaneously decode as many messages as possible even though some of them are not needed immediately.

5.4.1 Decoding in the Multiple Access Channel and the Broadcast Channel

Now, we revise the decoding scheme proposed by Sendonaris et al.[16]. Since node 1 and node 2 are symmetric and interchangeable in this scheme, although our analysis focuses on one node, this analysis also applies to the other node. At node 2, when W_{120} is decoded in the forward decoding stage, X_{10} is regarded as noise so that the constraint on R_{120} is (5.4). In terms of the number of messages embedded in the received signal, a similar situation also appears in both the Gaussian multiple access channel and the Gaussian broadcast channel. The decoding schemes in these two channels are different. The problem here is to determine which decoding scheme should be used in this scenario.

To solve this problem, it is crucial to recognize the difference between the decoding schemes for these two fundamental channels. Suppose that the communication scenario is as illustrated in Figure 5.8. There are 2 co-located sources. Signals X_1 and X_2 are obtained from W_1 and W_2 respectively, and transmitted from these two nodes. Since they are co-located, it is not necessary to tell which signal comes from which node. The noise

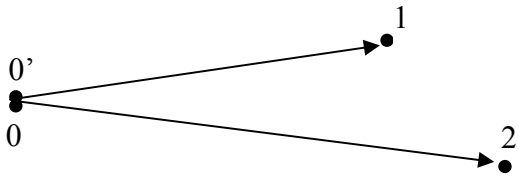

Figure 5.8: the network with 2 co-located sources, and 2 destinations

power spectrum densities at node 1 and node 2 are N_1 and N_2. The path gains are K_{01} and K_{02} respectively, and K_{01} is greater than K_{02}. At node 1, the received signal is $K_{01}(X_1 + X_2)$, and what is of interest is X_1. This received signal can be interpreted as that in the Gaussian multiple access channel or the Gaussian broadcast channel. In both channels, node 1 tries to decode W_1 and W_2. The constraint, however, is different.

In the Gaussian multiple access channel, the constraints are

$$R_1 < C\left(\frac{K_{01}^2 P_1}{N_1}\right) \tag{5.52}$$

$$R_2 < C\left(\frac{K_{01}^2 P_2}{N_1}\right) \tag{5.53}$$

$$R_1 + R_2 < C\left(\frac{K_{01}^2 (P_1 + P_2)}{N_1}\right). \tag{5.54}$$

This region is shown in Figure 5.9 as the outer pentagon. The horizontal line corresponds to the rate constraint on R_1 if X_2 is regarded as noise. As for the decoding in the Gaussian broadcast channel, W_2 is first decoded, X_2 is removed from the received signal, and finally, W_1 is decoded. Thus, the constraints are

$$R_1 < C\left(\frac{K_{01}^2 P_1}{N_1}\right) \tag{5.55}$$

$$R_2 < C\left(\frac{K_{01}^2 P_2}{N_1 + K_{01}^2 P_1}\right). \tag{5.56}$$

This region is the shaded rectangle in Figure 5.9. Notice that the vertex A is shared by both regions. Obviously, the region for the Gaussian multiple access channel is larger than the Gaussian broadcast channel, and it seems that the decoding approach in the multiple access channel is better. This puzzle is solved when we inspect node 2. For node 2 to

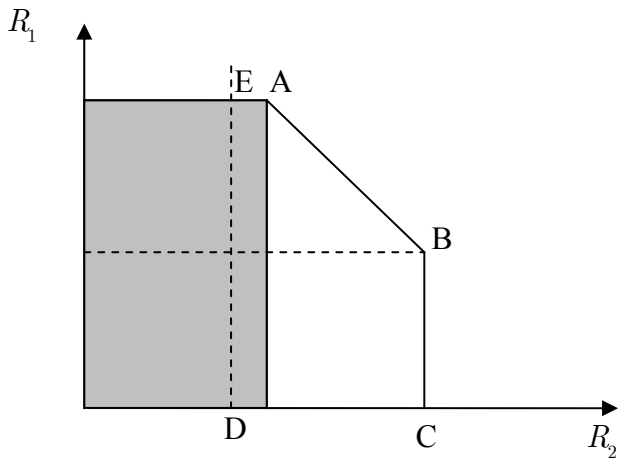

Figure 5.9: The achievable rate region for 2 decoding schemes at the closer node.

decode W_2, the constraint is

$$R_2 < C\left(\frac{K_{02}^2 P_2}{N_2 + K_{02}^2 P_1}\right). \tag{5.57}$$

Because X_1 is too weak, it is not worthwhile to decode W_1 at node 2. The constraint (5.57) is illustrated in Figure 5.9 as the vertical dashed line. Notice that vertex A is at the right hand side of this line, and that the remaining region after this pruning is identical for both decoding approaches at node 1. In other words, with fixed P_1 and P_2, even though node 1 can decode W_1 and W_2 coded at any rate pair in area ABCDE, node 2 cannot decode W_2 from the received signal for some rate pairs. Consequently, in the Gaussian broadcast channel in Figure 5.8, the achievable rate region is the same regardless of which decoding approach is employed at the closer node. No matter which scheme is used, the rate constraint on R_1 is increased from the horizontal line.

5.4.2 Joint Decoding and Sequential Decoding

Before proceeding to improve the achievable rate region proposed by Sendonaris, et

al.[16], we further explore these two decoding schemes when they are used in the Gaussian multiple access channel and propose a new decoding scheme to achieve the same achievable rate region as in [2]. This means that we consider node 1 only and remove node 2 from the scenario. The destination of both messages is node 1. With the joint decoding approach and the concept of jointly typical sequences [2], the achievable rate region is region ABCOF in Figure 5.10. If we choose to decode W_2 first and then W_1 as in the Gaussian broadcast channel, the rate pair must be within region ADOF so that messages can be decoded. Notice that this region is a subset of region ABCOF. We call this sequential decoding, as opposed to joint decoding. In contrast, if W_1 is decoded ahead of W_2, the achievable region with this scheme is region BCOE. Consequently, with these two sequential decoding alternatives, sequential decoding can achieve most of the area of the achievable rate region with joint decoding, i.e. region ABCOF. The only missing region is triangle ABG..

To achieve the rate pair in triangle ABG with sequential decoding, the above two

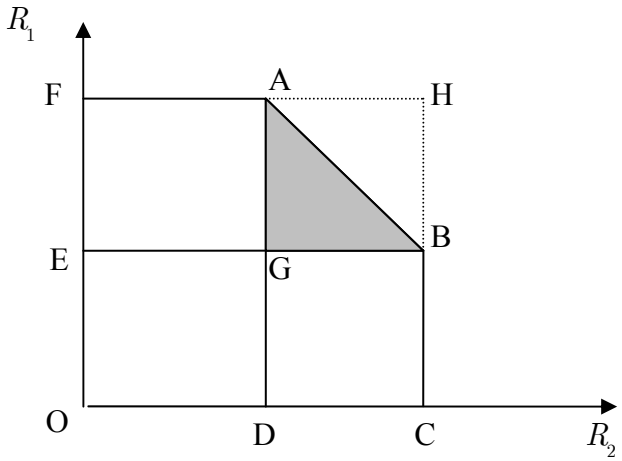

Figure 5.10: Difference between sequential and joint decoding schemes.

sequential decoding alternatives can be time-multiplexed as illustrated in Figure 5.11. For example, suppose the unfilled rectangle represents when the coding and decoding schemes operate at rate pair A in Figure 5.10, and the filled rectangle represents the rate pair B in Figure 5.10. By changing the time-duration ratio between these two choices, we can achieve any rate pair located on line section AB. As a result, any rate pair located in the rectangle ABG can be realized without resorting to the joint decoding approach.

It might be argued that additional information is required for the senders to determine the ratio of time durations. In other words, each sender must be informed of the existence of the other sender, and they cooperatively determine two transmission rate pairs in two sequential decoding alternatives respectively and how these two pairs are linearly combined. However, this kind of information is also needed if the joint decoding approach is used. To be specific, without the information about the other sender, sender 2 will consider any rate R_2 left to line CH to be achievable, and likewise sender 1 will consider any rate R_1 below line FH to be achievable, given the individual signal to noise ratios. If they encode messages individually and independently and the rate pair lies in triangle AHB, the messages cannot be decoded even with the joint decoding approach.

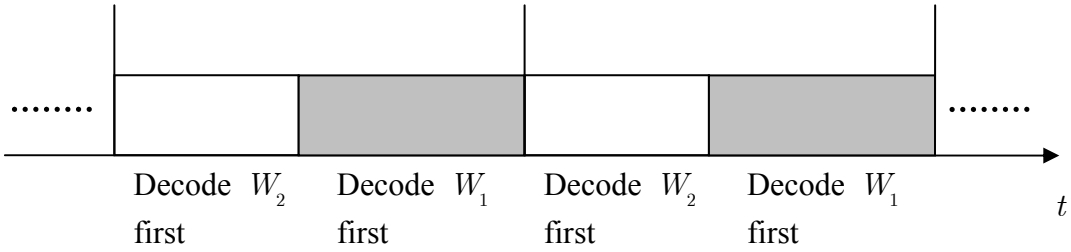

Figure 5.11: Multiplexing sequential decoding schemes in the Gaussian multiple access channel.

From this point of view, with sequential decoding, senders do not need more information than with joint decoding.

Although the discussion above is based on the situation with 2 transmitters, the same result can be obtained for any number of senders. For example, suppose there are three transmitters, labeled nodes 1, 2, and 3. They send X_1, X_2, and X_3, which are derived from W_1, W_2 and W_3 individually, to node 0. The received signal power values for each signals are P_1, P_2, and P_3. The noise power spectrum density is N_0. Obviously, there are six orders in which to decode messages sequentially. Their individual constraint sets are:

$$R_1 < C\left(\frac{P_1}{P_2+P_3+N_0}\right) \quad R_2 < C\left(\frac{P_2}{P_3+N_0}\right) \quad R_3 < C\left(\frac{P_3}{N_0}\right)$$
$$R_1 < C\left(\frac{P_1}{P_2+P_3+N_0}\right) \quad R_3 < C\left(\frac{P_3}{P_2+N_0}\right) \quad R_2 < C\left(\frac{P_2}{N_0}\right)$$
$$R_2 < C\left(\frac{P_2}{P_1+P_3+N_0}\right) \quad R_1 < C\left(\frac{P_1}{P_3+N_0}\right) \quad R_3 < C\left(\frac{P_3}{N_0}\right)$$
$$R_2 < C\left(\frac{P_2}{P_1+P_3+N_0}\right) \quad R_3 < C\left(\frac{P_3}{P_1+N_0}\right) \quad R_1 < C\left(\frac{P_1}{N_0}\right)$$
$$R_3 < C\left(\frac{P_3}{P_1+P_2+N_0}\right) \quad R_1 < C\left(\frac{P_1}{P_2+N_0}\right) \quad R_2 < C\left(\frac{P_2}{N_0}\right)$$
$$R_3 < C\left(\frac{P_3}{P_1+P_2+N_0}\right) \quad R_2 < C\left(\frac{P_2}{P_1+N_0}\right) \quad R_1 < C\left(\frac{P_1}{N_0}\right).$$

It can be easily verified that we can achieve any point in the achievable rate region through a linear combination of these six constraint sets.

5.4.3 Revision to the Scenario with Two Sources and One Destination

Now, we proceed to expand the achievable rate region proposed by Sendonaris et al.[16].

In the forward decoding stage, if node 2 tries to decode W_{10}, the constraint on R_{120} will be relaxed. As we discussed above, there are two choices. We may decode W_{10} first, and W_{120} after removing X_{10}. We call this broadcast decoding to highlight that it is used in the Gaussian broadcast channel. The rate constraints are

$$R_{10} < C\left(\frac{K_{12}^2 P_{10}}{K_{12}^2 P_{120} + N_2}\right) \tag{5.58}$$

$$R_{120} < C\left(\frac{K_{12}^2 P_{120}}{N_2}\right) \tag{5.59}$$

This achievable rate region is demonstrated as rectangle ADOF in Figure 5.12. Alternatively, if we decode W_{10} and W_{120} regarding them as signals to be decoded in the Gaussian multiple access channel, the rate constraints are

$$R_{10} < C\left(\frac{K_{12}^2 P_{10}}{N_2}\right) \tag{5.60}$$

$$R_{120} < C\left(\frac{K_{12}^2 P_{120}}{N_2}\right) \tag{5.61}$$

$$R_{10} + R_{120} < C\left(\frac{K_{12}^2 (P_{10} + P_{120})}{N_2}\right) \tag{5.62}$$

This achievable rate region is the pentagon ABCOF in Figure 5.12. We call this multiple access decoding. As we pointed out, the key point is at the place where W_{10} is intended to be decoded, i.e. node 0. For node 0 to decode W_{10}, the rate constraint is (5.6), shown as line GH in Figure 5.12. In contrast to Figure 5.9, this vertical line does not necessarily lie to the left of line AD because what is compared to $(N_2 + K_{12}^2 P_{120})/K_{12}^2$ is N_0/K_{10}^2, instead of $(N_0 + K_{10}^2 P_{120})/K_{10}^2$ as in Figure 5.9. In Figure 5.9, the further node cannot

decode the message intended for the closer node, whereas here this message is decoded at the farther node through backward decoding and coherent combining. Hence, $K_{10}^2 P_{120}$ is removed from the noise power. If broadcast decoding is used, we may underestimate the achievable rate region and lose the lighter shaded area if $(N_2 + K_{12}^2 P_{120}) / K_{12}^2 > N_0 / K_{10}^2$. If constraint (5.6) is ignored and multiple access decoding is used, W_{10}, which is encoded at the rate pair in region BCGJ, cannot be decoded at node 0 even in the backward decoding stage.

Therefore, for the achievable rate region proposed by Sendonaris et al., the constraint (5.4) is replaced by (5.61) and (5.62). Likewise, (5.5) should be replaced by

$$R_{210} < C\left(\frac{K_{21}^2 P_{210}}{N_1}\right) \tag{5.63}$$

$$R_{20} + R_{210} < C\left(\frac{K_{21}^2 (P_{20} + P_{210})}{N_1}\right). \tag{5.64}$$

The other constraints remain. Constraints (5.4), (5.61) and (5.62) are shown as lines BK,

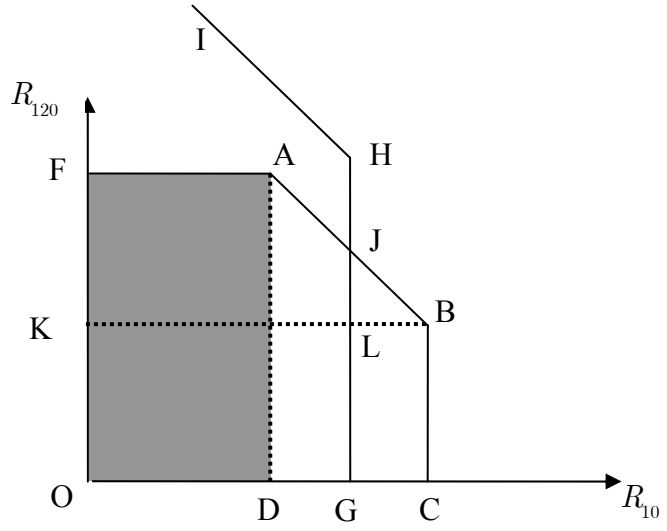

Figure 5.12: Relaxation of the constraint on R_{120}.

AF and AB in Figure 5.12, respectively. The effect of (5.9) is illustrated as line IH in Figure 5.12. This line changes with the summation of R_{20} and R_{210}. In other words, this line interacts with its counterpart in the R_{20} vs. R_{210} plane. However, it is reasonable to assume that this line and its counterpart are not effective, i.e., they do not shape the achievable rate region determined by other constraints. This is reflected in Figure 5.12. The right hand side of (5.9) contains the power related to coherent combining, which is not shown in other constraints. Thus, this constraint is supposed to be very loose. In addition, we neglect (5.8) in the following discussion. Unlike (5.9), (5.8) is effective in shaping the achievable rate region in Figure 5.12 when R_{20} is high enough. The consequence is that the constraint on R_{10} is replaced by

$$R_{10} < C\left(\frac{K_{10}^2 P_{10} + K_{20}^2 P_{20}}{N_0}\right) - R_{20}, \tag{5.65}$$

instead of (5.6). Nevertheless, in the following discussion of optimal power allocation, we will assume (5.8) is ineffective for the whole range of R_{20}. Thus, we remove the interaction between R_{10} vs. R_{120} and R_{20} vs. R_{210} planes and simplify the analysis. The achievable rate region of R_{10} and R_{120} is the region AJGOF. From this point of view, our analysis will provide a bound on power allocation if we take the effect of (5.8) into account.

As in the previous section, our objective is to find the optimal power allocation between P_{10} and P_{120} such that $R_1 = R_{10} + R_{120}$ is maximized, given that $P_{1,non-coherent} = P_{10} + P_{120}$ is fixed. When we vary the power allocation, lines IH and AB

are fixed. The maximum rate R_1 occurs whenever (R_{10}, R_{120}) is located on line section AJ assuming that point J is to the right of point A. If the relationship between lines AD and JG is indeed as depicted in Figure 5.12, we can guess that the optimal power allocation is a range. The reason is that if we slightly change the power allocation back and forth, the length of line section AJ is still nonzero. Thus, our task is to find out the range of power locations such that the length of line section AJ is greater than 0. When the length is zero, the intersection of lines AF and GJ lies on line AB, i.e.

$$C\left(\frac{K_{10}^2 P_{10}}{N_0}\right) + C\left(\frac{K_{12}^2 P_{120}}{N_2}\right) = C\left(\frac{K_{12}^2 (P_{10} + P_{120})}{N_2}\right).$$

Since it is a second order equation, there are two solutions. They are

$$P_{10} = \begin{cases} 0 \\ P_{1,non-coherent} + \dfrac{N_2}{K_{12}^2} - \dfrac{N_0}{K_{10}^2} \end{cases}, \quad P_{120} = \begin{cases} P_{1,non-coherent} \\ \dfrac{N_0}{K_{10}^2} - \dfrac{N_2}{K_{12}^2}. \end{cases}$$

With the additional physical restriction that P_{120} must be greater than 0, the range of the optimal power allocation is

$$P_{1,non-coherent} \geq P_{120} \geq \max\left(0, \frac{N_0}{K_{10}^2} - \frac{N_2}{K_{12}^2}\right)$$
$$P_{10} = P_{1,non-coherent} - P_{120}.$$

When P_{10} approaches 0, the achievable rate region is illustrated in Figure 5.13. Because points A, B, J and F coincide, the optimal rate pair is

$$R_{10} = 0$$
$$R_{120} = C\left(\frac{K_{12}^2 (P_{10} + P_{120})}{N_2}\right).$$

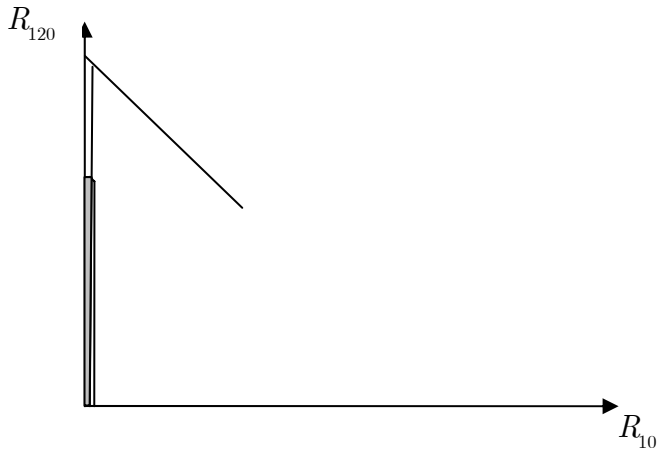

Figure 5.13: The achievable rate region when P_{10} is 0.

Sendonaris's achievable rate region is region KLGO in Figure 5.12. This region is unconditionally smaller than the new region AJGOF. The maximum rate R_1 in Sendonaris's region occurs at point L. This rate is less than the rate at line section AJ. The only exception is when P_{10} is zero. At this time, point L coincides with points A, B, J and J, and achieve the same R_1. Thus, for both decoding schemes, the maximum achievable rates R_1 are the same for fixed $P_{1,non-coherent}$, although the optimal power allocation in Sendonaris's region is a single point where it is a range in the new region.

When $P_{120} = N_0 / K_{10}^2 - N_2 / K_{12}^2 > 0$, it is at the critical point and the achievable rate region is shown in Figure 5.14. At this time, points A and J coincide, and this rate pair still lies on line AB. If P_{10} is increased further, line section GH will not intersect with line section AB, and thus the maximum rate R_1 will be decreased.

If $N_0 / K_{10}^2 - N_2 / K_{12}^2 < 0$, the range of optimal P_{10} is from 0 to $P_{1,non-coherent}$. That is, if all power is allocated to the direct path and node 2 does not relay any messages,

the maximum R_1 is still achieved. This can be explained as follows. The signals derived from W_{120} and W_{10} are transmitted from node 1, and received by node 0. From the point of view of node 0, these signals are alike in the forward decoding stage. W_{120} can also be decoded in the forward decoding stage although it is intended to be decoded in the backward decoding stage. However, if the relay node, i.e. node 2, can decode W_{120} at a higher rate than node 0, a higher R_{120} can be delivered to node 0 through coherent combining and backward decoding. Thus, P_{120} should at least account for the difference of decoding ability between node 2 and 0. This amount is $N_0 / K_{10}^2 - N_2 / K_{12}^2$. If this value is less than 0, that means that node 2 is noisier than node 0 and node 0 can decode whatever node 2 can decode. Consequently, we can allocate all power to the direct path. On the other hand, if some power is allocated to W_{120}, it can be decoded in the forward decoding stage without the help of node 2. Actually, when this happens, the simpler ap-

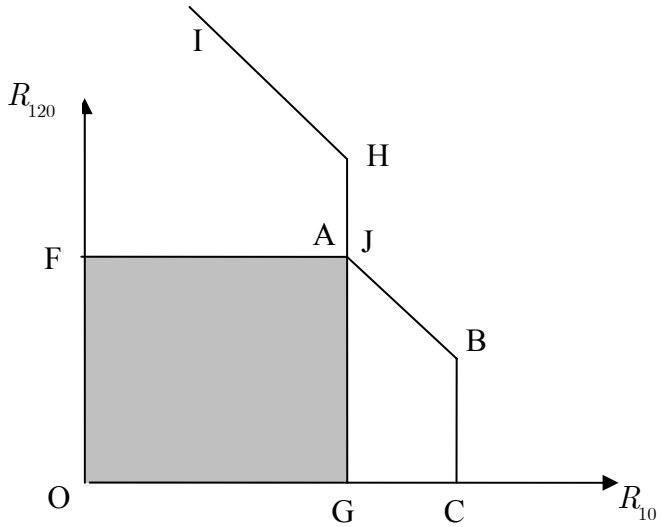

Figure 5.14: The achievable rate region at the critical point.

proach is to neglect node 2 completely, and the problem reduces to point-to-point communication.

When the power of the relay node is too low or the distance from node 1 and 2 to the destination, i.e. node 0, is too far, the right-hand side of (5.9) is decreased. Because this rate budget is split between R_1 and R_2, when

$$C\left(\frac{K_{10}^2(P_{10}+P_{120})}{N_0}\right)+C\left(\frac{K_{12}^2(P_{20}+P_{210})}{N_2}\right)<C\left(\frac{K_{10}^2P_1+K_{20}^2P_2+2K_{10}K_{20}\sqrt{P_{U10}P_{U20}}}{N_0}\right),$$

at least in one of R_{10} vs. R_{120} and R_{20} vs. R_{210} planes, constraint (5.9) becomes effective. In Figure 5.15, this is illustrated as line IH, which lies below line AB. This line represents

$$R_{10}+R_{120}<C\left(\frac{K_{10}^2P_1+K_{20}^2P_2+2K_{10}K_{20}\sqrt{P_{U10}P_{U20}}}{N_0}\right)-R_{20}-R_{210}.$$

On the contrary, line AB becomes ineffective. As in the previous case, in order to find the range of optimal power allocation, we have to solve the equation

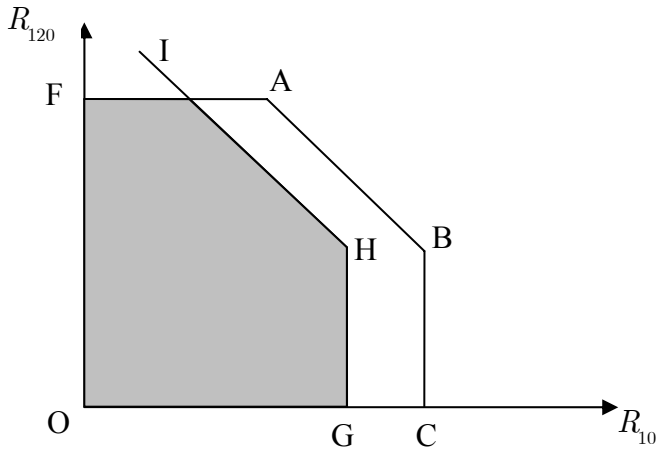

Figure 5.15: The achievable rate region when the relay power is too low.

$$C\left(\frac{K_{10}^2 P_{10}}{N_0}\right)+C\left(\frac{K_{12}^2 P_{120}}{N_2}\right)=C\left(\frac{K_{10}^2 P_1+K_{20}^2 P_2+2K_{10}K_{20}\sqrt{P_{U10}P_{U20}}}{N_0}\right)-R_{20}-R_{210}.$$

After some manipulation, this equation is rewritten as

$$\begin{aligned} f \triangleq & -P_{120}^2(K_{10}^2K_{12}^2)-P_{120}(N_2K_{10}^2-N_0K_{12}^2-K_{10}^2K_{12}^2P_{1,non-coherent}) \\ & -\left[(N_2P_{rx}+N_0N_2)/2^{2R_2}-N_2K_{10}^2P_{1,non-coherent}-N_0N_2\right]=0 \end{aligned},$$

where $P_{rx} \triangleq K_{10}^2P_1+K_{20}^2P_2+2K_{10}K_{20}\sqrt{P_{U10}P_{U20}}$. For the sake of brevity, we denote $(N_2P_{rx}+N_0N_2)/2^{2R_2}-N_2K_{10}^2P_{1,non-coherent}-N_0N_2$ by P_a. It is straightforward to obtain the solutions. We denote them by P_{120}^+ and P_{120}^-. There are some interesting observations: when P_a=0, P_{120}^-=0 and $P_{120}^+=P_{1,non-coherent}-N_2/K_{12}^2+N_0/K_{10}^2$. However, because node 2 is closer to node 1, $N_2/K_{12}^2<N_0/K_{10}^2$ and P_{120}^+ is infeasible. This is shown in Figure 5.16 as curve A . Thus, the feasible optimal power allocation is $P_{1,non-coherent}\geq P_{120}\geq 0$. When P_{120} approaches 0, the achievable rate region is shown in Figure 5.17. As P_a decreases, the curve moves up, as curve C in Figure 5.16, and the

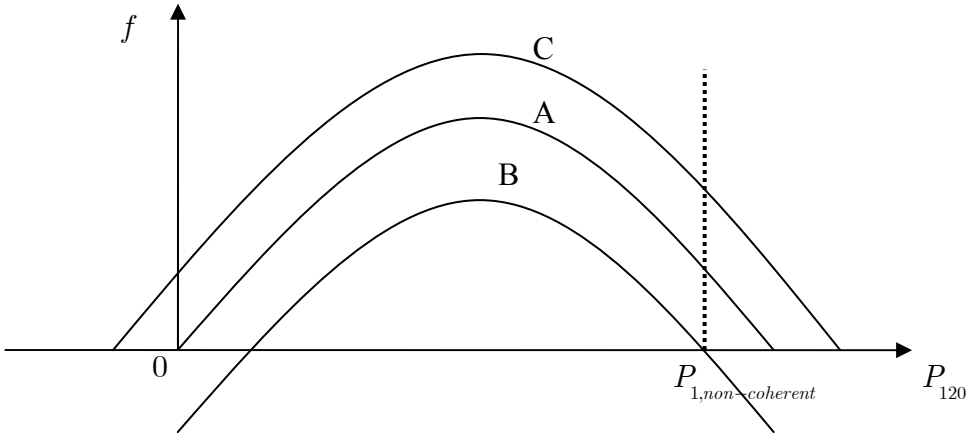

Figure 5.16: The solutions of P_{120} change with P_a.

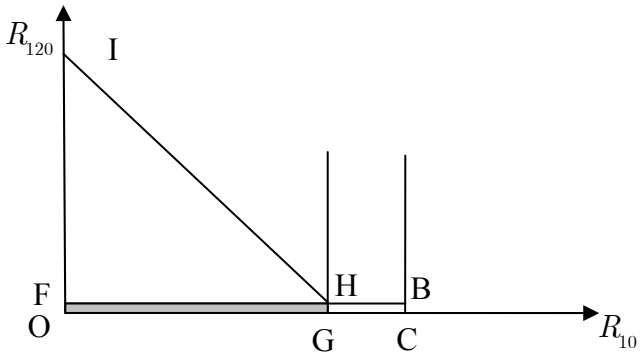

Figure 5.17: The achievable rate region when the relay power is too low and $P_{120} \to 0$.

feasible power allocation range stays the same. Actually, when the curve is above curve A, it means that the relay is not helpful enough so that the power allocation with $P_{120} = 0$ can even achieve the same R_1. When this is the case, the implication is similar to our previous explanation. It means that node 0 can decode W_{120} without the help of node 2, and the roles of W_{10} and W_{120} are the same from this point of view.

As P_a increases, the curve moves down and the range of optimal power allocation shrinks, as in curve B in Figure 5.16. P_{120}^- increases from 0, and the optimal power allocation of P_{120} is $P_{1,non-coherent} \geq P_{120} \geq P_{120}^-$. When $P_{120} = P_{120}^-$ and the value of f is between curve A and B, the achievable rate region is shown in Figure 5.18.

When P_a is high enough so that the values of f become curve B, P_{120}^+ is equal to $P_{1,non-coherent}$. This solution is identical to the solution when line AB lies below line IH, i.e., (5.62) becomes effective. Actually, at this point,

$$C\left(\frac{K_{12}^2(P_{10}+P_{120})}{N_2}\right) = C\left(\frac{K_{10}^2P_1 + K_{20}^2P_2 + 2K_{10}K_{20}\sqrt{P_{U10}P_{U20}}}{N_0}\right) - R_{20} - R_{210},$$

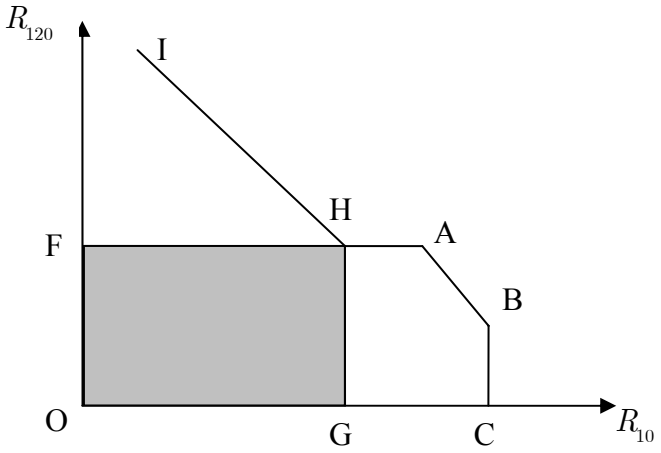

Figure 5.18: The achievable rate region when P_a increases.

and these two lines collocate. After this point, the analysis assuming (5.62) is effective applies.

To conclude, assuming (5.8) is ineffective, when

$$\begin{aligned} & C\left(\frac{K_{12}^2(P_{10}+P_{120})}{N_2}\right)+C\left(\frac{K_{21}^2(P_{20}+P_{210})}{N_1}\right) \\ & <C\left(\frac{K_{10}^2P_1+K_{20}^2P_2+2K_{10}K_{20}\sqrt{P_{U10}P_{U20}}}{N_0}\right), \end{aligned} \tag{5.66}$$

through proper rate allocation, line IH can lie above line AB in both R_{10} vs. R_{120} and R_{20} vs. R_{210} planes, and thus the optimal power allocation between P_{10} and P_{120} is

$$P_{1,non-coherent} \geq P_{120} \geq \frac{N_0}{K_{10}^2}-\frac{N_2}{K_{12}^2},$$

and $P_{10}=P_{1,non-coherent}-P_{120}$. When (5.66) does not hold, in at least one rate plane, line IH lies below line AB. In this plane, the optimal power allocation for P_{120} is

$$P_{1,non-coherent} \geq P_{120} \geq \max(0,P_{120}^{-}).$$

If (5.8) is taken into consideration, the influence is that the lower bounds of optimal P_{120}

and P_{210} will interact with each other through the interaction between lines GH in the two rate planes. Nevertheless, it is worthwhile to observe that the power allocation with $P_{120} = P_{1,non-coherent}$ and $P_{210} = P_{2,non-coherent}$ is always optimal in all situations.

5.5 Two Sources and Two Destinations

In this section, based on the same concept, we employ another approach to derive the achievable rate regions for several scenarios. First of all, we assume that all W's contained in the received signals are decodable at all nodes. Then, based on the relationships among noises for specific scenarios, we determine whether W's are indeed decodable. If a W is not decodable, it will be considered as noise in that node, and the whole achievable rate region is rewritten. This process may have to iterate several times to arrive at the final achievable rate region.

The network we consider is still the 3-node wireless network. There are 2 information sources, each with 2 information streams. This is illustrated in Figure 5.19, where nodes 0 and 1 are the information sources. Node 0 sends information messages $W_{0\to1}$ and $W_{0\to2}$ to nodes 1 and 2, respectively. Node 1 sends information messages $W_{1\to0}$ and $W_{1\to2}$ to nodes 0 and 2, respectively. As in the previous section, each message is di-

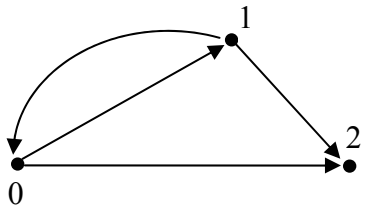

Figure 5.19: the network with 2 information sources, each with 2 information streams

vided into direct-path and relay-path messages. The information rates are divideded accordingly as

$$\begin{aligned} R_{0\to1} &= R_{01} + R_{021} \\ R_{0\to2} &= R_{02} + R_{012} \\ R_{1\to2} &= R_{12} + R_{102} \\ R_{1\to0} &= R_{10} + R_{120} \end{aligned}.$$

The transmission also continues for B blocks of length n each. The concept of the encoder design is unchanged. The direct-path signal is a function of the associated direct-path message in the current block and all relay-path messages which were transmitted or had to be decoded in the previous block. The relay-path signal is a function of the associated relay-path message in the current block and all relay-path messages which were transmitted or had to be decoded in the previous block. The coherent combining signal from a node to an information destination is a function of the relay-path messages which were transmitted or had to be decoded for the information destination in the previous block. Therefore, the transmitted signals are

$$\begin{aligned} X_0 &= X_{01} + X_{02} + X_{021} + X_{012} + U_{01} + U_{02} \\ X_1 &= X_{10} + X_{12} + X_{120} + X_{102} + U_{10} + U_{12} \\ X_2 &= U_{21} + U_{21}, \end{aligned}$$

where the constituent signals are outputs of encoders:

$$\begin{aligned} U_{01} &= \sqrt{P_{U01}}\tilde{U}_1(W_{021}(i-1)) \\ U_{02} &= \sqrt{P_{U02}}\tilde{U}_2(W_{012}(i-1), W_{102}(i-1)) \\ U_{10} &= \sqrt{P_{U10}}\tilde{U}_0(W_{120}(i-1)) \\ U_{12} &= \sqrt{P_{U12}}\tilde{U}_2(W_{012}(i-1), W_{102}(i-1)) \\ U_{20} &= \sqrt{P_{U20}}\tilde{U}_0(W_{120}(i-1)) \end{aligned}$$

$$U_{21} = \sqrt{P_{U21}}\tilde{U}_1(W_{021}(i-1))$$
$$X_{01} = \sqrt{P_{01}}\tilde{X}_{01}(W_{01}(i), W_{012}(i-1), W_{021}(i-1), W_{102}(i-1))$$
$$X_{02} = \sqrt{P_{02}}\tilde{X}_{02}(W_{02}(i), W_{012}(i-1), W_{021}(i-1), W_{102}(i-1))$$
$$X_{021} = \sqrt{P_{021}}\tilde{X}_{021}(W_{021}(i), W_{012}(i-1), W_{021}(i-1), W_{102}(i-1))$$
$$X_{012} = \sqrt{P_{012}}\tilde{X}_{012}(W_{012}(i), W_{012}(i-1), W_{021}(i-1), W_{102}(i-1))$$
$$X_{10} = \sqrt{P_{10}}\tilde{X}_{10}(W_{10}(i), W_{012}(i-1), W_{120}(i-1), W_{102}(i-1))$$
$$X_{12} = \sqrt{P_{12}}\tilde{X}_{12}(W_{12}(i), W_{012}(i-1), W_{120}(i-1), W_{102}(i-1))$$
$$X_{120} = \sqrt{P_{120}}\tilde{X}_{120}(W_{120}(i), W_{012}(i-1), W_{120}(i-1), W_{102}(i-1))$$
$$X_{102} = \sqrt{P_{102}}\tilde{X}_{102}(W_{102}(i), W_{012}(i-1), W_{120}(i-1), W_{102}(i-1)).$$

Notice U_{01} is designed to combine coherently with U_{21}, so they use the same encoder $\tilde{U}_1$. The same concept applies between U_{02} and U_{12} and between U_{20} and U_{10}.

The received signals are

$$Y_0 = K_{10}(X_{10} + X_{12} + X_{120} + X_{102} + U_{10} + U_{12}) + K_{20}(U_{20} + U_{21}) + Z_0$$
$$Y_1 = K_{01}(X_{01} + X_{02} + X_{021} + X_{012} + U_{01} + U_{02}) + K_{21}(U_{20} + U_{21}) + Z_1$$
$$Y_2 = K_{02}(X_{01} + X_{02} + X_{021} + X_{012} + U_{01} + U_{02})$$
$$+K_{12}(X_{10} + X_{12} + X_{120} + X_{102} + U_{10} + U_{12}) + Z_2.$$

The decoding also includes the forward and backward stages. As in the last section, we assume that all direct-path messages are intended to be decoded in the backward decoding stage although some can be decoded in the forward decoding stage. In the forward decoding stage, node 2 has to decode W_{021} and W_{120}, node 1 has to decode W_{012}, and node 0 has to decode W_{102}, if these messages are employed. Now, we look at the first block in the forward decoding stage. As in the last section, all messages are initialized to zero and known to all nodes. Thus all coherent combining signals can be removed from

the received signals. If node 2 can decode all data contained in the signals, the channel is like the multiple access channel[2] from the point of view of node 2. Consequently the achievable rate region is

$$R_{01} < C\left(\frac{K_{02}^2 P_{01}}{N_2}\right) \tag{5.67}$$

$$R_{02} < C\left(\frac{K_{02}^2 P_{02}}{N_2}\right) \tag{5.68}$$

$$R_{12} < C\left(\frac{K_{12}^2 P_{12}}{N_2}\right) \tag{5.69}$$

$$R_{10} < C\left(\frac{K_{12}^2 P_{10}}{N_2}\right) \tag{5.70}$$

$$R_{012} < C\left(\frac{K_{02}^2 P_{012}}{N_2}\right) \tag{5.71}$$

$$R_{102} < C\left(\frac{K_{12}^2 P_{102}}{N_2}\right) \tag{5.72}$$

$$\boldsymbol{R}_{021} < \boldsymbol{C}\left(\frac{\boldsymbol{K}_{02}^2 \boldsymbol{P}_{021}}{\boldsymbol{N}_2}\right) \tag{5.73}$$

$$\boldsymbol{R}_{120} < \boldsymbol{C}\left(\frac{\boldsymbol{K}_{12}^2 \boldsymbol{P}_{120}}{\boldsymbol{N}_2}\right) \tag{5.74}$$

$$R_{01} + R_{02} < C\left(\frac{K_{02}^2 (P_{01} + P_{02})}{N_2}\right) \tag{5.75}$$

$$R_{01} + R_{12} < C\left(\frac{K_{02}^2 P_{01} + K_{12}^2 P_{12}}{N_2}\right) \tag{5.76}$$

$$\vdots$$

$$\begin{aligned} &R_{01} + R_{02} + R_{12} + \ldots + R_{120} \\ &< C\left(\frac{K_{02}^2 (P_{01} + P_{02} + P_{012} + P_{021}) + K_{12}^2 (P_{12} + P_{10} + P_{102} + P_{120})}{N_2}\right) \end{aligned} \tag{5.77}$$

Among all W's that may be decoded by node 2, it is required to decode W_{021} and W_{120} so that a relay can take place in the next block. Thus, no matter if node 2 can decode other messages, this node must impose constraints on R_{021} and R_{120} as long as W_{021} and W_{120} are employed. In other words, (5.73) and (5.74) must be satisfied, regardless of the network scenario. They are called criterion constraints and are shown in bold fonts. The importance of criterion constraints will be further explained later. Similarly, for node 0, the conjectured rate constraints are

$$R_{12} < C\left(\frac{K_{10}^2 P_{12}}{N_0}\right) \tag{5.78}$$

$$R_{10} < C\left(\frac{K_{10}^2 P_{10}}{N_0}\right) \tag{5.79}$$

$$R_{120} < C\left(\frac{K_{10}^2 P_{120}}{N_0}\right) \tag{5.80}$$

$$\boldsymbol{R}_{102} < \boldsymbol{C}\left(\frac{\boldsymbol{K}_{10}^2 \boldsymbol{P}_{102}}{\boldsymbol{N}_0}\right) \tag{5.81}$$

$$R_{12} + R_{10} < C\left(\frac{K_{10}^2 (P_{12} + P_{10})}{N_0}\right) \tag{5.82}$$

$$R_{12} + R_{120} < C\left(\frac{K_{10}^2 (P_{12} + P_{120})}{N_0}\right) \tag{5.83}$$

$$\vdots$$

$$R_{12} + R_{10} + R_{120} + R_{102} < C\left(\frac{K_{10}^2 (P_{12} + P_{10} + P_{120} + P_{102})}{N_0}\right). \tag{5.84}$$

Among them, node 0 has to decode W_{102}, and thus impose the constraint on R_{102}. For node 1, the constraints are

$$R_{01} < C\left(\frac{K_{01}^2 P_{01}}{N_1}\right) \tag{5.85}$$

$$R_{02} < C\left(\frac{K_{01}^2 P_{02}}{N_0}\right) \tag{5.86}$$

$$R_{021} < C\left(\frac{K_{01}^2 P_{021}}{N_2}\right) \tag{5.87}$$

$$\boldsymbol{R}_{012} < \boldsymbol{C}\left(\frac{\boldsymbol{K}_{01}^2 \boldsymbol{P}_{012}}{\boldsymbol{N}_1}\right) \tag{5.88}$$

$$R_{01} + R_{02} < C\left(\frac{K_{01}^2 (P_{01} + P_{02})}{N_1}\right) \tag{5.89}$$

$$R_{01} + R_{021} < C\left(\frac{K_{01}^2 (P_{01} + P_{021})}{N_1}\right) \tag{5.90}$$

$$\vdots$$

$$R_{01} + R_{02} + R_{021} + R_{012} < C\left(\frac{K_{01}^2 (P_{01} + P_{02} + P_{021} + P_{012})}{N_0}\right). \tag{5.91}$$

Among them, node 1 has to decode W_{012}, and thus impose the constraint on R_{012}.

In the backward decoding stage, node 0 has to decode W_{10} and W_{120}. The constraints will be relaxed if W_{12} can be decoded as well, instead of being considered as noise. Thus, the constraints are

$$R_{12} < C\left(\frac{K_{10}^2 P_{12}}{N_0}\right) \tag{5.92}$$

$$\boldsymbol{R}_{10} < \boldsymbol{C}\left(\frac{\boldsymbol{K}_{10}^2 \boldsymbol{P}_{10}}{\boldsymbol{N}_0}\right) \tag{5.93}$$

$$R_{10} + R_{12} < C\left(\frac{K_{10}^2 (P_{12} + P_{10})}{N_0}\right) \tag{5.94}$$

$$\begin{aligned}&\boldsymbol{R}_{10}+\boldsymbol{R}_{12}+\boldsymbol{R}_{120}\\&<\boldsymbol{C}\left(\frac{\boldsymbol{K}_{10}^{2}(\boldsymbol{P}_{12}+\boldsymbol{P}_{10}+\boldsymbol{P}_{120}+\boldsymbol{P}_{U10})+\boldsymbol{K}_{20}^{2}\boldsymbol{P}_{U20}+2\boldsymbol{K}_{10}\boldsymbol{K}_{20}\sqrt{\boldsymbol{P}_{U10}\boldsymbol{P}_{U20}}}{\boldsymbol{N}_{0}}\right).\end{aligned}\tag{5.95}$$

Notice that signals associated other messages, such as W_{102}, are removed from the received signal because these messages have been obtained in the forward decoding stage. In the same way, for node 1, if all messages are decoded, the constraints are

$$R_{02}<C\left(\frac{K_{01}^{2}P_{02}}{N_{1}}\right)\tag{5.96}$$

$$\boldsymbol{R}_{01}<\boldsymbol{C}\left(\frac{\boldsymbol{K}_{01}^{2}\boldsymbol{P}_{01}}{\boldsymbol{N}_{1}}\right)\tag{5.97}$$

$$R_{01}+R_{02}<C\left(\frac{K_{01}^{2}(P_{01}+P_{02})}{N_{1}}\right)\tag{5.98}$$

$$\begin{aligned}&\boldsymbol{R}_{01}+\boldsymbol{R}_{02}+\boldsymbol{R}_{021}\\&<\boldsymbol{C}\left(\frac{\boldsymbol{K}_{01}^{2}(\boldsymbol{P}_{01}+\boldsymbol{P}_{02}+\boldsymbol{P}_{021}+\boldsymbol{P}_{U01})+\boldsymbol{K}_{21}^{2}\boldsymbol{P}_{U21}+2\boldsymbol{K}_{01}\boldsymbol{K}_{21}\sqrt{\boldsymbol{P}_{U01}\boldsymbol{P}_{U21}}}{\boldsymbol{N}_{1}}\right).\end{aligned}\tag{5.99}$$

Among them, W_{01} and W_{021} are required to be obtained. For node 2, it is necessary to decode W_{02}, W_{12}, W_{012}, and W_{102} if they are employed. The conjectured constraints are

$$R_{01}<C\left(\frac{K_{02}^{2}P_{01}}{N_{2}}\right)\tag{5.100}$$

$$R_{10}<C\left(\frac{K_{12}^{2}P_{10}}{N_{2}}\right)\tag{5.101}$$

$$\boldsymbol{R}_{02}<\boldsymbol{C}\left(\frac{\boldsymbol{K}_{02}^{2}\boldsymbol{P}_{02}}{\boldsymbol{N}_{2}}\right)\tag{5.102}$$

$$\boldsymbol{R}_{12}<\boldsymbol{C}\left(\frac{\boldsymbol{K}_{12}^{2}\boldsymbol{P}_{12}}{\boldsymbol{N}_{2}}\right)\tag{5.103}$$

$$R_{01} + R_{10} < C\left(\frac{K_{02}^2 P_{01} + K_{12}^2 P_{10}}{N_2}\right) \tag{5.104}$$

$$R_{01} + R_{02} < C\left(\frac{K_{02}^2 P_{01} + K_{02}^2 P_{02}}{N_2}\right) \tag{5.105}$$

$$\vdots \tag{5.106}$$

$$R_{01} + R_{10} + R_{02} + R_{12} < C\left(\frac{K_{02}^2 (P_{01} + P_{02}) + K_{12}^2 (P_{10} + P_{12})}{N_2}\right) \tag{5.107}$$

$$\begin{aligned} &\boldsymbol{R}_{02} + \boldsymbol{R}_{12} + \boldsymbol{R}_{012} + \boldsymbol{R}_{102} + \boldsymbol{R}_{10} + \boldsymbol{R}_{01} \\ &< \boldsymbol{C}\left(\frac{\boldsymbol{K}_{02}^2 (\boldsymbol{P}_{01} + \boldsymbol{P}_{02} + \boldsymbol{P}_{012} + \boldsymbol{P}_{U02}) + \boldsymbol{K}_{12}^2 (\boldsymbol{P}_{10} + \boldsymbol{P}_{12} + \boldsymbol{P}_{102} + \boldsymbol{P}_{U12})}{\boldsymbol{N}_0}\right. \\ &\left.\frac{+2\boldsymbol{K}_{02}\boldsymbol{K}_{12}\sqrt{\boldsymbol{P}_{U02}\boldsymbol{P}_{U12}}}{}\right) \end{aligned} \tag{5.108}$$

The set of constraints associated with a node and a decoding stage is termed a group. In total, there are six groups of constraints. Obviously, some inequalities may be redundant. For example, if (5.71) holds for a specific scenario, node 2 does not have to decode W_{012} again in the backward decoding stage. This means it is not necessary for node 1 to relay signals from node 0 to node 2 since node 2 can know what they would transmit coherently. As a result, the operation on W_{012} is identical to W_{02}. Therefore, W_{012} is not considered in the communication scheme. P_{102} is set to 0. Consequently, some constraints are not meaningful for a specific scenario. We list all of them because these constraints will be used as the foundation for several scenarios. For each scenario, we will derive a reduced set of constraints from these.

There are six normalized noise measures to be considered. In the rate constraints, there are three types of quantities: signal power, path gain, and noise power. Signal power

is our design variable, whereas path gain and noise are determined by the network scenarios. Our goal is to derive achievable rate regions for various scenarios. This means we have to consider a variety of combinations of path gain and noise power. Nevertheless, there are only six combinations, and their appearance can be interpreted easily. There are three noise components. For each component, the other two nodes have different perceptions. For a fixed signal power, if the path gain is low, i.e., attenuation is high, the noise appears more substantial. Consequently, noise power should be normalized by the square of path gain. Assuming the path gains are reciprocal, which means $K_{ij} = K_{ji}$, this normalization ends up with six quantities: N_2 / K_{12}^2, N_2 / K_{02}^2, N_1 / K_{21}^2, N_1 / K_{01}^2, N_0 / K_{10}^2, and N_0 / K_{20}^2.

5.5.1 $\frac{N_2}{K_{12}^2} < \frac{N_2}{K_{02}^2} < \frac{N_1}{K_{01}^2}, \frac{N_0}{K_{10}^2}$

We consider several kinds of relationships among them. Each relationship can be associated with a specific network configuration. First, we consider the configuration where node 2 is located between node 0 and 1, as depicted in Figure 5.20. We assume that the power spectrum densities are the same and the path gains are inversely proportional to the distance with an exponent whose value is greater than 1. Thus, the relationship among the normalized noise components is

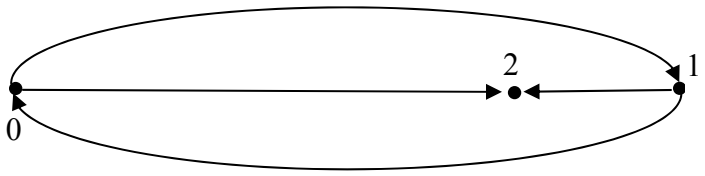

Figure 5.20: node 2 is in between node 0 and node 1, and closer to node 1.

$$\frac{N_2}{K_{12}^2} < \frac{N_2}{K_{02}^2} < \frac{N_1}{K_{01}^2}, \frac{N_0}{K_{10}^2}. \tag{5.109}$$

Notice that N_1 / K_{21}^2 and N_0 / K_{20}^2 do not emerge in (5.109). The reason is that they do not show up in any inequality, and thus their values are irrelevant. With (5.109), we can determine which inequalities in the conjectured rate region hold, and then we can obtain a reduced set of constraints. Now, we focus on the constraints of R_{10} in the form $R_{10} < C(\bullet)$, which include (5.70), (5.79), (5.93), and (5.101). Among these four constraints, (5.93) must hold in order to decode W_{10} at node 1, regardless of the relationship among normalized noise measures. This decoding is compulsory in this communication scheme. Thus, it is more like a given condition from this point of view, and so called the criterion constraint. (5.70), (5.79), or (5.101) are inequalities to be verified. If (5.70), (5.79), or (5.101) is satisfied for a specific relationship between normalized noise measures, it will facilitate the decoding, in the sense of relaxing the criterion constraint, for the node from which the constraint comes. With (5.109), all regions of (5.70), (5.79), or (5.101) contain the region of (5.93). When (5.70) holds, for example, node 2 is able to decode W_{10}, instead of regarding it as noise, at the same time it tries to decode other messages. Consequently, the noise power is reduced by $K_{12}^2 P_{10}$ and it is easier to decode other W's at node 2. Meanwhile, this additional and beneficial decoding does not impose a tighter constraint for node 0 to decode W_{10}. In other words, this decoding is transparent to node 0.

Obviously, it is imperative to identify the criterion constraints first. These are the

constraints associated with the W's that must be decoded at each node. We have pointed out these W's. To summarize, in the forward decoding stage, they are W_{021} and W_{120} at node 2, W_{102} at node 0, and W_{012} at node 1. In the backward decoding stage, they are W_{10} and W_{120} at node 0, W_{01} and W_{021} at node 1, and W_{02}, W_{12}, W_{012} and W_{102} at node 2. They correspond to (5.73), (5.74), (5.81), (5.88), (5.93), (5.95), (5.97), (5.99), (5.102), (5.103) and (5.108).

Rather than considering constraints for each R, as demonstrated above for R_{10}, it is easier to start from the relationship of normalized noise measures. First, we notice that N_2 / K_{12}^2 is the smallest, i.e.

$$\frac{N_2}{K_{12}^2} < \frac{N_2}{K_{02}^2}, \frac{N_1}{K_{01}^2}, \frac{N_0}{K_{10}^2}.$$

Then, we search for inequalities containing N_2 / K_{12}^2. They are (5.101), (5.72), (5.69), (5.103) and (5.70). Among them, (5.103) is one of the criterion constraints, and thus must be excluded for verification. For each of the other three inequalities, compare it with the corresponding criterion constraint to determine if it is true given the criterion constraint. For example, the criterion constraint for (5.101) is (5.93), and $C(K_{12}^2 P_{10} / N_2)$ is greater than $C(K_{10}^2 P_{10} / N_0)$. Consequently, (5.101) holds. In the same way, (5.72) and (5.70) hold. (5.69) also holds because it is identical to its criterion constraint (5.103).

Similarly, we start another series of determinations from

$$\frac{N_2}{K_{02}^2} < \frac{N_1}{K_{01}^2}, \frac{N_0}{K_{10}^2}.$$

(5.67), (5.71) and (5.100) are valid. (5.68) is identical to its criterion constraint (5.102).

At this moment, all simple inequalities, which are those with only one rate component at the left hand side, for node 2 in the forward decoding stage, including criterion and non-criterion ones, hold. We call the status in which all constraints in a group are valid as being verified. Then, the group is invulnerable to other groups in the sense that the achievable rate region determined by this group is fixed regardless of what happens to other groups. Notice that we do not have to pay attention to constraints which are neither simple nor criterion constraints. These non-simple constraints do not cut the original achievable rate region before expansion. In other words, they do not impose any tighter constraint. In Figure 5.12, the non-simple constraint which shows up after rate expansion and the original constraint intersect at point B. However, the original achievable rate region is also constrained by line GH, which lies to the left of point B. Therefore, the non-simple constraint is looser than the original constraint, given that the associated simple constraints hold.

If a group is not verified, the verified simple constraints in that group may become invalid or the criterion constraints may change after a constraint in that group is determined to be invalid. For example, if (5.78) does not hold for a specific network scenario, while other simple inequalities, i.e., (5.79) and (5.80) in that group have been verified as valid, then W_{12} has to be regarded as noise by node 0 in the forward decoding stage. Thus, the whole achievable rate region for that group has to be rewritten as

$$R_{10} < C\left(\frac{K_{10}^2 P_{10}}{N_0 + K_{10}^2 P_{12}}\right) \tag{5.110}$$

$$R_{120} < C\left(\frac{K_{10}^2 P_{120}}{N_0 + K_{10}^2 P_{12}}\right) \tag{5.111}$$

$$\boldsymbol{R}_{102} < \boldsymbol{C}\left(\frac{\boldsymbol{K}_{10}^{2}\boldsymbol{P}_{102}}{\boldsymbol{N}_{0}+\boldsymbol{K}_{10}^{2}\boldsymbol{P}_{12}}\right) \tag{5.112}$$

$$R_{10}+R_{120} < C\left(\frac{K_{10}^{2}(P_{10}+P_{120})}{N_{0}+K_{10}^{2}P_{12}}\right) \tag{5.113}$$

$$R_{10}+R_{102} < C\left(\frac{K_{10}^{2}(P_{10}+P_{102})}{N_{0}+K_{10}^{2}P_{12}}\right) \tag{5.114}$$

$$R_{120}+R_{102} < C\left(\frac{K_{10}^{2}(P_{120}+P_{102})}{N_{0}+K_{10}^{2}P_{12}}\right) \tag{5.115}$$

$$R_{10}+R_{120}+R_{102} < C\left(\frac{K_{10}^{2}(P_{10}+P_{120}+P_{102})}{N_{0}+K_{10}^{2}P_{12}}\right). \tag{5.116}$$

Although the rate constraints for R_{10} and R_{120} were verified, (5.110) and (5.111) have to verified again because the constraint is tighter now and it may not be looser than the criterion constraint anymore. If this happens to the new verification of a simple constraint, this simple constraint changes to be not valid. Then it has to be regarded as noise and other constraints are required to be rewritten.

In addition, the modification is not limited to the same group. Since (5.112) is a criterion constraint, after it is tightened, the constraints on R_{102} in other groups have to be verified again. Consequently, the inequalities that did not hold may turn out to be valid, while those that were valid still hold.

Now, the first group is verified and the achievable rate region determined by this group is not subject to changes of inequalities in other groups. This region suggests that node 2 could decode all W's contained in the received signal, including W_{012} and W_{102}. However, W_{012} and W_{102} were originally intended to be decoded from the coherently combined signal in the backward decoding stage. For example, W_{012} should be decoded

by node 1 in the forward decoding stage. Then, node 0 and node 1 transmit signals which combine coherently. Finally, node 2 decodes W_{012} based on the combined signal in the backward decoding stage. Now, since node 2 can and should decode W_{012} in the forward decoding stage, it is worthless for node 0 and 1 to cooperate. Accordingly, U_{12} and U_{02} are not functions of W_{012}. Therefore, the role played by W_{012} is exactly identical to W_{02}. In other words, messages starting from node 0 and ending at node 2 do not have to be relayed by node 1, and W_{012} should be absorbed in W_{02}. Similarly, we can conclude W_{102} should not be employed. This is equivalent to setting P_{012} and P_{102} to 0.

Since W_{102} is not used anymore, node 0 does not have to decode W_{102} and or do any other additional decoding to facilitate the decoding of W_{102} in the forward decoding stage. The criterion constraint (5.81) as well as other constraints (5.78)—(5.84) in the second group are all removed, regardless of whether they hold. Likewise, node 1 is not required to decode W_{012}, and (5.85)—(5.91) are eliminated.

Also, W_{02} and W_{12} should now be decoded in the forward decoding stage. Originally, they were intended to be decoded with W_{012} and W_{102} by node 2 in the backward decoding stage. Now that W_{012} and W_{102} are not used, W_{02} and W_{12} can be decoded in the forward decoding stage and the achievable rate region constrained by (5.100)—(5.108) can be removed. Notice that two criterion constraints (5.102) and (5.103) are among what is removed. Because W_{02} is now obtained in the forward decoding stage, the new criterion constraint for R_{02} is (5.68). In the same way, (5.69) replaces

(5.103) as the criterion constraint.

At this point, what remains are (5.67)—(5.77), (5.92)—(5.95), and (5.96)—(5.99). Among them, (5.67)—(5.77) have be verified. In (5.92)—(5.95), and (5.96)—(5.99), the simple inequalities which are not criterion ones are (5.92) and (5.96). Compared with their criterion constraints, i.e., (5.69) and (5.68), respectively, both of them do not hold. Therefore, they should be regarded as noise of values $K_{10}^2 P_{12}$ and $K_{01}^2 P_{02}$. Consequently, the constraints in the fourth and the fifth groups should be rewritten. At this moment, all simple inequalities either have been verified or are criterion ones. The achievable rate region is thus as follows.

In the forward decoding stage, for node 2:

$$R_{01} < C\left(\frac{K_{02}^2 P_{01}}{N_2}\right) \tag{5.117}$$

$$R_{02} < C\left(\frac{K_{02}^2 P_{02}}{N_2}\right) \tag{5.118}$$

$$R_{12} < C\left(\frac{K_{12}^2 P_{12}}{N_2}\right) \tag{5.119}$$

$$R_{10} < C\left(\frac{K_{12}^2 P_{10}}{N_2}\right) \tag{5.120}$$

$$\boldsymbol{R}_{021} < \boldsymbol{C}\left(\frac{\boldsymbol{K}_{02}^2 \boldsymbol{P}_{021}}{\boldsymbol{N}_2}\right) \tag{5.121}$$

$$\boldsymbol{R}_{120} < \boldsymbol{C}\left(\frac{\boldsymbol{K}_{12}^2 \boldsymbol{P}_{120}}{\boldsymbol{N}_2}\right) \tag{5.122}$$

$$R_{01} + R_{02} < C\left(\frac{K_{02}^2 (P_{01} + P_{02})}{N_2}\right) \tag{5.123}$$

$$R_{01} + R_{12} < C\left(\frac{K_{02}^2 P_{01} + K_{12}^2 P_{12}}{N_2}\right) \tag{5.124}$$

$$\vdots$$

$$R_{01} + R_{02} + R_{12} + \ldots + R_{120}$$
$$< C\left(\frac{K_{02}^2(P_{01} + P_{02} + P_{012} + P_{021}) + K_{12}^2(P_{12} + P_{10} + P_{102} + P_{120})}{N_2}\right) \tag{5.125}$$

In the backward decoding stage, for node 0

$$\boldsymbol{R}_{10} < \boldsymbol{C}\left(\frac{\boldsymbol{K}_{10}^2\boldsymbol{P}_{10}}{\boldsymbol{N}_0 + \boldsymbol{K}_{10}^2\boldsymbol{P}_{12}}\right) \tag{5.126}$$

$$\boldsymbol{R}_{10} + \boldsymbol{R}_{120} < \boldsymbol{C}\left(\frac{\boldsymbol{K}_{10}^2(\boldsymbol{P}_{12} + \boldsymbol{P}_{120} + \boldsymbol{P}_{U10}) + \boldsymbol{K}_{20}^2\boldsymbol{P}_{U20} + 2\boldsymbol{K}_{10}\boldsymbol{K}_{20}\sqrt{\boldsymbol{P}_{U10}\boldsymbol{P}_{U20}}}{\boldsymbol{N}_0 + \boldsymbol{K}_{10}^2\boldsymbol{P}_{12}}\right) \tag{5.127}$$

In the backward decoding stage, for node 1

$$\boldsymbol{R}_{01} < \boldsymbol{C}\left(\frac{\boldsymbol{K}_{01}^2\boldsymbol{P}_{01}}{\boldsymbol{N}_1 + \boldsymbol{K}_{01}^2\boldsymbol{P}_{02}}\right) \tag{5.128}$$

$$\boldsymbol{R}_{01} + \boldsymbol{R}_{021} < \boldsymbol{C}\left(\frac{\boldsymbol{K}_{01}^2(\boldsymbol{P}_{01} + \boldsymbol{P}_{021} + \boldsymbol{P}_{U01}) + \boldsymbol{K}_{21}^2\boldsymbol{P}_{U21} + 2\boldsymbol{K}_{01}\boldsymbol{K}_{21}\sqrt{\boldsymbol{P}_{U01}\boldsymbol{P}_{U21}}}{\boldsymbol{N}_1 + \boldsymbol{K}_{01}^2\boldsymbol{P}_{02}}\right) \tag{5.129}$$

Obviously, (5.117) and (5.120) contain their respective criterion constraints (5.128) and (5.126), and thus are redundant. There are listed there to emphasize that R_{01}, R_{10}, $K_{02}^2P_{01}$, and $K_{12}^2P_{10}$ are considered in (5.123)—(5.125). The substream flows are demonstrated in Figure 5.21—Figure 5.24, corresponding the achievable rate region. Different types of lines are used for different substreams. Note that the decoding which is beneficial to the criterion constraints is not shown. For example, at node 2 in the forward decoding stage, the decoding of W_{01} and W_{10} is not shown in Figure 5.21 and Figure 5.22 because they are not intended to node 2.

This achievable rate region is reasonable. Node 2 is located between node 0 and node 1. Between node 0 and 1, if one node wants the other node to relay signals to node 2,

it has to emanate signals, and the signals will also be received by node 2. As the signal to noise ratio at node 2 is higher, node 2 is also able to decode the signals intended to be relayed. As a result, any information stream ending in node 2 is not necessary for cooperative communications. By contrast, node 2 can help relay messages from either node 1 to 0or from node 0 to 1. When node 2 relays signals, each signal is combined coherently with the signal from the information source node. In this sense, node 2 is the hub of in-

Figure 5.21: Node 2 decodes W_{12} and W_{120} in the forward decoding stage.

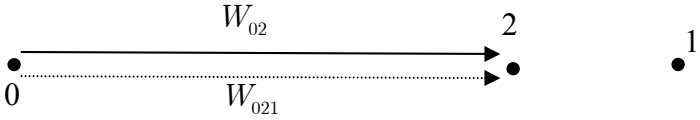

Figure 5.22: Node 2 decodes W_{02} and W_{021} in the forward decoding stage.

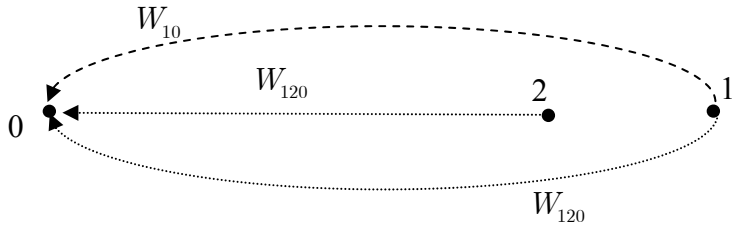

Figure 5.23: Node 0 decodes W_{10} and coherently combined W_{120} in the backward decoding stage.

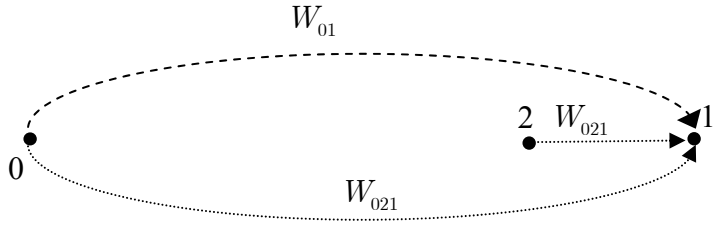

Figure 5.24: Node 1 decodes W_{01} and coherently combined W_{021} in the backward decoding stage.

formation flows.

5.5.2 $\frac{N_2}{K_{12}^2} < \frac{N_1}{K_{01}^2} = \frac{N_0}{K_{10}^2} < \frac{N_2}{K_{02}^2}$

In this subsection, we will derive an achievable rate region for the network scenario as depicted in Figure 5.25. As in the last subsection, there are also four information streams: node 0 to nodes 1 and 2, and node 1 to nodes 0 and 2. The only difference is the node location. Nodes 1 and 2 are close to each other, and they are both far from node 0. Between nodes 1 and 2, node 1 is closer to node 0.

We will use the same concept as in the previous subsection to derive the achievable rate region. We start from the same sets of conjectured constraints (5.67)—(5.108). To start with, we assume that the relationship between normalized noise measures is

$$\frac{N_2}{K_{12}^2} < \frac{N_1}{K_{01}^2} = \frac{N_0}{K_{10}^2} < \frac{N_2}{K_{02}^2}. \tag{5.130}$$

Again, we assume N_0, N_1 and N_2 are roughly in the same order. Thus, (5.130) corresponds to the setting in Figure 5.25, and we focus on the influences of distances between nodes. If the unnormalized noise power values varies over a wide range so that (5.130) does not hold, the achievable rate region will be different. For example, if the relationship among unnormalized noise power values is (5.109), the achievable rate region

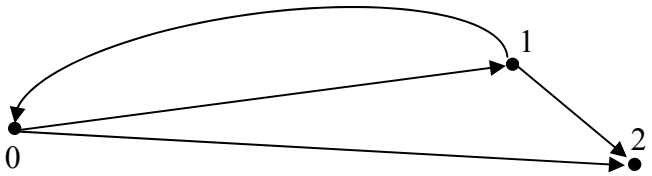

Figure 5.25: node 0 is far from nodes 1 and 2, while node 1, compared with node 2, is closer to node 0

is the same as that in the last subsection even if the network setting is like Figure 5.25. As the derivation proceeds, we will investigate several relationships of unnormalized noise measures, all of which obey (5.130).

Since what is required to be decoded in both stages is unchanged before derivation, the criterion constraints are still (5.73), (5.74), (5.81), (5.88), (5.93), (5.95), (5.97), (5.99), (5.102), (5.103) and (5.108). As the derivation proceeds based on (5.130), the set of criterion constraints will change. The derivation for this network is more involved than in the last subsection. Some issues which are briefly mentioned in the last subsection will occur here. In this subsection, there are two events that may happen and will make the derivation more difficult. First, the verified simple constraint in an unverified group may become invalid if another simple constraint in that group does not hold and thus the noise power in the verified constraint is increased. Secondly, the invalid constraint may become valid if the noise power in its criterion constraint increases. We will point out some of these events when they happen. Even with these two annoyances, nevertheless, the constraints in a verified group are still fixed. Because the group is verified, the first annoyance will not happen. Because there is no invalid constraint, the second annoyance is also avoided. Therefore, our objective is to identify and construct verified groups. We did not explicitly mention this objective in the last subsection because the configuration there is simpler and the derivation can proceed without this objective in mind. Without this objective in mind in this subsection, it is difficult to obtain the achievable rate region. Actually, they are just different orders of verification, and both orders lead to the same result.

We find out that (5.85) is identical to its criterion constraint (5.97). Because

$N_1 / K_{01}^2 < N_2 / K_{02}^2$, (5.86) and (5.87) hold, compared with their criterion constraints (5.102) and (5.73) respectively. Now, all simple and non-criterion constraints (5.85)—(5.87) in the third group have been verified, and thus this group is verified and fixed. From these inequalities, it is beneficial to decode W_{01}, W_{02}, and W_{021} for node 1 in the forward decoding stage. Notice that W_{01} and W_{021} were originally decoded in the backward decoding stage. Now, this stage is not required. W_{021} is decoded by node 1 before it is relayed by node 2. Thus the role of W_{021} can be replaced by W_{01} and so $P_{021} = 0$. The new conjectured achievable rage region is determined by (5.131)—(5.137), and (5.131) becomes the new criterion constraint on R_{10}.

Since this group is fixed, the criterion constraints, (5.131) and (5.133) in this group are also fixed. Then, if we proceed from these inequalities, we can avoid the second annoyance. First, (5.67) and (5.100) do not hold, compared with (5.131), and $K_{02}^2 P_{01}$ is thus regarded as noise in both groups. Secondly, (5.71) does not hold, compared with (5.133), and $K_{02}^2 P_{012}$ is regarded as noise.

Although W_{012} is not decoded in the current block, when we proceed to the next block, W_{012} is encoded in signals again because it is a relay-path signal. Actually, it is encoded in several signals, including the coherent combining ones. At this block, if W_{012} is not decoded from these signals, it is very difficult to decode other messages. As a matter of fact, since it is encoded in several signals, it is very easy to decode this message now. Thereafter, we make this assumption whenever this kind of situation occurs, and

ignore the constraint to decode this message. Now, we are going to make a further classification on normalized noise measures. It is helpful to list the constraints we have developed:

For node 1 in the forward decoding stage:

$$\boldsymbol{R}_{01} < \boldsymbol{C}\left(\frac{\boldsymbol{K}_{01}^2\boldsymbol{P}_{01}}{\boldsymbol{N}_1}\right) \tag{5.131}$$

$$R_{02} < C\left(\frac{K_{01}^2 P_{02}}{N_0}\right) \tag{5.132}$$

$$\boldsymbol{R}_{012} < \boldsymbol{C}\left(\frac{\boldsymbol{K}_{01}^2\boldsymbol{P}_{012}}{\boldsymbol{N}_1}\right) \tag{5.133}$$

$$R_{01} + R_{02} < C\left(\frac{K_{01}^2(P_{01} + P_{02})}{N_1}\right) \tag{5.134}$$

$$R_{01} + R_{012} < C\left(\frac{K_{01}^2(P_{01} + P_{012})}{N_1}\right) \tag{5.135}$$

$$R_{02} + R_{012} < C\left(\frac{K_{01}^2(P_{02} + P_{012})}{N_1}\right) \tag{5.136}$$

$$R_{01} + R_{02} + R_{012} < C\left(\frac{K_{01}^2(P_{01} + P_{02} + P_{012})}{N_1}\right). \tag{5.137}$$

For node 0 in the forward decoding stage,

$$R_{12} < C\left(\frac{K_{10}^2 P_{12}}{N_0}\right) \tag{5.138}$$

$$R_{10} < C\left(\frac{K_{10}^2 P_{10}}{N_0}\right) \tag{5.139}$$

$$R_{120} < C\left(\frac{K_{10}^2 P_{120}}{N_0}\right) \tag{5.140}$$

$$\boldsymbol{R}_{102} < \boldsymbol{C}\left(\frac{\boldsymbol{K}_{10}^2\boldsymbol{P}_{102}}{\boldsymbol{N}_0}\right) \tag{5.141}$$

$$R_{12} + R_{10} < C\left(\frac{K_{10}^2(P_{12} + P_{10})}{N_0}\right) \tag{5.142}$$

$$R_{12} + R_{120} < C\left(\frac{K_{10}^2(P_{12} + P_{120})}{N_0}\right) \tag{5.143}$$

$$\vdots$$

$$R_{12} + R_{10} + R_{120} + R_{102} < C\left(\frac{K_{10}^2(P_{12} + P_{10} + P_{120} + P_{102})}{N_0}\right). \tag{5.144}$$

For node 2 in the forward decoding stage,

$$R_{02} < C\left(\frac{K_{02}^2 P_{02}}{N_2 + K_{02}^2 P_{01} + K_{02}^2 P_{012}}\right) \tag{5.145}$$

$$R_{12} < C\left(\frac{K_{12}^2 P_{12}}{N_2 + K_{02}^2 P_{01} + K_{02}^2 P_{012}}\right) \tag{5.146}$$

$$R_{10} < C\left(\frac{K_{12}^2 P_{10}}{N_2 + K_{02}^2 P_{01} + K_{02}^2 P_{012}}\right) \tag{5.147}$$

$$R_{102} < C\left(\frac{K_{12}^2 P_{102}}{N_2 + K_{02}^2 P_{01} + K_{02}^2 P_{012}}\right) \tag{5.148}$$

$$\boldsymbol{R}_{120} < \boldsymbol{C}\left(\frac{\boldsymbol{K}_{12}^2 \boldsymbol{P}_{120}}{\boldsymbol{N}_2 + \boldsymbol{K}_{02}^2 \boldsymbol{P}_{01} + \boldsymbol{K}_{02}^2 \boldsymbol{P}_{012}}\right) \tag{5.149}$$

$$\boldsymbol{R}_{021} < \boldsymbol{C}\left(\frac{\boldsymbol{K}_{02}^2 \boldsymbol{P}_{021}}{\boldsymbol{N}_2 + \boldsymbol{K}_{02}^2 \boldsymbol{P}_{01} + \boldsymbol{K}_{02}^2 \boldsymbol{P}_{012}}\right) \tag{5.150}$$

$$R_{02} + R_{12} < C\left(\frac{K_{02}^2 P_{02} + K_{12}^2 P_{12}}{N_2 + K_{02}^2 P_{01} + K_{02}^2 P_{012}}\right) \tag{5.151}$$

$$R_{02} + R_{10} < C\left(\frac{K_{02}^2 P_{02} + K_{12}^2 P_{10}}{N_2 + K_{02}^2 P_{01} + K_{02}^2 P_{012}}\right) \tag{5.152}$$

$$\vdots$$

$$\begin{aligned} &R_{02} + R_{12} + R_{10} + R_{102} + R_{120} \\ &< C\left(\frac{K_{02}^2 P_{02} + K_{12}^2 (P_{12} + P_{10} + P_{102} + P_{120})}{N_2 + K_{02}^2 P_{01} + K_{02}^2 P_{012}}\right) \end{aligned} \tag{5.153}$$

For node 0 in the backward decoding stage,

$$R_{12} < C\left(\frac{K_{10}^2 P_{12}}{N_0}\right) \tag{5.154}$$

$$\boldsymbol{R}_{10} < \boldsymbol{C}\left(\frac{\boldsymbol{K}_{10}^2 \boldsymbol{P}_{10}}{\boldsymbol{N}_0}\right) \tag{5.155}$$

$$R_{10} + R_{12} < C\left(\frac{K_{10}^2 (P_{12} + P_{10})}{N_0}\right) \tag{5.156}$$

$$\begin{aligned}&\boldsymbol{R}_{10} + \boldsymbol{R}_{12} + \boldsymbol{R}_{120} \\ &< \boldsymbol{C}\left(\frac{\boldsymbol{K}_{10}^2(\boldsymbol{P}_{12} + \boldsymbol{P}_{10} + \boldsymbol{P}_{120} + \boldsymbol{P}_{U10}) + \boldsymbol{K}_{20}^2 \boldsymbol{P}_{U20} + 2\boldsymbol{K}_{10}\boldsymbol{K}_{20}\sqrt{\boldsymbol{P}_{U10}\boldsymbol{P}_{U20}}}{\boldsymbol{N}_0}\right).\end{aligned} \tag{5.157}$$

For node 2 in the backward decoding stage

$$R_{10} < C\left(\frac{K_{12}^2 P_{10}}{N_2 + K_{02}^2 P_{01}}\right) \tag{5.158}$$

$$\boldsymbol{R}_{02} < \boldsymbol{C}\left(\frac{\boldsymbol{K}_{02}^2 \boldsymbol{P}_{02}}{\boldsymbol{N}_2 + \boldsymbol{K}_{02}^2 \boldsymbol{P}_{01}}\right) \tag{5.159}$$

$$\boldsymbol{R}_{12} < \boldsymbol{C}\left(\frac{\boldsymbol{K}_{12}^2 \boldsymbol{P}_{12}}{\boldsymbol{N}_2 + \boldsymbol{K}_{02}^2 \boldsymbol{P}_{01}}\right) \tag{5.160}$$

$$R_{01} + R_{10} < C\left(\frac{K_{02}^2 P_{01} + K_{12}^2 P_{10}}{N_2 + K_{02}^2 P_{01}}\right) \tag{5.161}$$

$$R_{01} + R_{02} < C\left(\frac{K_{02}^2 P_{01} + K_{02}^2 P_{02}}{N_2 + K_{02}^2 P_{01}}\right) \tag{5.162}$$

$$\vdots$$

$$R_{10} + R_{02} + R_{12} < C\left(\frac{K_{02}^2 (P_{01} + P_{02}) + K_{12}^2 (P_{10} + P_{12})}{N_2 + K_{02}^2 P_{01}}\right) \tag{5.163}$$

$$\begin{aligned}
&\boldsymbol{R}_{02}+\boldsymbol{R}_{12}+\boldsymbol{R}_{012}+\boldsymbol{R}_{102}+\boldsymbol{R}_{10}\\
&<\boldsymbol{C}\left(\frac{\boldsymbol{K}_{02}^{2}(\boldsymbol{P}_{02}+\boldsymbol{P}_{012}+\boldsymbol{P}_{U02})+\boldsymbol{K}_{12}^{2}(\boldsymbol{P}_{10}+\boldsymbol{P}_{12}+\boldsymbol{P}_{102}+\boldsymbol{P}_{U12})}{\boldsymbol{N}_{0}+\boldsymbol{K}_{02}^{2}\boldsymbol{P}_{01}}\right.\\
&\left.\frac{+2\boldsymbol{K}_{02}\boldsymbol{K}_{12}\sqrt{\boldsymbol{P}_{U02}\boldsymbol{P}_{U12}}}{}\right)
\end{aligned}\tag{5.164}$$

In (5.131)—(5.164), there is only one verified group (5.131)—(5.137). We have not constructed new verified groups from this verified group. It seems that we cannot make further simplifications. However, there are two groups with only one simple constraint which is not verified and not a criterion constraint. These two constraints are (5.154) and (5.158). There is a delicate relationship between them. The criterion constraint of (5.154) is (5.160). (5.160) may change if (5.158) is not verified. The reason that (5.158) cannot be verified is that its criterion constraint (5.155) may change if (5.154) is not verified. It seems as if there is a bottleneck among these four inequalities. To loosen this bottleneck, we notice that for the first type of annoyance to occur, it takes at least two simple constraints which are neither criterion constraints nor verified in a group. There is only one such constraint in each of these two groups. Thus, the first annoyance cannot happen. However, the second annoyance may still happen. Therefore, we should start from the constraint that can be verified (as valid). For this verified constraint, even if the noise power of its criterion constraint is increased later, this verified constraint is further valid.

5.5.2.1 $\frac{\boldsymbol{N}_{2}+\boldsymbol{K}_{02}^{2}\boldsymbol{P}_{01}}{\boldsymbol{K}_{12}^{2}}<\frac{\boldsymbol{N}_{0}}{\boldsymbol{K}_{10}^{2}}$

Among (5.154), (5.160), (5.158) and (5.155), the noise power of concern is $(N_2+K_{02}^2P_{01})/K_{12}^2$ and N_0/K_{10}^2. If

$$\frac{N_2 + K_{02}^2 P_{01}}{K_{12}^2} < \frac{N_0}{K_{10}^2}, \tag{5.165}$$

(5.158) holds and (5.158)—(5.164) is a verified group. (5.154) does not hold. Thus, the noise power in (5.155) is increased. The new constraints are (5.166) and (5.167). This group is also fixed.

$$\boldsymbol{R}_{10} < \boldsymbol{C}\left(\frac{\boldsymbol{K}_{10}^2 \boldsymbol{P}_{10}}{\boldsymbol{N}_0 + \boldsymbol{K}_{10}^2 \boldsymbol{P}_{12}}\right) \tag{5.166}$$

$$\boldsymbol{R}_{10} + \boldsymbol{R}_{120} < \boldsymbol{C}\left(\frac{\boldsymbol{K}_{10}^2(\boldsymbol{P}_{10} + \boldsymbol{P}_{120} + \boldsymbol{P}_{U10}) + \boldsymbol{K}_{20}^2 \boldsymbol{P}_{U20} + 2\boldsymbol{K}_{10}\boldsymbol{K}_{20}\sqrt{\boldsymbol{P}_{U10}\boldsymbol{P}_{U20}}}{\boldsymbol{N}_0 + \boldsymbol{K}_{10}^2 \boldsymbol{P}_{12}}\right). \tag{5.167}$$

Now, we have three more fixed criterion constraints, (5.159), (5.160) and (5.166), coming from two verified groups. We proceed to determine that (5.138), (5.145) and (5.146) do not hold. As a result, (5.145)—(5.153) are replaced by

$$R_{10} < C\left(\frac{K_{12}^2 P_{10}}{N_2 + K_{02}^2 P_{01} + K_{02}^2 P_{012} + K_{02}^2 P_{02} + K_{12}^2 P_{12}}\right) \tag{5.168}$$

$$R_{102} < C\left(\frac{K_{12}^2 P_{102}}{N_2 + K_{02}^2 P_{01} + K_{02}^2 P_{012} + K_{02}^2 P_{02} + K_{12}^2 P_{12}}\right) \tag{5.169}$$

$$\boldsymbol{R}_{120} < \boldsymbol{C}\left(\frac{\boldsymbol{K}_{12}^2 \boldsymbol{P}_{120}}{\boldsymbol{N}_2 + \boldsymbol{K}_{02}^2 \boldsymbol{P}_{01} + \boldsymbol{K}_{02}^2 \boldsymbol{P}_{012} + \boldsymbol{K}_{02}^2 \boldsymbol{P}_{02} + \boldsymbol{K}_{12}^2 \boldsymbol{P}_{12}}\right) \tag{5.170}$$

$$R_{10} + R_{102} < C\left(\frac{K_{12}^2 P_{10} + K_{12}^2 P_{102}}{N_2 + K_{02}^2 P_{01} + K_{02}^2 P_{012} + K_{02}^2 P_{02} + K_{12}^2 P_{12}}\right) \tag{5.171}$$

$$R_{10} + R_{120} < C\left(\frac{K_{12}^2 P_{10} + K_{12}^2 P_{120}}{N_2 + K_{02}^2 P_{01} + K_{02}^2 P_{012} + K_{02}^2 P_{02} + K_{12}^2 P_{12}}\right) \tag{5.172}$$

$$R_{102} + R_{120} < C\left(\frac{K_{12}^2 P_{102} + K_{12}^2 P_{120}}{N_2 + K_{02}^2 P_{01} + K_{02}^2 P_{012} + K_{02}^2 P_{02} + K_{12}^2 P_{12}}\right) \tag{5.173}$$

$$\begin{aligned} &R_{10} + R_{102} + R_{120} \\ &< C\left(\frac{K_{12}^2 (P_{10} + P_{102} + P_{120})}{N_2 + K_{02}^2 P_{01} + K_{02}^2 P_{012} + K_{02}^2 P_{02} + K_{12}^2 P_{12}}\right). \end{aligned} \tag{5.174}$$

(5.138)—(5.144) are replaced by

$$R_{10} < C\left(\frac{K_{10}^2 P_{10}}{N_0 + K_{10}^2 P_{12}}\right) \tag{5.175}$$

$$R_{120} < C\left(\frac{K_{10}^2 P_{120}}{N_0 + K_{10}^2 P_{12}}\right) \tag{5.176}$$

$$\boldsymbol{R}_{102} < \boldsymbol{C}\left(\frac{\boldsymbol{K}_{10}^2 \boldsymbol{P}_{102}}{\boldsymbol{N}_0 + \boldsymbol{K}_{10}^2 \boldsymbol{P}_{12}}\right) \tag{5.177}$$

$$R_{102} + R_{120} < C\left(\frac{K_{10}^2 (P_{120} + P_{10})}{N_0 + K_{10}^2 P_{12}}\right) \tag{5.178}$$

$$R_{10} + R_{102} < C\left(\frac{K_{10}^2 (P_{10} + P_{102})}{N_0 + K_{10}^2 P_{12}}\right) \tag{5.179}$$

$$R_{120} + R_{102} < C\left(\frac{K_{10}^2 (P_{120} + P_{102})}{N_0 + K_{10}^2 P_{12}}\right) \tag{5.180}$$

$$R_{10} + R_{120} + R_{102} < C\left(\frac{K_{10}^2 (P_{10} + P_{120} + P_{102})}{N_0 + K_{10}^2 P_{12}}\right). \tag{5.181}$$

In these two groups, there are four simple non-criterion constraints, (5.168), (5.169), (5.175), and (5.176). The situation is like (5.154)—(5.164). (5.169), (5.176) and their criterion constraints (5.170) and (5.177) form the bottleneck mentioned above. In addition, we have (5.168) and (5.175), which are both constraints on R_{10}. (5.175) is identical to its criterion constraint (5.166), while (5.168) cannot be determined unless we can determine the relationship between

$$\frac{N_2 + K_{02}^2 P_{01} + K_{02}^2 P_{012} + K_{02}^2 P_{02} + K_{12}^2 P_{12}}{K_{12}^2}$$

and $(N_0 + K_{10}^2 P_{12}) / K_{10}^2$.

The relationship

$$\frac{N_2 + K_{02}^2 P_{01} + K_{02}^2 P_{012} + K_{02}^2 P_{02}}{K_{12}^2} < \frac{N_0}{K_{10}^2} \tag{5.182}$$

occurs when the geographic locations of nodes are as demonstrated in Figure 5.26. Node 2 is very close to node 1 such that the left side of (5.182) is less than the right side even with three additional noise components. If (5.182) holds, then (5.168) as well as (5.169) hold while (5.176) does not. Now, (5.168)—(5.174) is a verified group, and they will not change no matter what happens to (5.175). Furthermore, according to (5.169), it is advantageous for node 2 to decode W_{102} in the forward decoding stage: node 0 does not have to decode and relay it. Because decoding W_{102} was the only requirement for node 0, it is now not required to decode any message in the forward decoding stage. Thus, W_{102} is incorporated with W_{12}, and P_{102} is set to 0. To conclude, when

$$\frac{N_2 + K_{02}^2 P_{01} + K_{02}^2 P_{012} + K_{02}^2 P_{02}}{K_{12}^2} < \frac{N_0}{K_{10}^2} = \frac{N_1}{K_{01}^2} < \frac{N_2}{K_{02}^2},$$

the achievable rate region is as follows:

For node 2 in the forward decoding stage,

$$R_{10} < C\left(\frac{K_{12}^2 P_{10}}{N_2 + K_{02}^2 P_{01} + K_{02}^2 P_{012} + K_{02}^2 P_{02} + K_{12}^2 P_{12}}\right) \tag{5.183}$$

$$\boldsymbol{R}_{120} < \boldsymbol{C}\left(\frac{\boldsymbol{K}_{12}^2 \boldsymbol{P}_{120}}{\boldsymbol{N}_2 + \boldsymbol{K}_{02}^2 \boldsymbol{P}_{01} + \boldsymbol{K}_{02}^2 \boldsymbol{P}_{012} + \boldsymbol{K}_{02}^2 \boldsymbol{P}_{02} + \boldsymbol{K}_{12}^2 \boldsymbol{P}_{12}}\right) \tag{5.184}$$

$$R_{10} + R_{120} < C\left(\frac{K_{12}^2 P_{10} + K_{12}^2 P_{120}}{N_2 + K_{02}^2 P_{01} + K_{02}^2 P_{012} + K_{02}^2 P_{02} + K_{12}^2 P_{12}}\right). \tag{5.185}$$

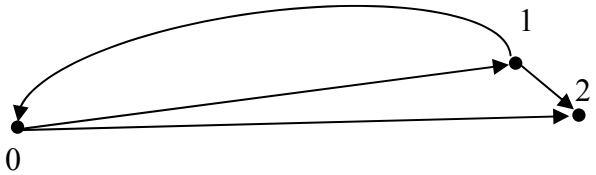

Figure 5.26: Node 2 is very close to node 1.

For node 1 in the forward decoding stage, the constraints are (5.131)—(5.137).

For node 0 in the backward decoding stage, the constraints are (5.166) and (5.167).

For node 2 in the backward decoding stage, the constraints are (5.158)—(5.164).

The flows of substreams are depicted in Figure 5.27—Figure 5.30. The first term in (5.182) can be interpreted as the thermal noise power plus all the received signal power from node 0, normalized by K_{12}^2. Because node 0 is too far from nodes 1 and 2, it cannot relay the information stream from node 1 to node 2. By contrast, since node 1 is in between, it can relay information from node 0. Besides, node 2, which is not in between node 0 and 1, but closer to node 1, can relay the information stream whose destination is node 0. Then, nodes 1 and 2 make their signals combine coherently at node 0.

Figure 5.27: Node 2 decodes W_{120} in the forward decoding stage.

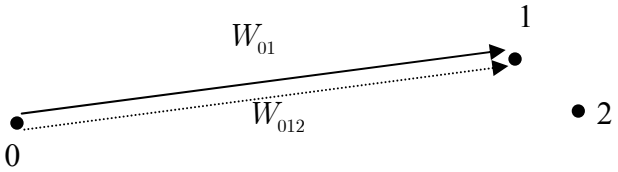

Figure 5.28: Node 1 decodes W_{01} and W_{012} in the forward decoding stage.

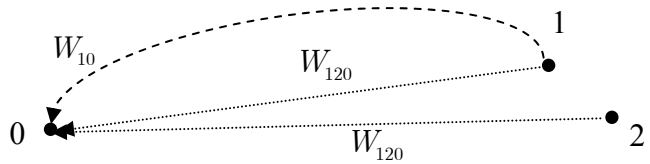

Figure 5.29: Node 0 decodes W_{120} and W_{10} in the backward decoding stage.

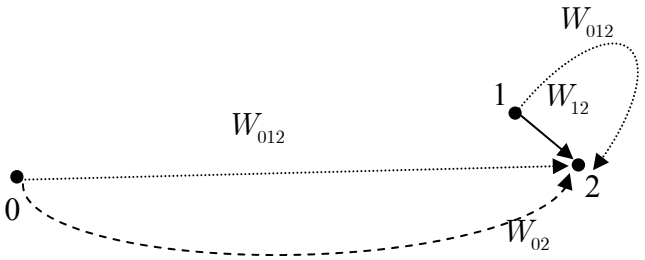

Figure 5.30: Node 2 decodes W_{012}, W_{12} and W_{02} in the backward decoding stage.

On the other hand, if node 2 is not so close to node 1, as demonstrated in Figure 5.31, then (5.182) does not hold. Consequently, (5.176) is valid while (5.168) and (5.169) are not. This is exactly the opposite outcome for the bottleneck among (5.169), (5.170), (5.176), and (5.177). Now, (5.175)—(5.181) is a verified group. With this verification, it is helpful for node 0 to decode W_{120} in the forward decoding stage. Thus, node 2 is not required to relay W_{120}, and this message should be incorporated with W_{10}. Consequently, node 2 does not have to perform any decoding in the forward decoding stage. Also, node 0 does not have this message to decode in the backward decoding stage. The other message W_{10} that node 0 intends to decoding in the backward decoding stage is now decoded in the forward decoding stage, as shown in (5.175). Therefore, node 0 is not required to perform any decoding in the backward decoding. To conclude, when

$$\frac{N_2 + K_{02}^2 P_{01}}{K_{12}^2} < \frac{N_0}{K_{10}^2} = \frac{N_1}{K_{01}^2} < \frac{N_2}{K_{02}^2} \tag{5.186}$$

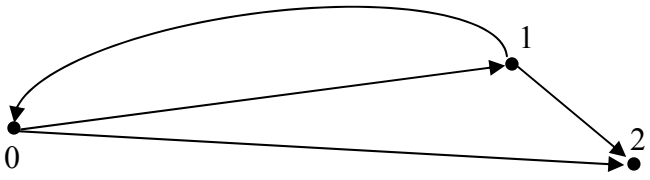

Figure 5.31: Node 2 is not so close to node 1.

and

$$\frac{N_2 + K_{02}^2 P_{01} + K_{02}^2 P_{012} + K_{02}^2 P_{02}}{K_{12}^2} > \frac{N_0}{K_{10}^2}, \tag{5.187}$$

the achievable rate region is composed of the following constraints:

For node 0 in the forward decoding stage,

$$R_{10} < C\left(\frac{K_{10}^2 P_{10}}{N_0 + K_{10}^2 P_{12}}\right) \tag{5.188}$$

$$\boldsymbol{R}_{102} < \boldsymbol{C}\left(\frac{\boldsymbol{K}_{10}^2 \boldsymbol{P}_{102}}{\boldsymbol{N}_0 + \boldsymbol{K}_{10}^2 \boldsymbol{P}_{12}}\right) \tag{5.189}$$

$$R_{10} + R_{102} < C\left(\frac{K_{10}^2 (P_{10} + P_{102})}{N_0 + K_{10}^2 P_{12}}\right) \tag{5.190}$$

For node 1 in the forward decoding stage, the constraints are (5.131)—(5.137).

For node 2 in the backward decoding stage, the constraints are (5.158)—(5.164).

The flows of substreams are shown in Figure 5.32—Figure 5.34. In this scenario, node 2 is not close enough to node 1 to make the left hand side of (5.187) less than the right hand side although (5.186) still holds. Therefore, node 2 cannot help node 1 to relay messages to node 0 as in the last scenario. By contrast, node 0 is able to help node 1 now. Meanwhile, node 1 can still help node 0. In the backward decoding stage, node 2 decodes both W_{102} and W_{012}. In this sense, node 0 and 1 are more as if in a cluster than node 1 and 2, although node 1 is closer to node 2 than to node 0. The reason is that node 2 would have up to 4 messages, i.e. W_{12}, W_{102}, W_{01}, and W_{012}, from the other two nodes to decode if it would like to help other nodes. On the contrary, because messages starting from node 0 are certainly known to node 0, node 0 has only up to 2 messages to decode, and thus it can afford to relay W_{102}.

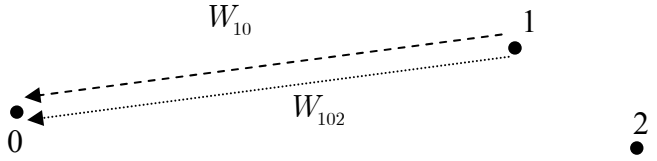

Figure 5.32: Node 0 decodes W_{10} and W_{102} in the forward decoding stage.

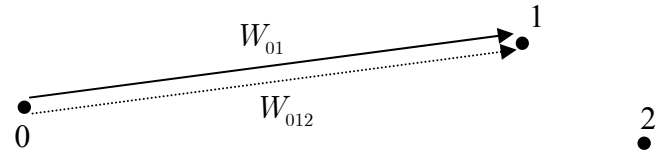

Figure 5.33: Node 1 decodes W_{01} and W_{012} in the forward decoding stage.

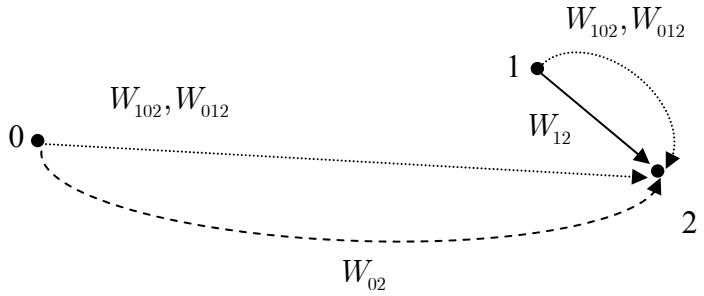

Figure 5.34: Node 2 decodes W_{02}, W_{12}, W_{102} and W_{012} in the backward decoding stage.

5.5.2.2 $\frac{\boldsymbol{N}_2 + \boldsymbol{K}_{02}^2 \boldsymbol{P}_{01}}{\boldsymbol{K}_{12}^2} > \frac{\boldsymbol{N}_0}{\boldsymbol{K}_{10}^2}$

Now, we consider the situation when (5.165) does not hold, i.e.

$$\frac{N_2 + K_{02}^2 P_{01}}{K_{12}^2} > \frac{N_0}{K_{10}^2}, \tag{5.191}$$

while

$$\frac{N_2}{K_{12}^2} < \frac{N_0}{K_{10}^2} = \frac{N_1}{K_{01}^2} < \frac{N_2}{K_{02}^2}$$

still holds. The geographic locations of sensors are demonstrated in Figure 5.35. We start

from (5.131)—(5.164), where the relationship between $(N_2 + K_{02}^2 P_{01})/K_{12}^2$ and N_0/K_{10}^2 has not been taken into consideration, and (5.131)—(5.137) are a verified group.

Now we face the bottleneck among (5.154), (5.155), (5.158), and (5.160) again. Because of (5.191), (5.154) holds, compared with its criterion constraint (5.160) even if the noise power in (5.160) increases. (5.154)—(5.157) form another verified group. In addition, (5.158) does not hold, compared with (5.155). Thus, the noise component for node 2 in the backward decoding stage becomes $N_2 + K_{02}^2 P_{01} + K_{12}^2 P_{10}$, (5.158)—(5.164) are replaced by (5.195)—(5.198), and they become a verified group. (5.147) is not valid, compared with (5.155), and thus the noise power in (5.145)—(5.153) increases by $K_{12}^2 P_{10}$. Consequently, modified (5.145) and (5.146) are not valid compared with their new criterion constraints (5.195) and (5.196). Thus, the noise power for node 2 in the forward decoding stage is increased. (5.145)—(5.153) are replaced by (5.192)—(5.194). Now, the constraints are composed of the following:

For node 2 in the forward decoding stage, the constraints are

$$\boldsymbol{R}_{102} < \boldsymbol{C}\left(\frac{\boldsymbol{K}_{12}^2 \boldsymbol{P}_{102}}{\boldsymbol{N}_2 + \boldsymbol{K}_{02}^2 \boldsymbol{P}_{01} + \boldsymbol{K}_{02}^2 \boldsymbol{P}_{012} + \boldsymbol{K}_{12}^2 \boldsymbol{P}_{10} + \boldsymbol{K}_{02}^2 \boldsymbol{P}_{02} + \boldsymbol{K}_{12}^2 \boldsymbol{P}_{12} + \boldsymbol{K}_{12}^2 \boldsymbol{P}_{10}}\right) \quad (5.192)$$

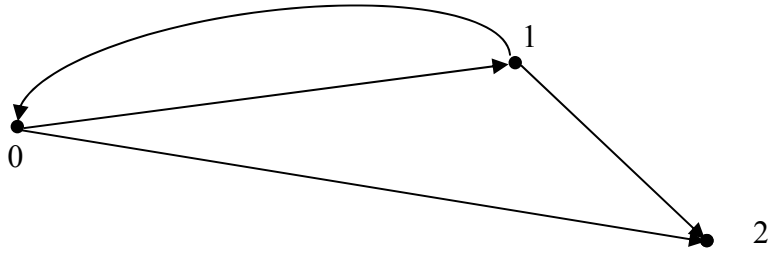

Figure 5.35: Node 2 is further away from node 1.

$$\boldsymbol{R}_{120} < \boldsymbol{C}\left(\frac{\boldsymbol{K}_{12}^2\boldsymbol{P}_{120}}{\boldsymbol{N}_2 + \boldsymbol{K}_{02}^2\boldsymbol{P}_{01} + \boldsymbol{K}_{02}^2\boldsymbol{P}_{012} + \boldsymbol{K}_{12}^2\boldsymbol{P}_{10} + \boldsymbol{K}_{02}^2\boldsymbol{P}_{02} + \boldsymbol{K}_{12}^2\boldsymbol{P}_{12} + \boldsymbol{K}_{12}^2\boldsymbol{P}_{10}}\right) \quad (5.193)$$

$$R_{102} + R_{120} < C\left(\frac{K_{12}^2(P_{102} + P_{120})}{N_2 + K_{02}^2P_{01} + K_{02}^2P_{012} + K_{12}^2P_{10} + K_{02}^2P_{02} + K_{12}^2P_{12} + K_{12}^2P_{10}}\right). \quad (5.194)$$

For node 0 in the forward decoding stage, the constraints are (5.138)—(5.144).

For node 1 in the forward decoding stage, the constraints are (5.131)—(5.137).

For node 0 in the backward decoding stage, the constraints are (5.154)—(5.157).

For node 2 in the backward decoding stage, the constraints are

$$\boldsymbol{R}_{02} < \boldsymbol{C}\left(\frac{\boldsymbol{K}_{02}^2\boldsymbol{P}_{02}}{\boldsymbol{N}_2 + \boldsymbol{K}_{02}^2\boldsymbol{P}_{01} + \boldsymbol{K}_{12}^2\boldsymbol{P}_{10}}\right) \quad (5.195)$$

$$\boldsymbol{R}_{12} < \boldsymbol{C}\left(\frac{\boldsymbol{K}_{12}^2\boldsymbol{P}_{12}}{\boldsymbol{N}_2 + \boldsymbol{K}_{02}^2\boldsymbol{P}_{01} + \boldsymbol{K}_{12}^2\boldsymbol{P}_{10}}\right) \quad (5.196)$$

$$R_{02} + R_{12} < C\left(\frac{K_{02}^2P_{02} + K_{12}^2P_{12}}{N_2 + K_{02}^2P_{01} + K_{12}^2P_{10}}\right) \quad (5.197)$$

$$\boldsymbol{R}_{02} + \boldsymbol{R}_{12} + \boldsymbol{R}_{012} + \boldsymbol{R}_{102}$$
$$< \boldsymbol{C}\left(\frac{\boldsymbol{K}_{02}^2(\boldsymbol{P}_{02} + \boldsymbol{P}_{012} + \boldsymbol{P}_{U02}) + \boldsymbol{K}_{12}^2(\boldsymbol{P}_{12} + \boldsymbol{P}_{102} + \boldsymbol{P}_{U12}) + 2\boldsymbol{K}_{02}\boldsymbol{K}_{12}\sqrt{\boldsymbol{P}_{U02}\boldsymbol{P}_{U12}}}{\boldsymbol{N}_0 + \boldsymbol{K}_{02}^2\boldsymbol{P}_{01} + \boldsymbol{K}_{12}^2\boldsymbol{P}_{10}}\right). \quad (5.198)$$

Among them, (5.131)—(5.137), (5.154)—(5.157), and (5.195)—(5.198) are the verified set. As we proceed, we find out (5.138) and (5.139) are valid, compared with (5.196) and (5.155) respectively. Again, we face a bottleneck among (5.192), (5.193), (5.140), and (5.141), where (5.193) and (5.141) are criterion constraints. Actually, the problem here is not so harsh. (5.140) is valid if (5.192) is valid. If (5.192) does not hold, the noise power in (5.193) intensifies, and it makes (5.140) more valid. Thus, (5.140) is valid unconditionally, and (5.138)—(5.144) form another verified group. Now, node 0 can decode W_{120} in the forward decoding stage. Therefore, we do not need node 2 to relay this mes-

sage. Because decoding W_{120} was the only requirement for node 2, node 2 is not required to perform any decoding anymore. Since W_{120} is incorporated with W_{10}, all constraints regarding node 0 in the backward decoding stage are removed. To conclude, when

$$\frac{N_2}{K_{12}^2} < \frac{N_1}{K_{01}^2} = \frac{N_0}{K_{10}^2} < \frac{N_2}{K_{02}^2}$$

and

$$\frac{N_2 + K_{02}^2 P_{01}}{K_{12}^2} > \frac{N_0}{K_{10}^2},$$

the achievable rate region is composed of :

For node 0 in the forward decoding stage, the constraints are

$$R_{12} < C\left(\frac{K_{10}^2 P_{12}}{N_0}\right) \tag{5.199}$$

$$\boldsymbol{R}_{10} < \boldsymbol{C}\left(\frac{\boldsymbol{K}_{10}^2 \boldsymbol{P}_{10}}{\boldsymbol{N}_0}\right) \tag{5.200}$$

$$\boldsymbol{R}_{102} < \boldsymbol{C}\left(\frac{\boldsymbol{K}_{10}^2 \boldsymbol{P}_{102}}{\boldsymbol{N}_0}\right) \tag{5.201}$$

$$R_{12} + R_{10} < C\left(\frac{K_{10}^2 (P_{12} + P_{10})}{N_0}\right) \tag{5.202}$$

$$R_{12} + R_{102} < C\left(\frac{K_{10}^2 (P_{12} + P_{102})}{N_0}\right) \tag{5.203}$$

$$R_{10} + R_{102} < C\left(\frac{K_{10}^2 (P_{10} + P_{102})}{N_0}\right) \tag{5.204}$$

$$R_{12} + R_{10} + R_{102} < C\left(\frac{K_{10}^2 (P_{12} + P_{10} + P_{102})}{N_0}\right). \tag{5.205}$$

For node 1 in the forward decoding stage, the constraints are (5.131)—(5.137).

For node 2 in the backward decoding stage, the constraints are (5.195)—(5.198).

The flows of substreams are demonstrated in Figure 5.36—Figure 5.38.Comparing this achievable rate region with the region for (5.186) and (5.187), there are two differences because node 2 is noisier and further unable to decode messages. In the backward decoding stage, node 2 cannot decode W_{10} anymore. By contrast, in the forward decoding stage, node 0 can further decode W_{12}.

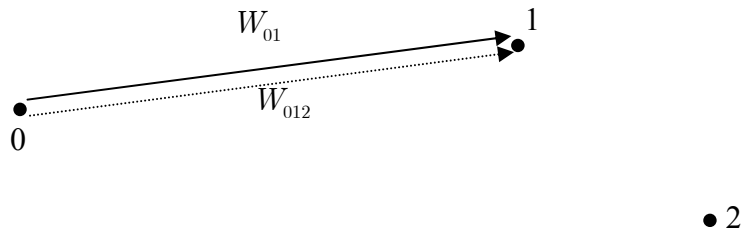

Figure 5.36: Node 1 decodes W_{01} and W_{012} in the forward decoding stage.

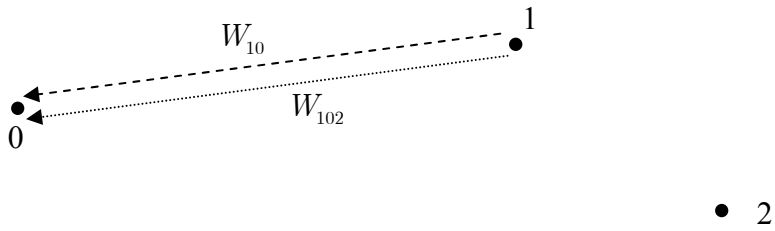

Figure 5.37: Node 0 decodes W_{10} and W_{102} in the forward decoding stage.

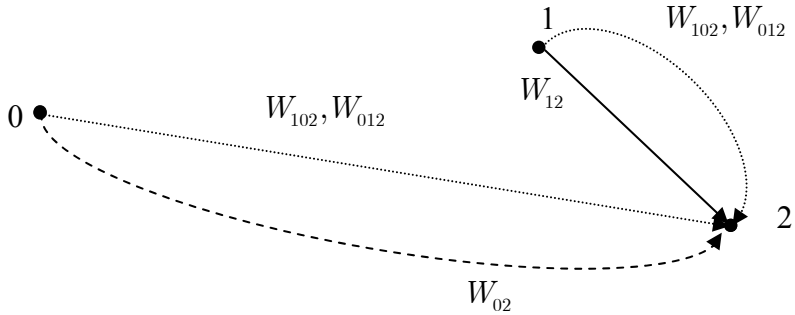

Figure 5.38: Node 2 decodes W_{02}, W_{12}, W_{102} and W_{012} in the backward decoding stage.

5.6 Conclusion

In this chapter, we have considered a wireless sensor network with three nodes and have explored some information-theoretic problems in this network. In the relay channel, the number of nodes is also three. However, in that configuration, only one information stream was considered. In [16], the configuration with two information streams with the common destination was examined. Based on the scheme of Sendonaris et al. and the associated achievable rate region, we have obtained the optimal power allocation point and have proved that this region collapses to the capacity of the physically degraded relay channel. Furthermore, we have proposed a concept to modify this scheme and have obtained a larger achievable rate. The concept is to decode signals intended for other nodes without imposing new rate constraints. With this scheme, the optimal power allocation turns out to be a range. The optimal power allocation under several conditions has then been derived. Finally, we have investigated the scenario with 2 information sources and each with 2 information streams. We have investigated several configurations with different distance relationships between nodes and noise power spectrum densities. Based on the proposed concept, the achievable rate regions have been derived.

To summarize, the achievable rate regions for the two sources and each with two destinations are listed for various relationships between normalized noise measures:

$$\frac{\boldsymbol{N}_2}{\boldsymbol{K}_{12}^2} < \frac{\boldsymbol{N}_2}{\boldsymbol{K}_{02}^2} < \frac{\boldsymbol{N}_1}{\boldsymbol{K}_{01}^2}, \frac{\boldsymbol{N}_0}{\boldsymbol{K}_{10}^2}:$$

In the forward decoding stage, for node 2, the constraints are (5.117)—(5.125).

In the backward decoding stage, for node 0, the constraints are (5.126) and (5.127).

In the backward decoding stage, for node 1, the constraints are (5.128) and (5.129).

$$\frac{\boldsymbol{N}_2}{\boldsymbol{K}_{12}^2} < \frac{\boldsymbol{N}_1}{\boldsymbol{K}_{01}^2} = \frac{\boldsymbol{N}_0}{\boldsymbol{K}_{10}^2} < \frac{\boldsymbol{N}_2}{\boldsymbol{K}_{02}^2}$$

if $\dfrac{\boldsymbol{N}_2 + \boldsymbol{K}_{02}^2 \boldsymbol{P}_{01}}{\boldsymbol{K}_{12}^2} < \dfrac{\boldsymbol{N}_0}{\boldsymbol{K}_{10}^2}$

if $\dfrac{\boldsymbol{N}_2 + \boldsymbol{K}_{02}^2 \boldsymbol{P}_{01} + \boldsymbol{K}_{02}^2 \boldsymbol{P}_{012} + \boldsymbol{K}_{02}^2 \boldsymbol{P}_{02}}{\boldsymbol{K}_{12}^2} < \dfrac{\boldsymbol{N}_0}{\boldsymbol{K}_{10}^2}$:

For node 2 in the forward decoding stage, the constraints are (5.183)—(5.185).

For node 1 in the forward decoding stage, the constraints are (5.131)—(5.137).

For node 0 in the backward decoding stage, the constraints are (5.166) and (5.167).

For node 2 in the backward decoding stage, the constraints are (5.158)—(5.164).

if $\dfrac{\boldsymbol{N}_2 + \boldsymbol{K}_{02}^2 \boldsymbol{P}_{01} + \boldsymbol{K}_{02}^2 \boldsymbol{P}_{012} + \boldsymbol{K}_{02}^2 \boldsymbol{P}_{02}}{\boldsymbol{K}_{12}^2} > \dfrac{\boldsymbol{N}_0}{\boldsymbol{K}_{10}^2}$

For node 0 in the forward decoding stage, the constraints are (5.188)—(5.190).

For node 1 in the forward decoding stage, the constraints are (5.131)—(5.137).

For node 2 in the backward decoding stage, the constraints are (5.158)—(5.164).

if $\dfrac{\boldsymbol{N}_2 + \boldsymbol{K}_{02}^2 \boldsymbol{P}_{01}}{\boldsymbol{K}_{12}^2} > \dfrac{\boldsymbol{N}_0}{\boldsymbol{K}_{10}^2}$

For node 0 in the forward decoding stage, the constraints are (5.199)—(5.205).

For node 1 in the forward decoding stage, the constraints are (5.131)—(5.137).

For node 2 in the backward decoding stage, the constraints are (5.195)—(5.198).

Chapter 6

Conclusion

This dissertation investigates communications in the physical layer of the wireless sensor network, where each sensor is equipped with one antenna. In terms of the number of transmit and receive antennas, the kind of communications is similar to multiple-input-multiple-output (MIMO) communications. However, differently from ordinary MIMO communications, some assumptions are not taken for granted. First, phase synchronization among antennas is not perfect and effortless. Secondly, beyond being unsynchronized, the phase offset between the received signal phase and the local clock phase may vary with time, instead of being fixed, for various reasons, such as antenna motion. Finally, the local information communication among antennas at either the transmit or the receive side does not come for free. Nevertheless, communications can be improved when sensors cooperate with each other, and this is called cooperative communications. In this dissertation, the consequences of three problems on communications are studied, and a type of cooperative communications is provided.

Chapter 2 considers the stationary configuration of multiple transmit antennas without synchronization and one receive antenna in the additive white Gaussian noise (AWGN) channel. It is demonstrated that cooperative communications can be accomplished if signals from each transmit antenna combine coherently at the receive antenna. This combining can occur only if clock phases of all transmit antenna clocks are adjusted

at the phase level. In addition to synchronization, pre-compensation at transmission is also required to account for different propagation delays. The synchronization is implemented by the phase-locked loop, with the help of CDMA. The value of pre-compensation for each transmit antenna is recursively estimated, based on signals sent from transmit antennas and dedicated for synchronization. The respective estimates are fed back to each transmit antenna. The phase error for coherent combining comes from the phase-locked loop phase error and the estimation error due to AWGN. Its distribution is determined, and the power consumption dedicated for synchronization is included to determine the communication performance versus overall power consumption. The numerical results show coherent transmission outperforms communications without this technique, even with the synchronization overhead. Additionally, the optimal power distribution between synchronization overhead and data transmission are observed.

The non-stationary case is explored in Chapter 3. The single receive antenna is assumed to move at high speed, and thus the perfect phase pre-compensation value for coherent transmission varies with time. Coherent transmission can still be achieved if the dependency of the pre-compensation estimate on the previous one is removed. In addition to the Doppler due to antenna motion and AWGN, the forward and backward medium disturbances are also considered. Furthermore, the time correlation of the phase random process associated with the signals from transmit antennas is analytically quantified when we determine the communication performance. In spite of so many imperfections, the benefit of coherent transmission is still present, and it grows with the number of transmit antennas.

When there are many stationary transmit antennas in the AWGN channel, coherent combining turns out to be the combination of channel decomposition and the water-filling algorithm. If the antenna clocks, either at the transmit or the receive side, are not synchronized in phase, the perceived channel matrix will be different for different phase relationships. These channel matrixes are discussed in Chapter 4. It is shown that the channel capacity is identical for all channel matrixes derived from different phase relationships. This equalization can be realized at baseband with a phase rotation corresponding to the phase offset, leaving the channel decomposition and the water-filling algorithm unchanged. Instead, if the channel decomposition is executed whenever the phase relationship changes, it is revealing that the water-filling algorithm is unchanged, whereas the channel decomposition at two points in time can be related through the discrepancy of the two associated phase relationships.

Finally, in Chapter 5, we address the issue of power-consuming local communication by investigating the three-node wireless network with AWGN, where all transmission power consumption is included. In contrast to the relay channel, we consider multiple information streams. Each information stream is decomposed into the relay-path and the direct-path streams. The relay-path stream is first sent to the relay node and then transmitted to the destination with coherent combining, whereas the direct-path stream goes to the destination directly. We start from the scenario with two information sources and one common destination. Using the forward and backward decoding stages, we derive two sets of achievable rate regions for two sets of relationships among noise power spectrum densities normalized by the square of path gain. We also consider scenarios

with one common source and two destinations for two information streams, as well as two sources and two destinations for four information streams. For each scenario, the achievable rate regions are derived for several sets of normalized noise relationships. The derivation contains two major concepts. First, if the relay-path stream can be decoded by the destination while it is decoded by the relay node, we should employ the direct-path stream only. Secondly, if a node is able to decode the undesired signals, instead of regarding it as noise, without imposing a stronger constraint, this decoding should be realized and it can alleviate the decoding of the desired signal. From the achieved rate regions, generally speaking, for a specific information stream if the third node is closer to the source than the destination, this node should decode the relay-path signal and then implement coherent combining with the source in the following time block.

Regarding the extension of research on wireless sensor networks, one extension is to investigate configurations with multiple transmit sensors and multiple receive sensors. Indeed, there is more freedom to conduct cooperation, and interference could be a problem. Nevertheless, it is worthwhile to devise communication schemes for certain constraints. For example, we can organize a hierarchy of sensors where each hierarchy has its own bandwidth. Another example is to consider certain distributions of sensor locations. Although it may be difficult to derive the channel capacity, it would be a big contribution to obtain the asymptotic performance.

Bibliography

[1] T. M. Cover and A. El Gamal, "Capacity theorems for the relay channel," *IEEE Trans. Inform. Theory*, IT-25: 572-584, 1979.

[2] T. M. Cover and J. A. Thomas, *Elements of Information Theory*, New York: John Wiley & Sons, 1991.

[3] T. M. Cover, "Broadcast channels," *IEEE Trans. Inform. Theory*, IT-18: 2-14, 1972.

[4] G. J. Foschini, Jr. and M. J. Gans, "On limits of wireless communication in a fading environment when using multiple antennas," *Wireless Personal Commun*, 6:311-335, Mar. 1998.

[5] R. M. Gagliardi, *Satellite Communications*, Van Nostrand Reinhold, New York, 1991.

[6] M. Gastpar and M. Vetterli, "On the capacity of wireless networks: the relay case," in *Proc. IEEE INFOCOM'02*, pp. 1577-1586.

[7] J.-C. Guey, M. P. Fitz, M. R. Bell and W.-Y. Kuo, "Signal design for transmitter diversity wireless communication systems over Rayleigh fading channgles," in *Proc. IEEE VTC'96*, pp. 136–140.

[8] P. Gupta and P. R. Kumar, "Towards an information theory of large networks: An achievable rate region," in *IEEE Int. Symp. Info. Theory*, Washington DC, June 2001, (also submitted to *IEEE Trans Info Theory*, 2001.).

[9] W. C. Hagmann, "Network synchronization techniques for satellite communication systems," Ph.D. dissertation, USC, Los Angeles, CA, 1981.

[10] J. N. Laneman, D N. C. Tse, and G. W. Wornell, “Cooperative diversity in wireless netowkrs: efficient protocols and outage behavior,” submitted to *IEEE Trans. Inform. Theory,* Jan. 2002.

[11] J. S. Lee and L. E. Miller, *CDMA systems engineering handbook*. Boston: Arch House, 1998.

[12] W. C. Lindsey, F. Ghazvinian, W. C. Hagmann, and K. Dessouky, “Network synchronization,” *Proc. IEEE*, vol. 73, pp. 1445–1467, Oct. 1985.

[13] H. Meyr, and G. Ascheid, *Synchronization in Digital Communications*, John Wiley & Sons, 1990.

[14] J. G. Proakis, *Digital Communications*, 4th ed., New York: McGraw-Hill, 2000.

[15] K. Quirk, “The Effects of Estimation Errors on Direct Sequence Spread Spectrum Receiver Performance,” Ph.D. disserattion, University of California, San Diego, CA, 2000.

[16] A. Sendonaris, E. Erkip, and B. Aazhang, “User Cooperation Diversity-Part I: System Description,”

[17] V. Tarokh, N. Seshadri, and A. R. Calderbank, “Space-time codes for high data rate wireless communication: performance criterion and code construction,” *IEEE Trans. Inform. Theory*, vol. 44, pp. 744–765, Mar. 1998.

[18] E. Telatar, “Capacity of multi-antenna Gaussian channels,” *AT&T-Bell Labs Internal Tech. Memo.*, June 1995.

[19] Paul A. Tipler, *Foundations of Modern Physics*, Worth Publishers, New York, NY, 1969.

[20] E. C. Van der Meulen, “A Survey of Multi-way Channels in Information Theory,” *IEEE Trans. Inform. Theory*, IT-23: 1-37, 1977.

[21] A. J. Viterbi, *Principles of Coherent Communication*. New York: McGraw-Hill, 1966.

[22] W. J. Webber, III, “Performance of Phase-Locked Loops in the Presence of Fading Communication Channels,” *IEEE Trans. Commun*., vol. 24, pp. 487-499, May 1976.